Dissertation
submitted to the
Combined Faculties of the Natural Sciences and for Mathematics
of the Ruperto-Carola University of Heidelberg, Germany
for the degree of
Doctor of Natural Sciences

presented by
Master-Physicist: Hany El-Gamal
born in: El-Menoufia, Egypt
Oral examination: 08.06.2005

Environmental tracers in groundwater as tools to study hydrological questions in arid regions

Referees: **Prof. Dr. Werner Aeschbach-Hertig**
Prof. Dr. Kurt Roth

Zusammenfassung

In der vorliegenden Arbeit werden Umwelttracer wie Edelgase, stabile Isotope, Tritium und SF_6 verwendet um hydrologische Fragen in ariden Regionen zu studieren. Theoretische Modelle und numerische Methoden zur Behandlung des Phänomens von Luftüberschüssen in Grundwasser werden diskutiert. Das Potential dieser Ansätze zur Beschreibung des Phänomens der Entgasung, das in einigen Grundwasserleitern gefunden wird, wird ausgelotet. Diese Arbeit enthält zwei bedeutende Anwendungen von Umwelttracern um Grundwasser in Gebieten mit sehr aridem Klima zu studieren. Das Hauptziel dieser Studien war, den Ursprung und das Alter des Grundwassers an solchen Standorten zu bestimmen. Die erste Studie untersucht Aquifere welche neu entwickelte "reclamation areas" südwestlich des Nildeltas in Ägypten mit Wasser versorgen. In diesem Gebiet wird das Grundwasser hauptsächlich aus dem Nil erneuert, wenn auch mit einer niedrigen Rate. Die meisten Proben wurden vor der Fertigstellung des Assuan Staudamms im Jahre 1969 infiltriert und haben Alter > 50 a, nur wenige in der Nähe des Oberflächenwassers gelegene Brunnen liefern jüngeres Wasser. Die zweite Studie untersucht Quellen, welche Oasen in den Bergen des nördlichen Oman versorgen. Das Wasser dieser Quellen wird durch Niederschlag auf Zeitskalen von Jahren bis höchstens wenige Dekaden erneuert. Die meisten Proben haben junge Alter im Bereich von 2-10 a.

Abstract

Environmental tracers such as noble gases, stable isotopes, tritium, and SF_6 are used in this work to study hydrological questions in arid regions. Theoretical models and numerical methods to treat the excess air phenomenon in groundwater are discussed. The potential of these approaches to describe the phenomenon of degassing, which is found in some aquifers, is explored. This work contains two major applications of environmental tracers to study groundwater in areas with very arid climate. The main goal of these studies was to determine the origin and age of groundwater in such locations. The first study investigates aquifers supplying water to new reclamation areas southwest of the Nile Delta in Egypt. In this area, the groundwater is mainly recharged from the Nile River, albeit at a low rate. Most of the samples were recharged before the completion of the Aswan High Dam in 1969 and have ages > 50 yr, only few wells located near to the surface water yield younger water. The second study investigates springs supplying oases in the mountains of Northern Oman. These springs are recharged by precipitation on time scales of years to at most a few decades. Most of the samples have young ages ranging between 2-10 yr.

Contents

Chapter 1

1 Introduction

1.1 Outline

This thesis is organized as follows:

Chapter 1 gives a brief introduction to groundwater, its role as a precious resource in arid regions, and the use of environmental tracers to study this resource. This discussion explains the motivation for this work, which is to develop and apply tools that will help to better manage the scarce groundwater resources in arid countries such as Egypt and Oman, where the main field studies (described in chapter 5 and 6) have been conducted.

Chapter 2 discusses the noble gases and their application in groundwater. The different origins of noble gases, their solubility and other processes affecting their concentrations in groundwater are described. After groundwater infiltration, the concentrations of noble gases in groundwater reflect the atmospheric equilibrium concentrations modified by an additional atmospheric component known as 'excess air'. The reasons for the presence of this excess air component in groundwater are not yet completely understood. However, the problem of the generation and composition of the excess air component is crucial to any interpretation of the results of the noble gas thermometer, and to all dating methods based on gaseous tracers. The ^{3}H-^{3}He method, which is the main noble gas based dating technique for groundwater, is also discussed in this chapter.

Chapter 3 outlines the different models, which describe the excess air phenomenon that is present in groundwater. These models are: i) the unfractionated excess air model (UA-model), which assumes complete dissolution of small air bubbles trapped in soil pores; ii) the partial re-equilibration model (PR-model) involving complete dissolution of entrapped air bubbles followed by partial re-equilibration (PR) with the atmosphere (Stute et al., 1995); iii) the closed system model (CE-model), the basic assumption of which is that a finite volume of initially air saturated water attains solubility equilibrium with a finite volume of gas (bubbles), which initially contained atmospheric air. The PR-model results in diffusivity-controlled fractionation of the excess air with respect to atmospheric air, whereas in the case of the CE-model the fractionation is controlled by the solubilities. The main goal of this chapter is to find a theoretical description of the degassing process, which might take place during sampling or because of formation of gas bubbles in the aquifers themselves. The Ledo-Paniselian aquifer (Belgium) is considered as a field example for testing and

applying the theoretical concepts. A comparison between the new model and the one described by Lippmann et al. (2003) is also explained in this chapter.

Chapter 4 discusses two transient gas tracers that have been used in our field studies to date young groundwater.

Sulfur hexafluoride (SF_6) is a relatively new tracer in groundwater hydrology. It is primarily of anthropogenic origin but also occurs naturally. Groundwater can be dated with SF_6 if equilibrates with atmospheric SF_6 at the time of recharge and does not contain significant SF_6 from non-atmospheric sources. Excess air usually contributes a significant component to the observed SF_6 concentration, but it can be accounted for. The calculation of the solubility and excess air components, and finally the SF_6 age is discussed. SF_6 can be collected in stainless steel cylinders, and we developed a method to transfer water samples from the cylinder to a special glass bottle for subsequent analysis using a gas chromatographic system.

Chlorofluorocarbons (CFCs) are stable and synthetic anthropogenic organic compounds, which can be used as tracers and dating tools of young groundwater (<50 years). The atmospheric mixing ratios of CFC-11, CFC-12 and CFC-113 have been reconstructed over the past 50 years. Groundwater dating by CFCs basically depends on the comparison between the atmospheric concentration history and the measured concentrations of CFCs in groundwater samples. In this chapter we focus on the application of CFCs as a dating tool for groundwater samples and explain the processes that affect CFC apparent age.

Chapter 5 discusses the results from a field study conducted in Egypt. The investigation area lies south-west of the Nile Delta in Egypt, where groundwater is pumped to supply water to new settlements and plantations, so called reclamation areas, in the former desert. This studied region is extremely arid, and the Nile River is the only relevant renewable source of water in it. The main goal of this study is to quantify the groundwater renewal rate as a basis for a sustainable management of this crucial resource.

The water-bearing formations in the investigation area are classified into five aquifers, (Recent, Pleistocene, Pliocene, Miocene and Oligocene), the hydrogeological and hydrochemical conditions of which are discussed.

Stable isotopes prove that the main source of recharge in the investigation area is the Nile water, and show that most of this recharge took place before the completion of the Aswan High Dam. For the relatively few wells that contain water that recharged after the construction of the dam in 1969, the ^3H-^3He and SF_6 methods have successfully been used to date the shallow groundwater. A comparison between the results of the two methods is made in this chapter. The noble gas data provide the basis for a clear interpretation and correction of the excess air component and show that no significant change of the climate conditions is recorded in the groundwater in the study area.

Chapter 6 deals with the tracer data obtained from springs in the mountains of Oman, also an area characterized by an arid climate. The chapter outlines the application of the ^{3}H-^{3}He, SF_6 and CFCs methods to date the groundwater from these springs. The interpretation of the Oman samples is unusually complicated because of sampling under difficult and not well controlled conditions. As a result, the noble gas compositions of a significant part of the samples did not show the same consistency as in the samples from Egypt. Furthermore, tritium concentrations in modern Oman precipitation are very low, the recharge altitudes of the groundwater from a mountainous area are not exactly known, and the high recharge temperatures affect the SF_6 dating method, because they lead to low SF_6 concentrations and large excess air corrections. Despite these difficulties, we succeeded to apply our methods, although with higher uncertainties than usual. The obtained results refer to the occurrence of young water (< 10 yr) in most springs, and to old water in some localities. The application of stable isotopes indicated that the origin of groundwater in the investigation areas is from a combination between the northern and southern moisture sources.

1.2 Groundwater

Groundwater is water that is found in the subsurface in cracks and pore spaces in soil, sand and rocks. These materials form what is called the groundwater reservoir or aquifer. Groundwater is found in two different zones. The first is the unsaturated zone, which lies immediately below the land surface; in this zone the spaces between the rock and soil particles are filled with a mixture of air and water. The second zone is the saturated zone in which all the pore spaces is completely filled with water. The top of the saturated zone is called water table, which may be found at widely varying depths. The water table may rise due to heavy rains or melting snow, it also may fall during periods of dry weather and because of overpumping, which takes place in areas depending mainly on groundwater for agriculture or as drinking water, like the area south-west of the Nile Delta in Egypt (chapter 5).

Groundwater is recharged generally by rainwater or snow melt, which infiltrate into the soil where some of it is evaporated, some is absorbed by plant roots, and some seeps down into the saturated zone. During long periods without rain the unsaturated zone may remain dry. In the saturated zone water infiltrates through the interconnected pore spaces, moving downward by the force of gravity, and upward toward zones of lower pressure. Where the water table intersects the surface, such as at a surface stream, lake, or swamp, the groundwater returns to the surface. Groundwater can also be extracted through a well drilled into the aquifer. A well is essentially a pipe in the ground that is perforated in some depth interval (called the well screen and usually located in the bottom part) through which it fills with groundwater. This water then can be brought to the surface by a pump.

In some areas of the world (e.g. south west Nile Delta, Egypt) people face serious water shortages because groundwater is used faster than it is naturally replenished. In other areas groundwater is polluted by different pollutants. In general the pollution of air, water, and land has an effect on the pollution and contamination of groundwater. For example, when the air is polluted, rainfall will settle many pollutants on the ground, which can then seep into and contaminate the groundwater resources. In addition, the overuse of fertilizers and pesticides for agricultural purposes, industrial and municipal solid waste, and leakages from tanks containing all kinds of liquids have also polluted groundwater. If groundwater becomes polluted, it will no longer be safe to drink. Cleaning up the contaminated aquifers is usually extremely difficult and expensive, or even unfeasible.

The movement and the amount of storage of groundwater depend on soil properties such as porosity and permeability. Porosity is defined as the ratio of the volume of pore space in a unit of material to the total volume of material; porosity is affected by the shape, size and the arrangement of the soil particles, e.g., the smaller particles could fill in the void spaces between the larger particles, which would result in a lower porosity. Permeability is a measure of a soil's or rock's ability to transmit water so that the size of pore space and interconnectivity of the spaces help determine permeability. Often the term hydraulic conductivity is used when discussing groundwater and aquifer properties. Hydraulic conductivity has the units of velocity.

Groundwater flow is driven by differences in pressure and elevation between two points in the aquifer, which are described in terms of the gradient of the so-called hydraulic head. The basic principle linking the specific discharge q (volume flow of water per crossectional area and time) to the hydraulic head h and the hydraulic conductivity k is Darcy's law, which for one-dimensional flow may be written as:

$$q = -k\frac{dh}{dx} \tag{1.1}$$

The specific discharge, as the hydraulic conductivity, has the dimensions of a velocity, and hence is also called the Darcy velocity.

1.3 Groundwater as a source of freshwater resources

More than 70 % of the surface of the Earth is covered with water, the most common substance in the environment. The total volume of water on Earth is about $1.4 \cdot 10^9$ km^3. Approximately 97.5 % of this water is salt water in the oceans and only 2.5 %, or about 35 million km^3 is fresh water (see Table 1.1). More than two thirds of the fresh water is locked up in ice caps and glaciers. Of the remaining liquid fresh water, the vast majority is groundwater, and only about 1.5 % is surface water (rivers, lakes and man-made reservoirs). Only this tiny fraction of about 0.01 % of all of the Earth's water is readily available to humans, other organisms and fresh water ecosystems which depend on this rare resource for their very existence.

Category	Storage (10^3 km^3)	% of total	% of liquid freshwater
Total global volume of water	1,384,000	100	
Oceans and salt water lakes	1,350,000	97.5	
Glaciers and ice caps	25,000	1.8	
Liquid fresh water (details see below)	9,000	0.65	100
Groundwater	8,847	0.64	98.3
Freshwater lakes	0,126	0.009	1.4
Soil moisture	0,0225	0.001	0.25
Man-made reservoirs	0,0027	-	0.03
Rivers	0,0018	-	0.02

Table 1.1: Global water reservoirs after Mather (1984). Similar numbers have been obtained by Shiklomanov and Rodda (2003).

The scarcity of water will be even more critical in the future, especially in arid and semi arid regions, which are characterized by receiving less than 200 to 250 mm/yr of precipitation, which may occur irregularly (Ingraham et al., 1998). Groundwater is considered as the main source of fresh water in arid and semi arid regions except in areas where large rivers are found such as the Colorado River in the American southwest and the Nile River in northeast Africa. Because of the steadily increasing demand for high quality fresh water due to population growth and rising standard of living, groundwater is frequently over-utilized. This results in a significant lowering of the groundwater table, allowing encroachment of saline water from the sea or from the deeper aquifers. For sustainable utilization of groundwater, the pumping has to be limited to the rate of groundwater recharge and the water quality has to be preserved.

Environmental tracers can be used to provide information about groundwater systems and their dynamics, in order to cope with the above mentioned guidelines for sustainable management. E.g., stable isotopes (δD and δ^{18}O) give information about the origin of groundwater and the effect of evaporation, anthropogenic tracers such as ^{3}H (possibly combined with ^{3}He), CFCs and SF_6 give information about groundwater ages, and noble gases can be used to determine the recharge conditions (especially temperature) in the past.

Environmental tracers have been used in this work to study groundwater in the area south-west of the Nile Delta, Egypt and in the Mountains of Oman, both of them belonging to arid regions. The main goal is to determine the origin of recharge and the recharge rate, which will help to define management guidelines for a sustainable use of groundwater in such areas.

Chapter 2

2 Noble gases in groundwater hydrology

Noble gases, also referred to as rare gases, are the elements He, Ne, Ar, Kr, and Xe (Rn is not considered here as it has no stable isotopes). They have proved to be valuable as tracers in hydrology, primarily due to their inherent chemical and biological inertness. The noble gases mainly enter the water phase through dissolution from air, and once they are in solution they remain unaffected by the chemical and physical environment through which they pass. They do not interact with any other species, except the most oxidizing of reagents, and even this only under extreme conditions. Thus, noble gases come very close to the ideal of a conservative tracer.

Noble gases in groundwater have different sources (Figure 2.1), e.g. an atmospheric source by gas exchange during infiltration, and a non atmospheric source from the water itself via the radioactive decay of tritium and from the Earth's mantle or crust.

Noble gases have been applied to the study of processes which affect the groundwater geochemistry in various geological settings. Some objectives of noble gas studies in groundwater are: (1) groundwater migration and age dating (2) paleoclimate assessment at recharge by measurement of the recharge temperature (3) investigation of deep crustal processes, e.g. $^{3}He/^{4}He$ systematics and fluxes of crustal and mantle derived gases, and (4) study of geochemical processes in the shallow crust, e.g. release of ^{40}Ar by alteration and increase in the N_2/Ar ratio because of denitrification. This work concentrates mainly on the application of groundwater dating and reconstruction of recharge conditions. The advantages of noble gases as tracers in groundwater studies are:

(1) There is no chemical or biological interaction between noble gases and other substances under natural conditions. The noble gases are ideal to study and trace physical processes because these processes such as diffusion, partitioning between different phases, and radiogenic production, govern their behavior in nature.

(2) The initial concentrations of the atmospheric noble gases in groundwater are mainly controlled by the ambient pressure, the altitude of the recharge area and the water temperature during recharge.

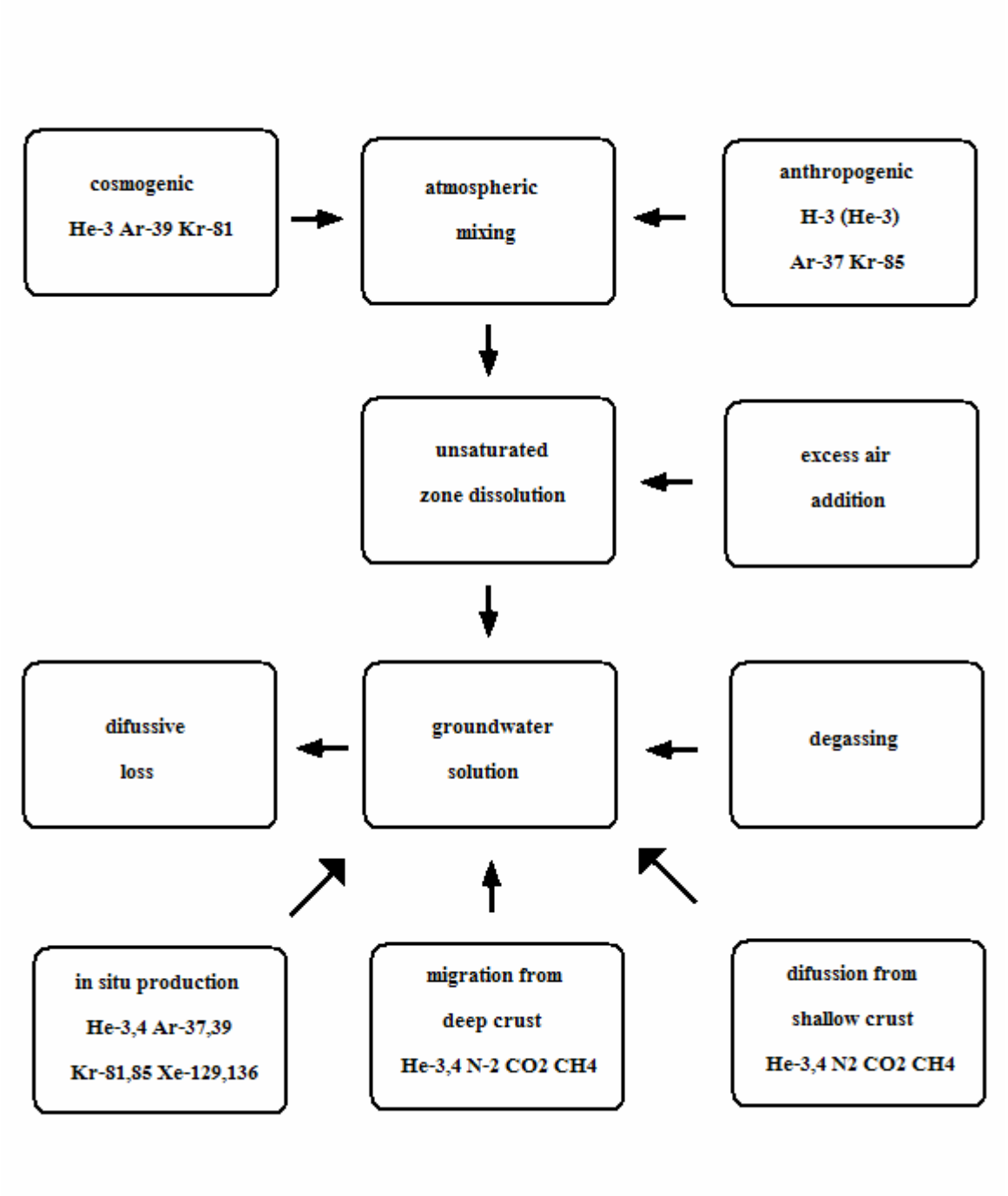

Figure 2.1: Source of stable and radioactive noble gas species and the pathways controlling the extent of their dissolution by groundwater (Andrews, 1992)

2.1 Sources of noble gases

The major reservoir of terrestrial noble gases is the atmosphere; air has a uniform composition that is generally constant over time. This is especially true for noble gases, which are volatile and non-reactive and therefore have very long residence times in the atmosphere. The mixing ratios and isotopic compositions of the noble gases in the atmosphere are listed in Tables 2.1 and 2.2. Most noble gas isotopes are of primordial origin, i.e., they stem from the time of the Earth's formation and have accumulated in the atmosphere as a result of degassing of the solid Earth. Some noble gas isotopes, however, are continuously produced in significant amounts.

Sources of helium isotopes:

The light noble gas isotopes ^{3}He and ^{4}He are the only stable noble gas isotopes that have a significant sink in the atmosphere, as they can escape from the upper atmosphere into space. Nevertheless, the atmospheric helium volume fraction below heights of 100 km is constant with a value of 5.24 ppm (Ozima and Podosek, 1983) and a ^{3}He/^{4}He ratio of $1.384 \cdot 10^{-6}$ (Clarke et al., 1976). The sink by loss to space appears thus to be balanced by sources, which are to be found in the solid earth. Both ^{3}He and ^{4}He are produced in the Earth's crust by in situ processes, the former by neutron irradiation of the lithium and the latter by α-decay of the natural radioelements;

$$^6Li(n,\alpha)^3H \rightarrow {}^3He \quad (2.1)$$

$$^{238}U \rightarrow {}^{206}Pb + 8\,{}^4He \quad (2.2)$$

$$^{235}U \rightarrow {}^{207}Pb + 7\,{}^4He \quad (2.3)$$

$$^{232}Th \rightarrow {}^{208}Pb + 6\,{}^4He \quad (2.4)$$

This crustal or radiogenic component is characterized by a ^{3}He/^{4}He ratio that is much lower than the ratio observed in the atmosphere. On the other hand, the helium stored in the Earth's mantle as well as that produced in surface rocks by cosmic radiation is enriched in ^{3}He relative to air, and deep crustal sources may be dominated by mantle stored helium containing a relatively high proportion of ^{3}He. Atmospheric helium, therefore, contains significant amounts of both cosmogenic and mantle derived ^{3}He,in addition to the dominant crustal source. The isotopic ratio for dissolved helium in groundwater may be the result of an admixture of these different sources.

In summary, the relative abundance of the two isotopes of He varies greatly among the various terrestrial reservoirs. Three major distinct reservoirs can be distinguished: (1) An atmospheric reservoir with a ^{3}He/^{4}He ratio of $1.384 \cdot 10^{-6}$ (Clarke et al., 1976). (2) A crustal reservoir with a ^{3}He/^{4}He ratio of 10^{-9}-10^{-7} and a typical value of $2 \cdot 10^{-8}$ (Mamyrin and Tolstikhin, 1984). (3) A mantle reservoir with a ^{3}He/^{4}He ratio of $1.1 \cdot 10^{-5}$ to $1.4 \cdot 10^{-5}$ (Ozima and Podosek, 1983).The separation of the total ^{3}He and ^{4}He in groundwater samples into their individual components will be discussed in section 2.5.

Noble gas	Volume fraction	Isotope	abundance
He	$(5.24 \pm 0.05) \cdot 10^{-6}$	^{3}He	0.001348
		^{4}He	~100
Ne	$(1.82 \pm 0.04) \cdot 10^{-5}$	^{20}Ne	90.50
		^{21}Ne	0.268
		^{22}Ne	9.23
Ar	$(9.34 \pm 0.01) \cdot 10^{-3}$	^{36}Ar	0.3371
		^{38}Ar	0.0632
		^{40}Ar	99.60
Kr	$(1.14 \pm 0.01).10^{-6}$	^{78}Kr	0.347
		^{80}Kr	2.257
		^{82}Kr	11.52
		^{83}Kr	11.48
		^{84}Kr	57.00
		^{86}Kr	17.40
Xe	$(8.7 \pm 0.1) \cdot 10^{-8}$	^{124}Xe	0.0951
		^{126}Xe	0.0887
		^{128}Xe	1.919
		^{129}Xe	26.44
		^{130}Xe	4.070
		^{131}Xe	21.22
		^{132}Xe	26.89
		^{134}Xe	10.43
		^{136}Xe	8.857

Table 2.1: Concentrations and isotopic abundances of noble gases in dry air (Ozima and Podosek, 1983)

Isotopes	Ratio
$^{3}He/^{4}He$	$1.384 \cdot 10^{-6}$
$^{3}He/^{20}Ne$	$4.408 \cdot 10^{-7}$
$^{4}He/^{20}Ne$	0.3185
$^{20}Ne/^{22}Ne$	9.80
$^{40}Ar/^{36}Ar$	295.5

Table 2.2: Atmospheric noble gas ratios

Sources of neon isotopes:

The neon concentration in the atmosphere is 18.18 ppm, which is higher than the helium concentration. The natural isotopic abundance of ^{20}Ne is 90.5%, for ^{21}Ne it is 0.268% and 9.23% for ^{22}Ne. ^{20}Ne which is the most abundant Ne isotope, has no significant radiogenic subsurface sources. ^{21}Ne and ^{22}Ne are produced in the crust but the produced concentration is usually too small to be detected compared to the large quantities derived from the atmosphere.

Sources of heavy noble gas isotopes:

The most frequent noble gas in the atmosphere is Ar (9340 ppm). The dominant isotopes are ^{40}Ar, ^{38}Ar and ^{36}Ar. The most abundant Ar isotope is ^{40}Ar which represents nearly 99.6% of the total amount of Ar in air and is largely the result of the production of ^{40}Ar from the decay of ^{40}K in the solid Earth.

Kr and Xe have several dominant isotopes in air, summing up to the total concentrations of 1.14 ppm for Kr and 0.087 ppm for Xe.

Minor sources of rare and radioactive noble gas isotopes:

Some noble gas isotopes have also been produced in anthropogenic sources, such as during nuclear weapons testing (^{3}H-^{3}He), in nuclear power reactors (^{37}Ar) and during nuclear fuel reprocessing (^{85}Kr). The in situ production of some radioisotopes occurs within geological formations as a result of cosmic proton and neutron induced reactions at shallow depths and of the in situ neutron flux at depths greater than 50 m (Andrews et al., 1989). In particular, the nuclides ^{37}Ar and ^{39}Ar are liable to be produced in groundwater by such underground processes, where as current estimates of the fission yield of ^{81}Kr suggest that it is very unlikely to be produced by uranium fission in an amount comparable to that of dissolved cosmogenic ^{81}Kr (Andrews et al., 1992).

2.2 Noble gas solubilities

Noble gas solubility is governed by Henry's law for dilute solutions. At equilibrium the concentration of gas i dissolved in the liquid phase is proportional to the concentration in the gas phase

$$C_{i,g} = H_i \cdot C_{i,l} \tag{2.5}$$

Where H_i is Henry's law constant which depends on the properties of the gas and the liquid and on temperature. H_i is called dimensionless if the concentration of gas and liquid are expressed in molar units (mol/L), but in reality the actual value of H_i implicitly depends on the choice of concentration units (e.g., it would be different if both concentrations were given in mol/kg). Therefore caution must be exercised if

related measures from different sources are compared. Concentrations in the gas phase are usually expressed as partial pressures, and Henry's law can then be written as follows

$$p_i = H_i' \cdot C_i^{eq} \tag{2.6}$$

Often, instead of Henry constants, the equilibrium concentration C_i^{eq} for p_i =1 atm is reported. This very convenient form of solubilities as a function of temperature and salinity for practical use has been reported by Weiss (1970, 1971) and Weiss and Kyser (1978), for ^{3}He, ^{4}He, Ne, Ar, Kr as well as for O_2 and N_2, both for fresh water and seawater. The corresponding values for He and Ne are commonly used in hydrological applications of the ^{3}H-^{3}He dating method (e.g., Solomon et al., 1992; Stute et al., 1997), oceanographic research (e.g. Jenkins., 1976; Schlosser et al., 1990), and limnological applications (e.g. Aeschbach-Hertig et al., 1996).

Benson and Krause (1976) re-evaluated the solubilities of noble gases in pure water, providing values with a very high precision (better than ± 0.2%). A critical evaluation of the literature on noble gas solubilities was published by Clever (1979a, b; 1980). In this review, the noble gas solubilities were expressed in terms of the mole fraction solubility X_i, which is defined as the number of moles of gas i per number of moles of solution when the partial pressure of the gas is 1 atm (Clever, 1979a, b, 1980). The coefficients and constants that were used to calculate the different noble gas solubilities are listed in appendix 1.

The solubilities of noble gases depend on salinity S in addition to temperature; the so-called salting out effect can be described by the Setchenow relation

$$\ln \frac{\beta_i(T,0)}{\beta_i(T,S)} = k_{s,i} \cdot C_{NaCl} \tag{2.7}$$

where $k_{s,i}$ is the salting coefficient of gas i, C_{NaCl} is the NaCl molarity and β is the Bunsen coefficient, which is defined as the volume of gas measured at STP (standard temperature: 0 ^{o}C and pressure: 1 atm) absorbed per unit volume of solution when the partial pressure of the gas is 1 atm. Smith and Kennedy (1983) reported the empirical salting coefficients for all noble gases in NaCl solutions. The complete sets of expressions for the noble gas solubilities can be obtained by combining the fresh water solubilities of Benson and Krause (1976) or Clever (1979a, b; 1980) and the data reported by Smith and Kennedy (1983).

Weiss and Price (1989) showed that the effect of salts on solubility depends mainly on the total mass of dissolved salt, thus the salting coefficient can be related to salinity by equating the mass of salt per unit volume:

$$C_{NaCl}(S) = \frac{S \cdot \rho(T,S)}{M_{NaCl}} \qquad \text{[mol/L]} \tag{2.8}$$

where M_{NaCl} is the molar mass of NaCl (58.443 g/mol) and ρ (T, S) is the density of a sea salt solution in kg/L.

In relatively fresh water (lakes, meteoric groundwater), S can be estimated from the electrical conductivity normalized to 20 °C (κ_{20}). For this purpose, the following relation established for $CaHCO_3$ dominated water can be used:

$$S(‰) = 0.87 \cdot 10^{-3} \cdot \kappa_{20} \quad (\mu S / cm) \tag{2.9}$$

Groundwater usually infiltrates with S ≈ 0, but can dissolve salt as it moves through the aquifer. This should however not affect the content of dissolved gases that has been set during infiltration.

The Bunsen coefficient β_i (see equation 2.7) and the salting coefficient k_s of Smith and Kennedy are used to introduce the salt dependence:

$$\beta_i(T,S) = \beta_i(T,0) \cdot e^{-k_{s,i} \cdot C_{NaCl}(S)} \quad [cm^3 STP/cm^3_{water}] \tag{2.10}$$

The Bunsen coefficient β_i of noble gas i can be converted to a moist air equilibrium concentration C_i^{eq} at a total atmospheric pressure P as follows:

$$C_i^{eq}(T,P,S) = \frac{\beta_i(T,S)(P - e(T))}{\rho(T,S)P_0} z_i \quad [cm^3\ STP/g_w] \tag{2.11}$$

where z_i is the volume fraction of gas i in dry air (Table 2.1), P_0 is the reference pressure at which β is given (1 atm) and e (T) is the saturated water vapor pressure as a function of T which is estimated according to Gill (1982)

$$e(T) = \frac{10^{\frac{a_1 + a_2 \cdot T}{b \cdot T + 1}}}{1013.25} \quad [atm] \tag{2.12}$$

with $a_1 = 0.7859$; $a_2 = 0.03477$; $b = 0.00412$

The literature values of Clever (1979a,b; 1980) for X_i in pure water can be converted to Bunsen coefficients β_i by:

$$\beta_i(T,0) = \frac{\rho(T,0) \cdot V_i}{M_w} X_i \quad [cm^3 STP/cm^3_{water}] \tag{2.13}$$

where ρ (T,0) is the density of pure water in g cm^{-3}, M_w is its molar mass (18.016 g/mol), and V_i is the molar volume of the gas i (in cm^3 STPgas/mol).

The dissolved concentration of gas in water with temperature T and salinity S at equilibrium with air at pressure P can finally be calculated from X_i by combining equations (2.10), (2.11) and (2.13) (Kipfer et al., 2002)

$$C_i^{eq}(T,P,S) = \frac{X_i}{M_w} \cdot \frac{(P - e(T))z_i}{P_0} \frac{\rho(T,0)}{\rho(T,S)} \cdot V_i \cdot e^{-k_{s,i} \cdot C_{NaCl}} \quad [\text{cm}^3\text{STP/g}] \quad (2.14)$$

The moist air equilibrium concentrations are not exactly proportional to P because of the water vapor pressure, the corrected pressure dependence is:

$$C_i^{eq}(T,P,S) = \frac{C_i^{eq}(T,S,P_0).(P - e(T))}{P_0 - e(T)} \quad [\text{cm}^3\text{STP/g}] \quad (2.15)$$

The total pressure P can be determined by using the barometric equation, in which P is related to the altitude H of the water surface.

$$P = P_s \exp\left(H \big/ H_0\right) \quad [\text{atm}] \quad (2.16)$$

where P_s is the pressure at sea level and H_0 is the typical scale height for a given meteorological situation. If the regional altitude-pressure function is not known, the constant values P_s = 1 atm and H_0 = 8300 m were used to determine P by equation (2.16).

2.3 Excess air

The concentrations of gases in ground water are often increased by the presence of excess air. Excess air occurs when air bubbles are trapped by fluctuations of the water table or during rapid recharge. These bubbles dissolve partially or entirely when the hydrostatic pressure increases (Heaton and Vogel, 1981; Andrews, 1991; Stute and Schlosser, 2000; Kipfer et al., 2002). Bubbles with diameter smaller than 1μm collapse under their surface tension and will inject all their gases in the water phase.

Assuming that excess air has the same composition as atmospheric air, the excess concentration of the noble gas i can be described by

$$C_i^{exc} = A \cdot z_i \quad [\text{cm}^3\text{STP/g}] \quad (2.17)$$

where A is the volume of dry air per gram of water and z_i is the volume fraction of the noble gas i in dry air. Because of their low solubility, the light noble gases (He, Ne) are more sensitive to excess air than the heavy noble gases. As their dissolved concentrations are small, addition of air creates comparatively large relative excesses of He and Ne. He excesses may also be due to radiogenic He, whereas Ne is of purely atmospheric origin. Therefore, it is useful to express the concentration of excess air as a relative Ne-excess (e.g., Stute and Schlosser, 2000):

$$\Delta Ne = \left(\frac{Ne_{mes} - Ne_{eq}}{Ne_{eq}} \right) \cdot 100 = \frac{Ne_{exc}}{Ne_{eq}} \cdot 100\% \,. \quad (2.18)$$

where Ne_{mes} is the measured Ne concentration, Ne_{exc} is the neon excess concentration and Ne_{eq} is the neon equilibrium concentration. Typical excess air in groundwater is about 10-100 % ΔNe.

The factors that control the excess air concentration in groundwater are not well understood. The first systematic investigation on the influence of lithology, precipitation rate and pore size on the concentration of excess air in groundwater was presented by Wilson and McNeill (1997). They studied the relationship between lithology and air entrainment by comparison of the mean and standard deviation of excess Ne contents for limestone, sandstone and granite-hosted groundwaters, respectively. The highest amounts of excess air were observed with limestone, less for sandstone and least for granite. The relative differences in air entrainment between the groundwater systems support a lithological control, such as porosity and morphology and are consistent with high quantities of excess air reported for limestones or karstic aquifers elsewhere (Herzberg and Mazor, 1979). On a microscopic scale, capillary forces within the unsaturated zone will be highest for the smaller pores and this may favor the entrapment of air bubbles (Heaton and Vogel, 1981). On the macroscopic scale however, the localized highly permeable fissured nature of most limestone aquifers are often associated with very rapid recharge which could entrap in large aliquots of air (Herzberg and Mazor, 1979).

With respect to the correlation between excess air and precipitation, the results of Wilson and McNeill (1997) are not conclusive, as a positive overall correlation was found, but a negative correlation was inferred if only data from sites of similar lithology were compared. A negative correlation can be explained if the recharge process in the unsaturated zone proceeds by the alternate admission at a constant rate of air and air-saturated water to the flow channels of the rock. Mean annual precipitation will then influence the amount of air entrainment because proportionately more air would be entrained when or where precipitation is lowest, and vice versa. The positive correlation may be explained by increased air entrainment during strong and rapid recharge. Such a correlation had been observed before in semi-arid regions, where in the past the recharge process had taken place under wetter conditions than today (Herzberg and Mazor, 1979). .

A positive correlation between excess air concentration and precipitation or recharge has later been assumed and confirmed by several studies. Stute and Talma (1998) interpreted a peak in excess air found in a groundwater record from Namibia as due to the water table rise at the onset of a wetter period. Aeschbach-Hertig et al. (2002) reported consistently high excess air concentrations in paleowaters from aquifers in semi-arid regions of Brazil, Niger, and Australia, and hypothesized that they might indicate higher precipitation in the past. Beyerle et al. (2003) found a correlation of excess Ne and stable isotopes in Niger, which indicated higher excess air formation during past wet periods. Kulongoski et al. (2004) studied groundwater from a sandstone aquifer located at ~1 km altitude in the Kalahari desert of central Botswana. They observed that the excess air component varied from 27 to 170 % ΔNe in the study area, and that the average excess-air content of post-LGM groundwaters

(ΔNe_{mean} = 117 ± 60 %) was higher than the average excess-air content of older (> 24 ka) groundwaters (ΔNe_{mean} = 83 ± 29%). They used the assumption of Beyerle et al. (2003) that periods of higher humidity may result in the entrainment of larger amounts of excess air in groundwater.

The assumption that excess air is formed simply by complete dissolution of small air bubbles trapped in soil pores is not generally applicable. Part of the excess air formed in this way may be lost by diffusive re-equilibration across the water table. The rate of this process depends on gas diffusion coefficients, temperature and matrix properties. The diffusive re-equilibration leads to a systematic elemental fractionation of the residual excess air. A similar fractionation occurs in the case of partial dissolution of air bubbles because the heavier gases are dissolved preferentially. The mentioned processes are the basis of two different models that were introduced to explain the formation of excess air in groundwater and the observed fractionation of the elemental composition of excess air relative to atmospheric air.

The first model (PR: Partial re-equilibration) was introduced by Stute et al. (1995), who postulated that entrapped air bubbles are initially completely dissolved, but later a part of the resulting excess is lost by molecular diffusion. The process of partial re-equilibration leads to a fractionation of the excess air component relative to atmospheric air in which the heavier noble gases are enriched relative to the light ones. The degree of re-equilibration can be characterized by introducing a new parameter which describes the remaining fraction of the initial Ne excess:

$$\frac{C_i^{exc}}{C_i^{exc}(0)} = \left[\frac{C_{Ne}^{exc}}{C_{Ne}^{exc}(0)}\right]^{\frac{D_i}{D_{Ne}}} \tag{2.19}$$

Where C_i^{exc} is the remaining excess of gas i after partial re-equilibration, $C_i^{exc}(0)$ is the initial excess and D_i is the molecular diffusion coefficient. Values for D_i (Table 2.3) were presented by Jähne et al. (1987) except for Ar.

The degassing term can be written in a way which refers to the underlying physical process by defining the re-equilibration parameter $R = -\ln(C_{Ne}^{exc} / C_{Ne}^{exc}(0))$ (Aeschbach-Hertig et al., 1999):

$$C_i^{exc} = C_i^{exc}(0) \cdot e^{-R(\frac{D_i}{D_{Ne}})} \tag{2.20}$$

Because the molecular diffusivity decreases with the mass of the isotopes, the PR-model predicts that the depletion of the initially unfractionated excess air is largest for the light noble gases, whereas the heavy gases are enriched relative to air in the remaining excess. In particular it is difficult to verify this prediction for helium isotopes because of the presence of a non-atmospheric helium component.

T (^oC)	D_{He} (10^{-5} cm^2/s)	D_{Ne} (10^{-5} cm^2/s)	D_{Ar} (10^{-5} cm^2/s)	D_{Kr} (10^{-5} cm^2/s)	D_{Xe} (10^{-5} cm^2/s)
5	5.1	2.61	1.63	1.02	0.774
10	5.74	2.94	1.87	1.2	0.929
15	6.3	3.28	2.13	1.41	1.12
20	7.22	4.16	2.69	1.84	1.47
25	8.48	4.82	3.29	2.4	1.94

Table 2.3: Molecular diffusivity of noble gases at different temperatures (Jähne et al., 1987; Stute, 1989). The diffusion coefficient for Ar was interpolated from the diffusion coefficients of the other noble gases assuming that D is inversely proportional to the square root of the atomic mass (Beyerle, 1999).

The second model (CE: Closed system equilibration) has been introduced by Aeschbach-Hertig et al. (2000). This model postulates that the entrapped air dissolves only partially and a new solubility equilibrium is attained in a closed system consisting initially of air saturated water and a finite volume of entrapped air under elevated total pressure. This model is described by the following equation (Aeschbach-Hertig et al., 2000):

$$C_i^{exc} = \frac{(1-F)Az_i}{1+FA\frac{z_i}{C_i^{eq}}} \tag{2.21}$$

where A is the initial STP-volume of entrapped air per unit mass of water (which is approximately equal to the initial volume ratio between entrapped air and water), and F is the model parameter describing the reduction of the gas volume by partial dissolution and compression.

The mentioned excess air models, in particular the CE-model will be discussed in more detail in chapter 3. The conceptual ideas of the models and the difference between them are summarized in Figure 2.2.

The CE-model in combination with data on the amount of entrapped air in soils provides a new view on the relationship of the excess air concentration and precipitation (Aeschbach-Hertig et al., 2002). It shows that usually the concentration of dissolved excess air is not limited by the amount of initially entrapped air, but by the available hydrostatic pressure that forces the gas into solution. The observed increase of ΔNe in periods of higher humidity in aquifers from semi-arid regions is thus not constrained by the availability of entrapped air, but is strongly correlated to the over-pressure acting on the entrapped air during recharge. The hydrostatic pressure increases due to the fluctuations in water table due to intensive but intermittent rainfalls (Heaton and Vogel, 1981). High ΔNe values therefore seem to indicate periods of strong but seasonal recharge in semi-arid regions.

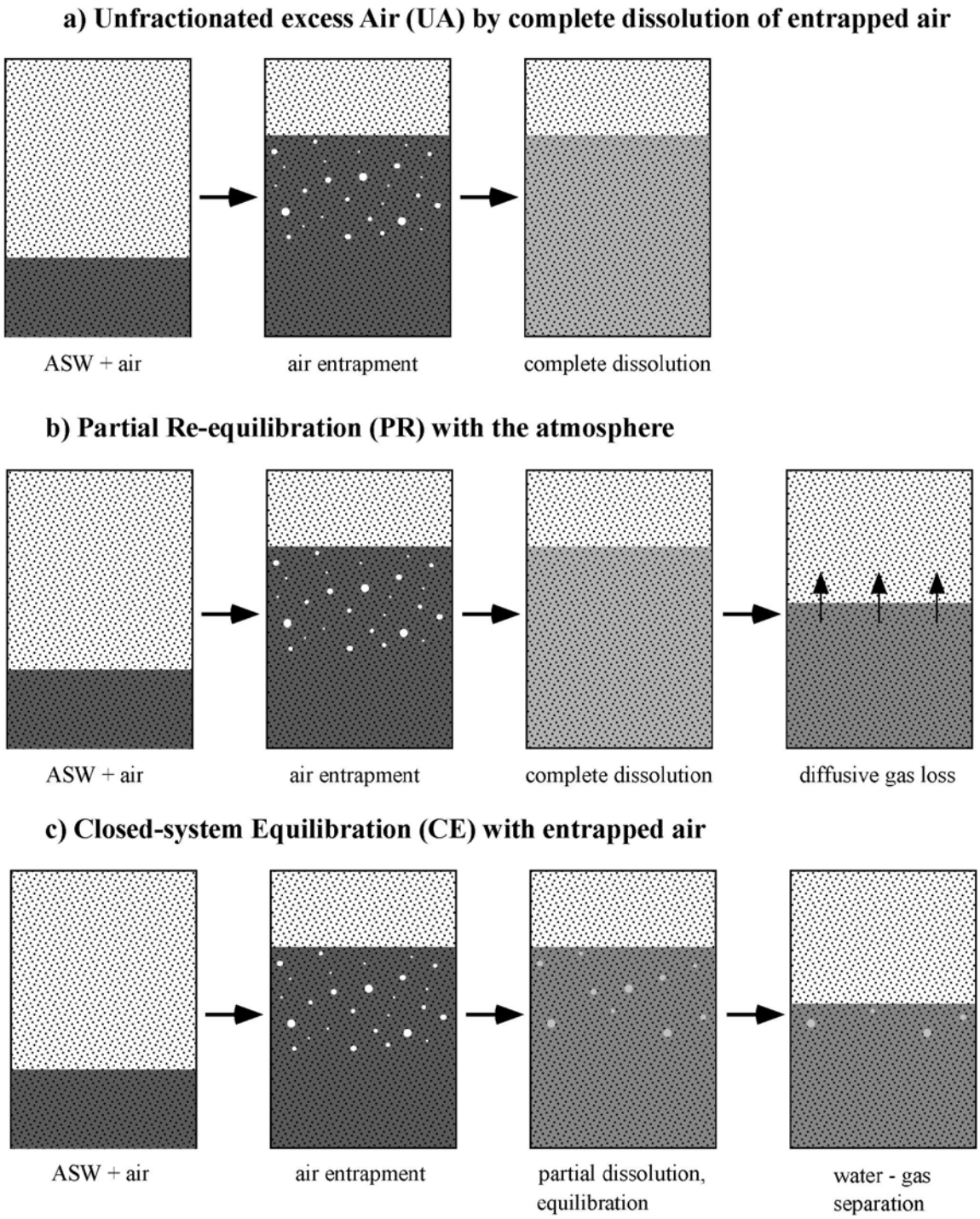

Figure 2.2: Schematic representation of the different model concepts for the formation of excess air (a) unfractionated excess air (UA) by complete dissolution of entrapped air, (b) Partial re-equilibration (PR) with atmosphere, (c) closed system equilibration (CE) with entrapped air (Kipfer et al., 2002)

2.4 Calculation of noble gas temperature and excess air

The concentrations of all gases in groundwater depend on atmospheric partial pressures and temperature. The equilibration temperature at the base of the unsaturated zone during recharge must be known to date groundwater with environmental tracers. In areas with thick unsaturated zones the recharge temperature is very close to the mean annual soil temperature and usually similar to the mean annual air temperature (Mazor, 1972; Herzberg and Mazor, 1979; Andrews and Lee, 1979; Heaton and Vogel, 1981; Stute and Schlosser, 1993). The recharge temperature can be different from the mean annual temperatures where the unsaturated zone is thin and the temperature just above the water table responds to the seasonal variations in the air temperature (Matthess, 1982).

The recharge temperature is not the mean air temperature during the rainy season or the temperature of the shallow groundwater (Stute and Schlosser, 1993). The main reason for this is that seasonal temperature variations are strongly damped in the soil at the depth where the final equilibration of the water with soil air takes place. The concentrations of noble gases and N_2 in oxic waters are excellent indicators of the recharge temperature (Heaton, 1981; Heaton and Vogel, 1981; Stute and Schlosser, 1993; Aeschbach- Hertig et al., 1999).

The atmospheric noble gas component is determined by the conditions prevailing at the last gas exchange with the atmosphere, such as water temperature and salinity, atmospheric pressure, and excess air. Usually it is possible to find reasonable values for the salinity and the atmospheric pressure. Therefore the amount of excess air and the temperature at recharge can be deduced from the atmospheric noble gas concentrations, provided a quantitative understanding of how the concentrations depend on the mentioned environmental conditions.

In the previous sections, an equation for the noble gas concentrations in solubility equilibrium (eq. 2.14) as well as two different model equations for the excess air component (eqs. 2.20 and 2.21) have been discussed. Together, this provides two complete models for atmospheric noble gases in water, given by

$$C_i(T,S,P,A,F) = C_i^{eq}(T,S,P) + Az_i \cdot e^{-F(D_i/D_{Ne})} \qquad (2.22a)$$

or

$$C_i(T,S,P,A,F) = C_i^{eq}(T,S,P) + \frac{(1-F)Az_i}{1+AF\dfrac{z_i}{C_i^{eq}}} \qquad (2.22b)$$

where C_i^{eq} is the equilibrium concentration of the noble gas i (i= Ne, Ar, Kr, Xe) as a function of the ambient temperature T, the salinity S and the pressure P (eq. 2.14), z_i is the volume fraction of gas i in dry air (Table 2.1), D_i is the molecular diffusion coefficient of the noble gas i (Table 2.3), and F is the fractionation parameter (which

is either the re-equilibration parameter R of the PR-model (eq. 2.20, 2.22a) or the partial dissolution parameter F of the CE-model (eq. 2.21, 2.22b). In addition to noble gases derived from atmospheric origin, some noble gas isotopes can originate from other sources as discussed before (section 2.1). Therefore, the equations (2.22) can be applied for He only if the presence of non-atmospheric He components can be excluded. Otherwise, the difference between the measured He concentration and the result of (2.22) evaluated for He yields the best estimate of the non-atmospheric He component (Aeschbach-Hertig et al., 1999). The equations (2.22) represent non-linear systems with five unknown parameters (T: temperature, S: salinity, P: pressure, A: amount of excess air, F: fractionation parameter) and one equation for each of the four or five applicable noble gases. It is advisable to look for a parameter combination that provides model predictions which agree with the measured data within the experimental error. The non- linear systems of equation (2.22) are over determined and can be solved, if some parameters are either known or prescribed: such that the number of free parameters becomes smaller than the number of applicable measured gases. As mentioned above, this can often be done for salinity S and pressure P, so that only three free parameters remain (T, A, and F). It should be mentioned that under the assumption of F = 0 (no fractionation), both model equations coincide and describe the simple case of total dissolution of the entrapped air to form unfractionated (purely atmospheric) excess air. In this special case, the number of free parameters is reduced to two.

In the following the method described by Aeschbach-Hertig et al. (1999) to solve the equation systems (2.22) for any subset of up to three of the five model parameters is outlined. The parameters are determined such that the sum of the weighted squared deviations between the modeled and measured concentrations is minimized. The goal function to be minimized is:

$$\chi^2 = \sum_i \frac{(C_i - C_i^{\mathrm{mod}})^2}{\sigma_i^2} \qquad (2.23)$$

where C_i^{mod} are the modeled concentrations, C_i are the measured concentrations, and σ_i are the experimental 1σ errors. The search for the minimum of the goal function in the parameter space is performed using standard numerical techniques in a special MATLAB-based software package called "NOBLEGAS" (Aeschbach-Hertig et al., 1999; Peeters et al., 2003).

This inverse approach to derive environmental parameters from noble gas concentrations in water is quite different from the traditional approach that was introduced by Stute (1989). The traditional approach looks for parameter values of A and F (P and S are prescribed) such that the spread of the temperatures calculated individually from Ne, Ar, Kr, and Xe is minimized, this means that temperature was used as a fit target. The temperature for each noble gas is calculated from the concentration after it has been corrected for excess air. This process is iteratively repeated with varying amounts of excess air (and if applicable various values of F) until optimum agreement between the four temperatures is reached. The noble gas

temperature is taken as the mean, its error as the standard deviation of the individual temperatures.

The inverse approach has a number of advantages compared to the traditional method which are summarized in the following:

- The inverse approach treats all physical parameters in the same way rather than focusing on temperature alone.
- The contribution of each noble gas to the goal function is weighted with the individual experimental errors. In the traditional approach, the experimental errors are not considered, and the temperature derived from each noble gas species has equal weight.
- The experimental errors can be used to judge the quality of the fit.
- The confidence intervals for the derived parameters can be calculated and the correlation between the parameters can be studied.

2.5 Dating groundwater with the ^{3}H-^{3}He method

The age of groundwater has a very important implication for water resources management; but the term age of groundwater can be a misleading term because of two reasons (Clark and Fritz, 1997):

Only tritium is part of the water molecule and can actually "date" the water. All other dating methods rely on dissolved constituents whose abundance in water is controlled by physicochemical and biological processes.

Hydrodynamic mixing and convergence of groundwater flow paths integrate a variety of recharge origins and ages. Only in well–defined and usually regional artesian aquifers age gradients along the flow path will be preserved. Because of these two reasons one should not talk about the age of groundwater but about "the groundwater mean residence time".

Assuming closed system behavior, the tritium concentration of a water parcel decreases by radioactive decay, according to

$$^3H(t) = {}^3H(t_0) \cdot e^{-\lambda(t-t_0)} \tag{2.24}$$

where ^{3}H(t) is the tritium concentration at time t, ^{3}H(t_0) is the initial tritium concentration and λ is the decay constant of tritium. As soon as the parcel is isolated from the atmosphere, the ^{3}He concentration increases as the ^{3}H concentration decreases (see Figure 2.3), according to

$$^3He_{tri}(t) = {}^3H(t) \cdot (e^{\lambda(t-t_0)} - 1) \tag{2.25}$$

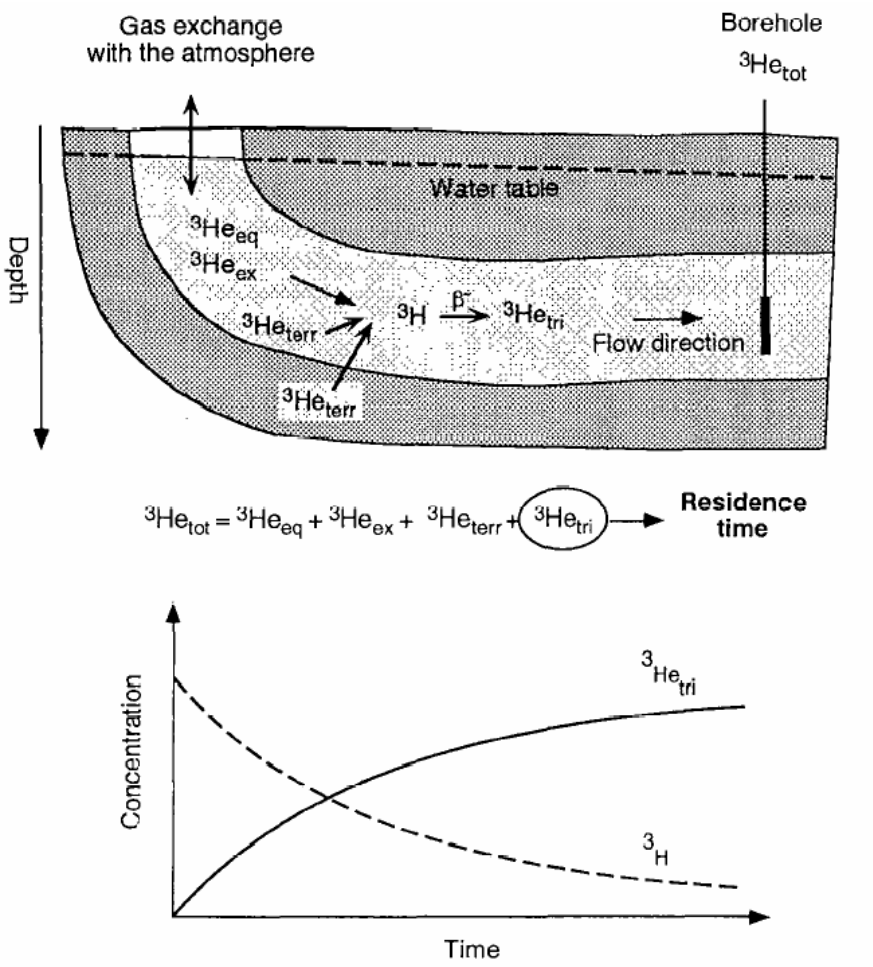

Figure 2.3: With increasing residence time of the water the ^3H concentration decreases whereas the $^3He_{tri}$ concentration increases. If the tritiogenic ^3He component ($^3He_{tri}$) can be determined from the measured ^3He concentration by correcting for the different non-tritiogenic ^3He components ($^3He_{eq}$: equilibrium, $^3He_{exc}$: excess air, and $^3He_{terr}$: terrigenic ^3He component), the so-called ^3H-^3He age can be calculated according to Eq (2.26) (Beyerle, 1999)

where $^3He_{tri}(t)$ in this case is the tritiogenic ^3He concentration at time t. From equation (2.25) one can deduce equation (2.26), which can be used to calculate the ^3H-^3He age $\tau = t - t_0$ of the groundwater. Determination of the age requires measurement of the concentrations of tritium and $^3He_{tri}$ (Tolstikhin, 1969):

$$\tau = \frac{1}{\lambda} \ln\left(1 + \frac{^3He_{tri}}{^3H}\right) \tag{2.26}$$

where ^3H and $^3He_{tri}$ are the tritium and tritiogenic ^3He concentrations of the water sample at the time t of sampling expressed in equal units, e.g. TU.

Note that the ^3H-^3He age defined in equation (2.26) is independent of the initial ^3H concentration $^3H(t_0)$ of the water parcel. This is the major advantage of the method because it circumvents problems due to the input of ^3H to a water system which is usually only vaguely known. It has to be further noted that the ^3H-^3He water age is an apparent age and can only be taken as the true age of the water if ^3He sources other

than ^{3}H decay can be corrected for, and if mixing of waters with different ^{3}H and ^{3}He concentrations can be excluded or can be quantified (Beyerle, 1999). The origin of the different ^{3}He components with regard to the ^{3}H-^{3}He dating method is outlined in Figure 2.3

The most difficult step in this method is the separation of $^3He_{tri}$ from the total ^{3}He ($^3He_{tot}$) dissolved in a groundwater sample. This can be achieved by analyses of the He and Ne concentration. The Ne concentration is used to estimate the atmospheric He components in order to calculate the non-atmospheric He components. This approach is based on the fact that Ne usually has only two components (equilibrium and excess air), whereas ^{4}He has one additional component (terrigenic), and ^{3}He has two non-atmospheric components (terrigenic and tritiogenic). The ^{3}He, ^{4}He and Ne composition can be represented by Figure 2.4.

The tritiogenic He ($^3He_{tri}$) of a groundwater sample can be calculated as the difference of the total measured ^{3}He ($^3He_{tot}$) and all other non-tritiogenic ^{3}He components (e.g., Schlosser, 1992):

$$^3He_{tri} = {}^3He_{tot} - {}^3He_{eq} - {}^3He_{exc} - {}^3He_{terr} \qquad (2.27)$$

The equilibrium concentration $^3He_{eq}$ is a function of water temperature, salinity and the atmospheric pressure prevailing during recharge. The NGT is considered as the best estimate of the recharge temperature. In cases where only He and Ne isotopes were analyzed, the in situ water temperature of the sample or the mean annual temperature of the recharge area can be taken to estimate the recharge temperature. The pressure can be calculated using the barometric equation. The salinity is considered to be zero at the time of recharge.

The excess air component $^3He_{exc}$ can be calculated by multiplying the excess air parameter A obtained from a model fit to the atmospheric noble gases by the volume fraction of ^{3}He in dry air if the excess air is not fractionated. In this case, the Ne concentration is normally a good enough measure to derive the atmospheric excess of ^{3}He:

$$^3He_{exc} = (^3He/Ne)_{air} \cdot (Ne_{tot} - Ne_{eq}) \qquad (2.28)$$

Caution has to be taken when excess air fractionation significantly influences the noble gas concentrations. If fractionation is not considered, the calculated $^3He_{exc}$ would overestimate the true excess, resulting in too small $^3He_{tri}$ and ^{3}H-^{3}He age.

The terrigenic component ($^3He_{terr} = {}^3He_{crust} + {}^3He_{mantle}$) may be present in aquifers where the rocks are enriched in U or Th, or in groundwater samples in which young water has mixed with relatively old water containing terrigenic, and in some cases, mantle He. In these cases, the Ne concentration must be measured and can be used to calculate the additional $^3He_{terr}$ (Bayer et. al, 1989).

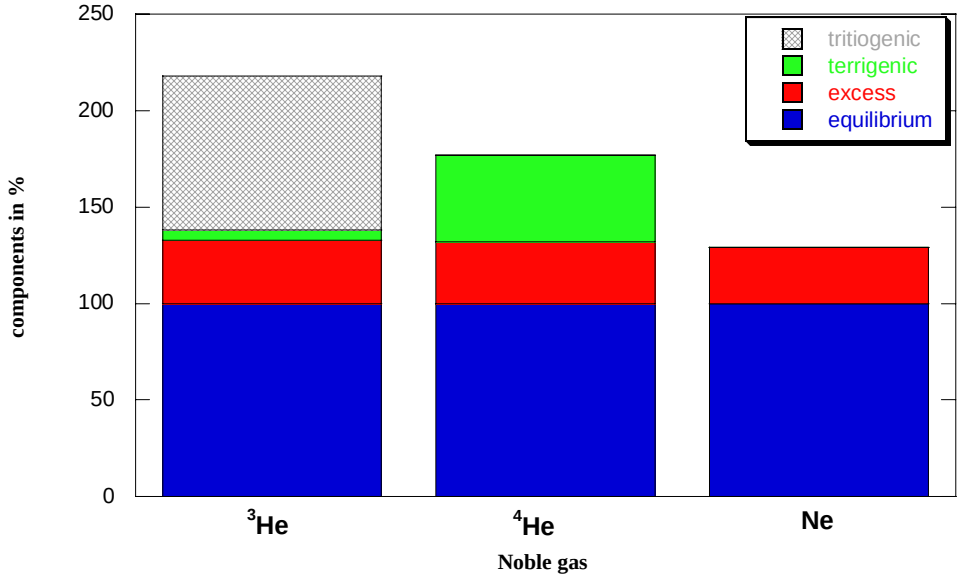

Figure 2.4: Example of the ^{3}He, ^{4}He and Ne components of a typical groundwater sample normalized to solubility equilibrium

$$^4He_{terr} = {}^4He_{tot} - (Ne_{tot} - Ne_{eq}) \cdot (^4He/Ne)_{atm} - {}^4He_{eq} \qquad (2.29a)$$

This equation can also be written in the form

$$^4He_{terr} = {}^4He_{tot} - L_{exc} \cdot Ne_{exc} - {}^4He_{eq} \qquad (2.29b)$$

where $^4He_{terr}$ is the terrigenic ^{4}He concentration, Ne_{tot} is the measured neon concentration, Ne_{eq} is the neon concentration in water in equilibrium with air, $(^4He/Ne)_{atm}$ is the atmospheric ratio (0.288), and L_{exc} is the elemental composition of the excess air (L_{exc}= $(He/Ne)_{exc}$), which is usually assumed to be atmospheric. If the excess air is fractionated, L_{exc} is always lower than L_{air} (L_{air}= $(^4He/Ne)_{atm}$ = 0.288). If the radiogenic ^{4}He is small and no ^{3}He from the mantle is present, the contribution of the $^3He_{terr}$ component to the measured ^{3}He is small or even negligible.

If there is no $^3He_{terr}$ in the sample, the concentration of $^3He_{tri}$ can be calculated by (Schlosser et al., 1989)

$$^3He_{tri} = {}^4He_{tot} \cdot (R_{tot} - R_a) + {}^4He_{eq} \cdot R_a (1-\alpha) \qquad (2.30)$$

where$^3He_{tri}$ is the tritiogenic ^{3}He, $^4He_{tot}$ is the measured ^{4}He content of the sample, $^4He_{eq}$ is the ^{4}He content of air equilibrated water at the recharge temperature, R_{tot} is the measured ^{3}He/^{4}He ratio of the sample, R_a, is the ^{3}He/^{4}He ratio of atmospheric air, which equals $1.384 \cdot 10^{-6}$, and α is the equilibrium isotope fractionation factor which equals 0.983 (Benson and Krause, 1980). If the water sample contains $^3He_{terr}$, the tritiogenic He can be calculated by the following equation (Schlosser et al., 1989)

$$
\begin{aligned}
{}^3He_{tri} &= {}^4He_{tot} \cdot R_{tot} - ({}^4He_{tot} - {}^4He_{terr}) \cdot R_a \\
&+ {}^4He_{eq} \cdot R_a (1-\alpha) - {}^4He_{terr} \cdot R_{terr}
\end{aligned}
\tag{2.31}
$$

where R_{terr} is the $^3He/^4He$ ratio of the terrigenic He source. R_{terr} can be determined from isotope measurements of tritium-free water in the aquifer under investigation, in our work we assume that R_{terr} is equal to the characteristic value $2 \cdot 10^{-8}$ (Mamyrin and Tolstikhin, 1984). If the $^3He_{tri}$ is confined in the aquifer, the apparent ^3H-^3He age of the water can be calculated from Eq. (2.26).

Chapter 3

3 Models to describe excess air and degassing in groundwater

Noble gases have several applications in groundwater studies, such as groundwater dating and paleoclimate assessment by measurement of the recharge temperature. These applications mainly depend on the concentrations of noble gases in groundwater samples, which usually are above solubility equilibrium as a result of excess air formation (section 2.3). However, some groundwater samples show gas undersaturation, rather than the usual excesses over solubility equilibrium. Of course this problem is a big challenge for the application of noble gases. In this chapter we will try to find a solution of this problem, by using models similar to or even equal to the excess air models as potential tools to describe the result of degassing in groundwater. To this end, we will first have a closer look at the excess air models, their derivation and the physical interpretation of their parameters. We will show how these models can be adapted to describe degassing. Finally the applicability of the presented models will be tested with some data sets from aquifers where degassing has been observed.

The models use two parameters to describe the excess air and its possible fractionation relative to atmospheric air. For simplicity, we will denote these parameters always as A and F, although their meaning is slightly different in the different models. Furthermore, the atmospheric pressure needed to define the atmospheric equilibrium concentrations is always denoted as P.

3.1 Unfractionated excess air model

The most straightforward explanation of the phenomenon of gas excesses above atmospheric equilibrium in groundwater is complete dissolution of small air bubbles trapped in soil pores (Heaton and Vogel, 1979, 1981). This traditional – but experimentally never directly verified – concept implies that the excess has the same composition as the entrapped gas, which is assumed to be atmospheric air, hence the name ‘excess air’. Because the composition of air is given by the constant and well-known volume fractions z_i of the individual noble gases, the model assuming unfractionated atmospheric excess air (UA-model) needs only one parameter to describe the excess air component, namely the amount of trapped and completely dissolved air per mass of water (A). The concentration C_i of the dissolved noble gas i can be written as (compare eq. 2.17):

$$C_i(T,S,P,A) = C_i^{eq}(T,S,P) + A \cdot z_i \qquad (3.1)$$

where C_i^{eq} (T,S,P) are the moist air solubility equilibrium concentrations as functions of temperature, salinity, and atmospheric pressure (see section 2.2), A is the concentration of totally dissolved dry air, and z_i are the noble gas volume fractions in dry air.

Formally, the UA-model with negative A would describe a situation with gas loss relative to equilibrium, however there is no physical reason that the lost gas should have atmospheric composition. This model is not discussed here further because it appears unsuitable to describe degassing and also because it is included as a special case in the more advanced models.

3.2 Partial re-equilibration and diffusive degassing models

The observation of a fractionation of the elemental composition of excess air with respect to atmospheric air led to propose a model involving complete dissolution of entrapped air followed by partial re-equilibration (PR) with the atmosphere (Stute et al., 1995). This PR-model results in diffusivity-controlled fractionation of the excess air and the concentrations C_i of the dissolved gases i are described by (compare eq. 2.22a):

$$C_i(T,S,P,A,F) = C_i^{eq}(T,S,P) + A \cdot z_i \cdot e^{-FD_i/D_{Ne}} \qquad (3.2)$$

where F is a new parameter describing the degree of re-equilibration, and D_i are the molecular diffusion coefficients (Table 2.3). For F = 0 the PR-model reduces to the UA-model.

Degassing may occur when high concentrations of dissolved gases (e.g., CH_4 or CO_2) in the groundwater force the formation of gas bubbles upon pressure release during sampling (Andrews, 1985). Dissolved atmospheric noble gases would then be transferred into the initially noble gas free gas phase, and if the water phase is preferentially sampled, a deficit of dissolved noble gases would be observed. Since only a short time is available for the degassing into bubbles formed during sampling, a non-equilibrium kinetic description of the gas exchange may be appropriate. In such a case, the extent of degassing is expected to be controlled by the diffusivities of the individual gases, as proposed by Stute (1989) and applied by Lippmann et al. (2003).

Diffusive degassing (DD) into an initially noble gas free gas phase can be described by a small modification of the PR-model equations (DD-model):

$$C_i(T,S,P,A,F) = \left(C_i^{eq}(T,S,P) + Az_i\right) \cdot e^{-FD_i/D_{Ne}} \qquad (3.3)$$

In contrast to the equation (3.2), the exponential degassing factor acts here on the total noble gas concentration (C_i^{eq} + Az_i) rather than only on the excess air term (Az_i). A further difference is that the temperature during degassing at the time of sampling may differ from that during equilibration at the time of infiltration, which is described

by the parameter T. Thus, whereas in applications of the PR-model the diffusion coefficients D_i are calculated using the parameter T, in the DD-model the sampling temperature should be prescribed and used to calculate the D_i (compare Lippmann et al., 2003).

Equation (3.3) is often used in a simplified form without the term Az_i (e.g. Lippmann et al., 2003). This corresponds to the assumption that before degassing, the water had been in atmospheric equilibrium. Since groundwater usually contains excess air, this simplification may not be appropriate. Even as it stands, eq. (3.3) is an approximation, because the possibility of initial fractionation of excess air (according to eq 3.2 or the CE-model described below) is not considered. Inclusion of such a fractionation would be difficult, because the large number of free and likely correlated parameters would render a solution of the equations problematic.

Because the diffusion coefficients of the light noble gases (in particular He) are larger than those of the heavier noble gases, the PR-model predicts a fractionation of the excess air component relative to atmospheric air, with a preferential loss of the light gases and consequently an enrichment of the heavier gases in the remaining excess. Similarly, the DD-model predicts a stronger degassing for the light noble gases, as it is usually observed. The conceptual ideas behind the PR- and DD-models and their effects on dissolved noble gas concentrations are shown in Figure 3.1.

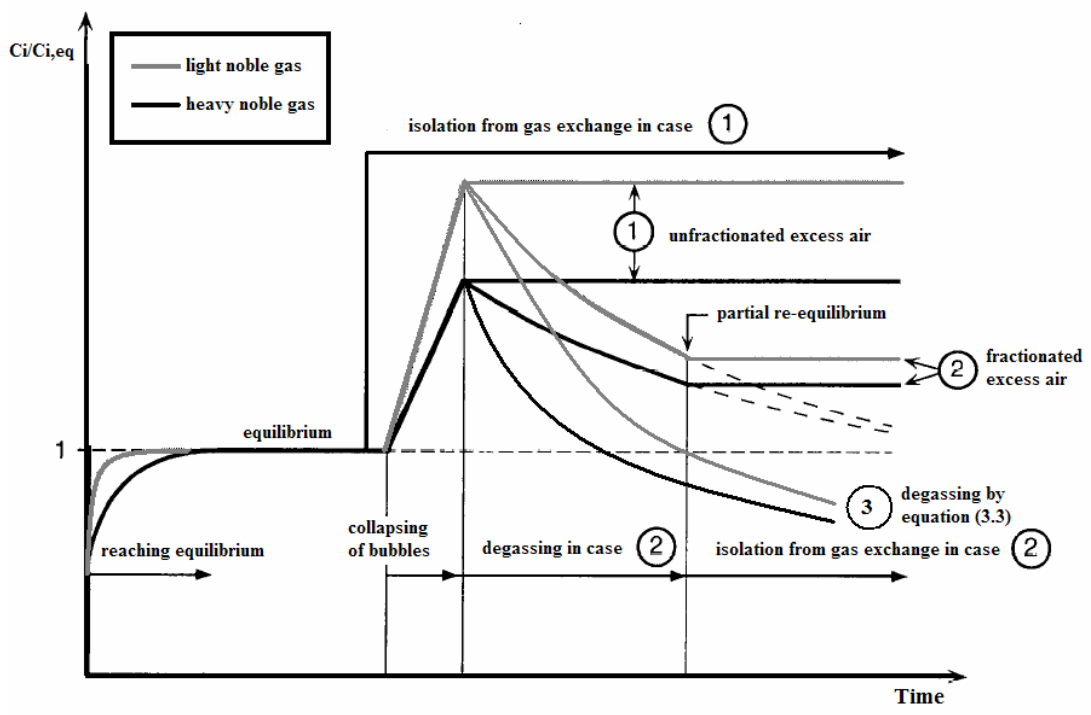

Figure 3.1: Formation of unfractionated and fractionated excess air plotted for light and heavy noble gas species. Case 1: The isolation from gas exchange happens before the complete dissolution of air bubbles. The result is an unfractionated excess air component (UA-model). Case 2: The isolation from gas exchange happens after the complete dissolution of air bubbles. In the mean time the supersaturated water starts to degas. The result is a fractionated excess air component (PR-model). Case 3: degassing according to equation 3.3, i.e. groundwater with unfractionated excess air degasses into a noble gas free gas phase (DD-model) (modified from Beyerle, 1999).

3.3 Closed-system equilibration model

The closed-system equilibration (CE) model provides an alternative description of the concentrations of dissolved atmospheric noble gases in groundwater. It has been developed by Aeschbach-Hertig et al. (2000) to account for the phenomenon of excess air, both fractionated and unfractionated relative to atmospheric air. The basic assumption of the model is that a finite volume of initially air saturated water attains solubility equilibrium with a finite volume of gas (bubbles), which initially contained atmospheric air. The conceptual idea is that soil air is trapped in small pockets in the pore space during a rise of the water table, and subsequently (partially) dissolved in the water under a certain hydrostatic pressure. After having reached solubility equilibrium with the gas phase, the water eventually flows through the aquifer to the point of sampling, whereas the gas bubbles remain trapped in their pores. However, during fluctuations of the water table, the gas phase is periodically replaced by soil air, which is assumed to be identical to atmospheric air in its composition (at least for noble gases).

The CE-model with the mentioned assumptions provides a description of the formation of excess air that has proved to be very useful and appropriate to describe observed noble gas concentrations in many groundwaters. We will show in the following that the same mathematical model with a more general conceptual interpretation can also be used to describe gas concentrations in degassed groundwaters. We will first derive a general form of the CE-model equation in order to clearly work out its possible physical interpretations. Next we introduce the additional assumptions that lead us to the form of the model equation that has been presented in the literature. We will finally propose a slightly modified equation and discuss its interpretation as a description for both excess air and degassing.

3.3.1 General derivation of the CE-model equation

We consider a closed, finite system of a water and a gas phase, which develops from a prescribed initial state into a final state of equilibrium. We want to calculate the noble gas concentrations in the water phase in the final state, as functions of the initial concentrations and the physical conditions in the two states. Of these conditions, pressure plays a central role. We define the initial state to be at atmospheric pressure P, which is different from the original derivation of Aeschbach-Hertig et al. (2000), and will have some subtle consequences on the definition of the model parameters. The pressure in the final state is the total pressure in the system with trapped bubbles, denoted as P_{tot}. This pressure is assumed to be the same in the water and the gas phase and only composed of atmospheric and hydrostatic pressure. Capillary pressure effects are neglected, although they certainly play a role in the process of gas bubble dissolution and collapse (Holocher et al., 2003). It is assumed that in the final state the gas phase is concentrated in relatively large bubbles, where capillary pressure is small. As a result, the actual spatial distribution of the two phases is irrelevant for the simplified description of the CE-model, only the total volume ratios play a role.

The water volume V_w remains constant (actually the water mass m_w, but the minor effects of temperature, pressure, and dissolved species on V_w can be ignored), whereas the gas volume can change from an initial value of V_g^* to V_g in the final state (quantities referring to the initial state are labeled with a star, those in the final state have no star). The change in the gas volume is due to changes in the total pressure (from $P^* = P$ to P_{tot}) and to changes in the total gas amount (from N^* to N) because of transformation of reactive gases or of redistribution of the gases between the two phases.

There are two essential assumptions that define the problem. The first is that the system is closed, the second that solubility equilibrium between the two phases is reached in the final state. The assumption of a closed system does not necessarily mean that the mass of all gas species is conserved, as some may undergo (bio-geochemical) transformations (e.g., O_2 consumption, production of CO_2 or CH_4). For the non-reactive noble gases, however, the total mass or number of moles is conserved. The condition of mass conservation can be written as:

$$n_{i,w}^* + n_{i,g}^* = n_{i,w} + n_{i,g} \tag{3.4}$$

where the left hand side describes the number of moles of gas i in the water and gas phase, respectively, in the initial state, and the right hand side describes the same quantities in the final state. The gas concentrations in the final state are related by the second assumption of solubility equilibrium. We can use this condition (i.e., Henry's law) to express the right hand side of equation (3.4) in terms of dissolved gas concentrations, which is the quantity we want to calculate. This is most easily done if we express Henry's law with molar concentrations (mol/L) in both phases, as in equation (2.5):

$$C_{i,g} = H_i\left(T,S\right)\cdot C_{i,w} \tag{3.5}$$

where $H_i(T,S)$ is the so-called dimensionless Henry's law constant which depends on temperature and salinity, whereas $C_{i,g} = n_{i,g}/V_g$ and $C_{i,w} = n_{i,w}/V_w$ are the molar concentrations of gas i in the gas and water phase, respectively. Rewriting the mass balance equation (3.4) in terms of concentrations and using equation (3.5) for the final state one obtains:

$$C_{i,w}^* V_w + C_{i,g}^* V_g^* = C_{i,w}\left(V_w + H_i V_g\right) \tag{3.6}$$

Dividing both sides of equation (3.6) by V_w and solving for $C_{i,w}$ yields:

$$C_{i,w} = \frac{C_{i,w}^* + C_{i,g}^* \dfrac{V_g^*}{V_w}}{1 + H_i\left(T,S\right)\dfrac{V_g}{V_w}} \tag{3.7}$$

This is, in essence, the most general form of the CE-model equation, giving the final dissolved gas concentrations as functions of the initial concentrations in the two phases, the gas/water volume ratios in both states, and the equilibrium conditions (temperature and salinity) in the final state. The original CE-model contains two additional assumptions that define the concentrations in the initial state: i) the initial gas volume V_g^* contains atmospheric air, and ii) the initial dissolved gas concentrations are at atmospheric equilibrium at the local atmospheric pressure P. In other words, Henry's law (equation 3.5) also applies for the initial state. This additional relation makes it possible to express also the initial concentrations in terms of dissolved concentrations, which we want in order to compare the final dissolved gas concentrations to the initial, atmospheric equilibrium concentrations. To avoid misunderstandings, it should be clearly defined what is meant by atmospheric equilibrium concentrations. They are the dissolved gas concentrations in water in equilibrium with water vapor saturated air at the local atmospheric pressure P and at the water temperature T^*, and can be written as follows:

$$C_{i,w}^{eq}\left(T^*,S^*,P\right)=\frac{C_{i,a}^{eq}\left(T^*,P\right)}{H_i\left(T^*,S^*\right)} \tag{3.8}$$

where $C_{i,a}^{eq}\left(T^*,P\right)$ denotes the gas concentrations in moist air at the indicated conditions. Applying equation (3.8) for the concentrations in the initial state, we can rewrite equation (3.7) as follows (dropping the index w, as we now only refer to dissolved concentrations in the water phase):

$$C_i=C_i^{eq}\left(T^*,S^*,P\right)\frac{1+H_i\left(T^*,S^*\right)\frac{V_g^*}{V_w}}{1+H_i\left(T,S\right)\frac{V_g}{V_w}} \tag{3.9}$$

To bring this equation to a form that more closely resembles the original CE-model equation of Aeschbach-Hertig et al. (2000), we introduce two model parameters:

i) the gas/water volume ratio in the initial state:

$$A=\frac{V_g^*}{V_w} \tag{3.10}$$

ii) the ratio of the gas volumes in the final and initial state:

$$F=\frac{V_g}{V_g^*} \tag{3.11}$$

Using these definitions, equation (3.9) becomes:

$$C_i = C_i^{eq}\left(T^*, S^*, P\right)\frac{1 + AH_i\left(T^*, S^*\right)}{1 + AFH_i\left(T, S\right)} \tag{3.12}$$

Alternatively, we could have defined a different model parameter, namely

iii) the gas/water volume ratio in the final state:

$$B = \frac{V_g}{V_w} = AF \tag{3.13}$$

Consequently, the model equation would be written as:

$$C_i = C_i^{eq}\left(T^*, S^*, P\right)\frac{1 + AH_i\left(T^*, S^*\right)}{1 + BH_i\left(T, S\right)} \tag{3.14}$$

The physical interpretation of the model parameters and their effects on the dissolved concentrations are quite obvious in this formulation. A describes the initial volume of entrapped air added per volume of water (the concentration of entrapped air), whereas B is the respective concentration of entrapped gas (now no longer of atmospheric composition) in the final state. In the case of B = F = 0, there is no final gas phase, and the entrapped air is completely dissolved. Equation (3.14) then reduces to the unfractionated excess air model (equation 3.1). The final dissolved gas concentrations then are always higher than the equilibrium concentrations. Alternatively, the case of A = 0 but with a finite B (while F is not defined in this case) describes degassing of an initially air-equilibrated water into a secondary gas phase. This case has been applied in the literature (Lippmann et al., 2003). Equation (3.14) simply becomes:

$$C_i = \frac{C_i^{eq}\left(T^*, S^*, P\right)}{1 + BH_i\left(T, S\right)} \tag{3.15}$$

The final dissolved gas concentrations in this case are always lower than the initial equilibrium concentrations due to degassing.

A rather trivial special case of equations (3.12) or (3.14) is A = B and F = 1, when the gas phase volume as well as the dissolved concentrations remains constant. The general case has both A and B > 0 and F = B/A either smaller or larger than 1. F < 1 is the classical excess air case, when the gas volume is reduced (B < A) and gases are forced into dissolution. F > 1 describes degassing, when the gas volume is increased (B > A) and gases are released into the gas phase.

For the conceptual interpretation of the model it is useful to look at the parameter F more closely. Using the ideal gas law, the gas volume ratio F can be related to ratios of pressure, temperature, and the total number of moles in the gas phase N_g (remembering that P refers to the initial atmospheric pressure, whereas the pressure in

the final state is denoted as P_{tot}, and otherwise quantities with stars refer to the initial state):

$$F = \frac{B}{A} = \frac{V_g}{V_g^*} = \frac{P}{P_{tot}} \frac{N_g}{N_g^*} \frac{T}{T^*} \tag{3.16}$$

This can be interpreted in the sense that changes in the gas volume are due to changes of pressure, temperature, or the total gas amount. In fact, each of these factors can drive contraction or expansion of the gas phase and consequently gas dissolution or exsolution (degassing).

Note that in this derivation the path of evolution between the initial and final state does not matter. For instance, the initially trapped gas may have been partly or completely dissolved and later redistributed between the water and a secondary gas phase, which could lead to degassing. However, we have explicitly retained the possibility that the equilibration conditions T and S are different in the initial and the final state. In the initial situation during groundwater recharge the atmospheric equilibrium concentrations are defined in the unsaturated zone or at the water table. They depend in particular on soil temperature T^*, which as the so-called recharge temperature is usually the parameter of most interest. In the case of excess air formation it can be assumed that the final equilibrium between the water and the gas phase is reached within the quasi-saturated zone in the recharge area at the same temperature and salinity as during the initial equilibration. In the case of degassing, however, it is possible that the final equilibrium is reached under different conditions, as they are present e.g. near the point of sampling.

The problem with including different equilibration conditions in the CE-model is that the number of unknown parameters becomes too big to solve for all of them based on the measured concentrations of only four atmosphere-derived noble gases (Ne, Ar, Kr, Xe). For this reason, we assume $T^* = T$ and $S^* = S$ for the time being, which also allows us to develop the original form of the CE-model equation. It should be noted, however, that including the possibility of different equilibration conditions may improve the performance of the model in describing degassing. This option could be explored in a case where reasonable estimates on the equilibration conditions in at least one state can be made.

Assuming thus that temperature and salinity are the same in the final and initial state, we can rewrite equation (3.12) to:

$$C_i = C_i^{eq}(T,S,P) \frac{1 + AH_i(T,S)}{1 + AFH_i(T,S)} = C_i^{eq} + \frac{(1-F) AH_i / C_i^{eq}}{1 + AFH_i} \tag{3.17}$$

This last form of the CE-model equation is equivalent to the one given in the literature (e.g. Aeschbach-Hertig et al., 2000; Kipfer et al., 2002), although it looks slightly different. The differences are essentially due to the choice of concentrations units and

consequently a slightly different definition of the parameter A. We think that the choice of units and parameters used above is the simplest and provides the best insight into the physical interpretation of the model and the parameters. The above equations are however not so convenient if they are to be applied to practical situations. On the one hand, noble gas concentrations in the atmosphere are well-known and reported in terms of the constant molar fractions z_i in dry air. On the other hand, concentrations of dissolved noble gases in water are usually reported in units of cm^3STP/g (STP: standard temperature T_0 = 273.15 K and standard pressure P_0 = 1 atm). It is therefore convenient to express the gas phase concentrations in terms of dry gas fractions and pressures and the water phase concentrations in cm^3STP/g.

3.3.2 The original formulation of the CE-model equation

The model equation in a notation referring to partial pressures and dry air mole or volume fractions is best derived again from scratch starting with the mass balance equation (3.4). The equilibrium condition for the final state (Henry's law) is now expressed as follows:

$$p_i = H_i^{'}(T,S)\cdot C_i \tag{3.18}$$

where $H_i^{'}$ is the Henry constant in units of [atm g cm^{-3}STP]. The partial pressures p_i are related to the number of moles in the gas phase $n_{i,g}$ by the ideal gas law:

$$p_i = \frac{n_{i,g} RT}{V_g} \tag{3.19}$$

The conversion of STP-volumes $V_{i,STP}$ to moles also follows from the ideal gas law, yielding the following relationship for dissolved gas concentrations:

$$C_i = \frac{V_{i,STP}}{m_w} = \frac{n_i V_0}{m_w} \text{ with } V_0 = \frac{RT_0}{P_0} \tag{3.20}$$

The atmospheric concentrations are now given as partial pressures $p_{i,a}$, which are related to the dry air mole fractions z_i by:

$$p_i^* = p_{i,a} = \left(P - e(T)\right) z_i \tag{3.21}$$

where e(T) denotes the saturation water vapor pressure (see eq. 2.12). The atmospheric equilibrium conditions for the initial state are now written as:

$$C_i^* = C_i^{eq}(T,S,P) = \frac{p_{i,a}}{H_i^{'}(T,S)} = \frac{\left(P - e(T)\right) z_i}{H_i^{'}(T,S)} \tag{3.22}$$

By inserting the relationships (3.18) to (3.22) into the mass balance equation (3.4) we arrive at an equation for the final dissolved gas concentrations, which is the equivalent of equation (3.9) in the new units:

$$C_i = \frac{C_i^{eq} + \frac{V_g^*}{m_w}\frac{P-e}{P_0}\frac{T_0}{T} z_i}{1 + \frac{V_g}{m_w}\frac{H_i'}{P_0}\frac{T_0}{T}} \tag{3.23}$$

From the expression in the numerator follows a convenient definition for the model parameter A, which now describes the initial dry air volume at standard conditions per unit mass of water, rather than simply the gas/water volume ratio as in equation (3.10):

$$A = \frac{V_g^*}{m_w}\frac{P-e}{P_0}\frac{T_0}{T} \tag{3.24}$$

Using this new definition of A but retaining the definition of $F = V_g / V_g^*$, and further using equation (3.22), equation (3.23) becomes:

$$C_i = \frac{C_i^{eq} + A z_i}{1 + AF\frac{z_i}{C_i^{eq}}} = C_i^{eq}\frac{1 + A\frac{z_i}{C_i^{eq}}}{1 + AF\frac{z_i}{C_i^{eq}}} \tag{3.25}$$

This is identical to the CE-model equation of Aeschbach-Hertig et al. (2000), which usually is expressed as follows (also compare equation 3.17):

$$C_i(T,S,P,A,F) = C_i^{eq}(T,S,P) + \frac{(1-F)Az_i}{1 + AF\frac{z_i}{C_i^{eq}}} \tag{3.26}$$

It should be noted again that there is a slight difference between the original derivation of the CE-model of Aeschbach-Hertig et al. (2000) and the one presented here. Aeschbach-Hertig et al. (2000) defined the pressure in the initial state to be the total (atmospheric plus hydrostatic) pressure and equal to the pressure in the final state. We define the initial state to be at atmospheric pressure. Consequently, Aeschbach-Hertig et al. (2000) referred the gas volume in the initial state and the parameter A to the total pressure, whereas we use the atmospheric pressure. Because the equilibrium condition in the initial state refers to the atmospheric pressure, Aeschbach-Hertig et al. (2000) had to introduce a pressure factor in the definition of F, which does not occur in the present formulation.

We also slightly change the interpretation of F compared to the one given above in equation (3.16). First, there is no temperature factor, since we assumed the

temperature to be constant. Furthermore, since the water vapor pressure e(T) is constant, changes in the total gas volumes V_g^* and V_g can be interpreted in terms of dry gas amounts and pressures, as follows:

$$F = \frac{V_g}{V_g^*} = \frac{P - e}{P_{tot} - e} \frac{N_{g,dry}}{N_{g,dry}^*} \tag{3.27}$$

where $N_{g,dry}$ refers to the total number of moles of gas in the gas phase except the contribution of water vapor.

Finally, we introduce a minor reformulation of the CE-model equation (3.26), which stresses the fact that the ratio z_i / C_i^{eq} is simply a special form of the gas solubilities. In analogy to the solubility function used by Warner and Weiss (1985) and Bullister et al. (2002), we define the moist air solubility G_i as follows:

$$G_i(T,S) \equiv \frac{C_i^{eq}(T,S,P_0)}{z_i} = \frac{P_0 - e(T)}{H_i^{'}(T,S)} \tag{3.28}$$

G_i is directly related to the moist air equilibrium concentration C_i^{eq} at a total atmospheric pressure of P_0 (1 atm). If P differs from P_0, the actual equilibrium concentration follows from:

$$C_i^{eq}(T,S,P) = \frac{P - e}{P_0 - e} G_i(T,S) z_i \equiv r G_i(T,S) z_i \tag{3.29}$$

with the dry gas pressure ratio

$$r \equiv \frac{P - e}{P_0 - e} \tag{3.30}$$

With these definitions, our final formulation of the CE-model equations becomes:

$$C_i(T,S,P,A,F) = C_i^{eq}(T,S,P) + \frac{(1-F) A z_i}{1 + AF / rG_i} \tag{3.31}$$

3.3.3 Interpretation of the CE-model and its parameters

As already discussed above, the CE-model can describe both the formation of excess air as well as the phenomenon of degassing, depending on the value of the fractionation parameter F. The degree of the concentration change, either by excess air or by degassing, also depends on the solubility G_i of the individual gas i (see equation 3.31). Therefore, the CE-model describes a solubility-controlled process of excess air formation or degassing.

To discuss the effect of the CE-model on gases of different solubilities, it is useful to look at the ratio of the gas excesses (or deficiencies) of two different gases. These excesses are given by the difference $C_i - C_i^{eq}$, which is simply the rightmost term in equations (3.31) or (3.26). For the ratio of two gases i and j we obtain (compare Peeters et al., 2003):

$$\frac{C_{i,ex}}{C_{j,ex}} = \frac{(1-F)Az_i}{1+AF/rG_i} \cdot \frac{1+AF/rG_j}{(1-F)Az_j} = \frac{z_i}{z_j} \cdot \frac{G_i}{G_j} \cdot \frac{rG_j + AF}{rG_i + AF} \qquad (3.32)$$

To understand the meaning of this equation, it is useful to discuss some limiting cases. One limit is F = 0, when the CE-model reduces to the UA-model, and the excess ratio of equation (3.32) simply becomes z_i/z_j, i.e., the atmospheric abundance ratio of the two gases. This is the case of unfractionated excess air. The other limit is reached when A or F are very large, such that AF >> rG_i or rG_j. Equation (3.32) then becomes:

$$\frac{C_{i,ex}}{C_{j,ex}} \approx \frac{z_i}{z_j} \cdot \frac{G_i}{G_j} = \frac{C_i^{eq}}{C_j^{eq}} \qquad (3.33)$$

Hence, for large AF, the ratio of the gas excesses approaches the ratio of the equilibrium concentrations, or the relative excesses (relative to the equilibrium concentration) of all gases become equal. This can be interpreted as a pressure effect, corresponding to equilibration of the water with the free atmosphere (or any very large air reservoir described by a high value of A) at a pressure different from the atmospheric pressure prevailing during the initial equilibration.

In realistic cases, the ratio of the two excesses (equation 3.32) will lie between these extremes, depending on the values of A, F, and the solubilities G_i and G_j. Heavy noble gases (Ar, Kr, Xe) have higher solubilities, i.e. higher values of G_i and lower values of H_i (compare equation 3.28) than light noble gases (He, Ne). Hence the ratio of the excess of a heavy noble gas i relative to a light noble gas j will be larger than the atmospheric ratio by a factor lying between one and the ratio G_i/G_j of the solubilities. This factor describes the fractionation of the excess air relative to atmospheric air, which leads to an enrichment of the heavy gases in the excess compared to the case of atmospheric excess air (F = 0). Yet, relative to the respective equilibrium concentrations, the excesses of the light gases will still be larger than those of the heavy gases. Similarly, in the case of degassing (F > 1), the light gases will be more susceptible to gas loss than the heavy ones, but compared to air the heavy gases will still be enriched in the lost gas.

The effects of different values of the fractionation parameter F on the concentration of dissolved light and heavy noble gases is illustrated in Figure 3.2.

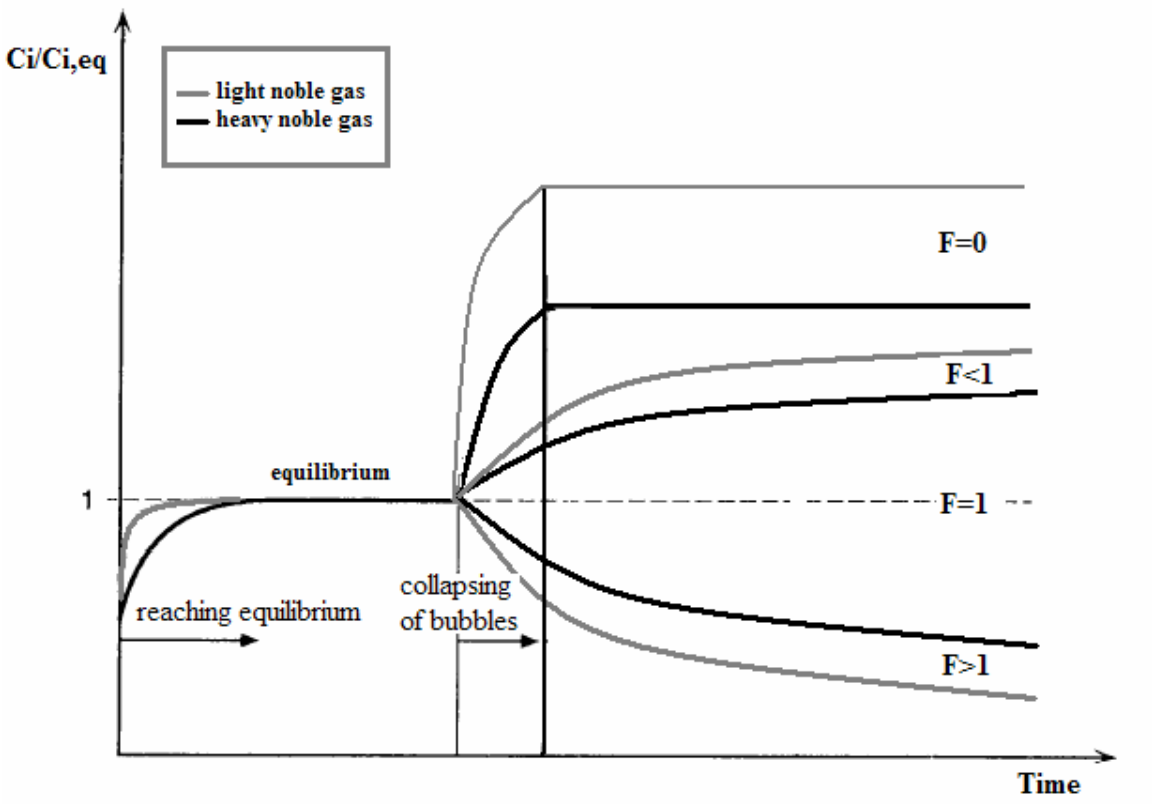

Figure 3.2: Formation of excess air and degassing according to the CE-model (equation 3.31). Different values of F refer to different processes, e.g. F = 0 refers to complete dissolution of entrapped air leading to purely atmospheric excess air (UA-model), F = 1 refers to no change of the equilibrium concentration, F < 1 refers to excess air formation, and F > 1 refers to degassing.

For a further discussion of the factors that lead to excess air formation or degassing according to the CE-model, it is useful to return to the physical interpretation of the fractionation parameter F. In analogy to the original derivation of the CE-model, we split F according to equation (3.27) in two factors v and q:

$$F \equiv \frac{v}{q} \quad \text{with} \quad v = \frac{N_{g,dry}}{N^*_{g,dry}} \quad \text{and} \quad q = \frac{P_{tot} - e}{P - e} \tag{3.34}$$

In this formulation, the physical interpretation of F is straightforward: F describes the change in the entrapped gas volume due to changes in the amount of dry gases (v) or the respective pressure (q). Values of F between 0 and 1 describe a contraction of the gas phase leading to an increase of the dissolved concentration (excess air), whereas values of F above 1 describe an expansion of the gas phase leading to a decrease of the dissolved concentrations (degassing). The question is which processes are responsible for changes in the pressure or the amount of gases.

Aeschbach-Hertig et al. (2002) showed that a relationship between the parameters q, v, and A exists, although they did not explicitly discuss the conditions for the validity of this relationship. The basis of this relationship is the physical requirement that the sum of the partial pressures of all gases in the trapped volume has to be equal to the total dry gas pressure (using equations 3.18 and 3.22):

$$P_{tot} - e = \sum_i p_i = \sum_i H_i' C_i = (P - e) \sum_i \frac{z_i}{C_i^{eq}} C_i \tag{3.35}$$

If, as tacitly assumed by Aeschbach-Hertig et al. (2002), the conservation condition (3.4) and therefore the CE-model equation (3.25) is valid for all gas species i, the above requirement can be rewritten as follows:

$$q = \frac{P_{tot} - e}{P - e} = \sum_i z_i \frac{1 + A\frac{z_i}{C_i^{eq}}}{1 + FA\frac{z_i}{C_i^{eq}}} = \sum_i z_i \frac{1 + A\frac{z_i}{C_i^{eq}}}{1 + \frac{v}{q} A\frac{z_i}{C_i^{eq}}} \tag{3.36}$$

This implicit equation couples the parameters q, A, and v (or F). I. e., if A and F are determined from fitting the model equation (3.26) to the data, q and v can be calculated from equation (3.36). However, as noted above, such a calculation of q and v is only valid if all gases behave conservatively, such that the CE-model applies for all of them. In this case, the sum on the right hand side is dominated by the most abundant atmospheric gases N_2, O_2, and Ar, which have relatively similar solubilities. Thus, it is a reasonable approximation to write equation (3.36) for a gas phase consisting of only one gas i = 0 ("N_2") with an atmospheric abundance z_0 of 1. We then arrive at the following condition for q and v:

$$\frac{q - 1}{1 - v} = \frac{A}{C_0^{eq}} \tag{3.37}$$

This equation imposes some restrictions on the range of possible values of q, v, and F. The right hand side of (3.37) is always positive, and q and v are also positive numbers according to their definition (eq. 3.34). Furthermore, the original assumption of the CE-model was that the pressure P_{tot} in the final state is the sum of the atmospheric and hydrostatic pressure, thus at least as large as the atmospheric pressure in the initial state. It follows $q \geq 1$ and, since in this case both the numerator and denominator on the left hand side of (3.37) have to be positive, we obtain $v \leq 1$. Since F = v/q, we find the condition $0 \leq F \leq 1$. This is, as discussed before, the case of excess air formation, where the gas phase volume (F) and gas amount (v) decrease due to increased pressure (q) and as a consequence the dissolved gas concentrations increase.

It may be useful to discuss the limiting cases for the values of F. Obviously, if F = 0 equation (3.26) reduces to $C_i = C_i^{eq} + Az_i$, or simple atmospheric excess air (UA-model). This case occurs if v = 0, which means that there is no gas left in the final state. This might in reality be achieved if the initial amount of entrapped air (A) is divided into many very small bubbles, which spontaneously collapse even under a very slight hydrostatic pressure. However, F also approaches zero if q goes to infinity. This means that the hydrostatic pressure is so large, that eventually all gas is forced into solution. Another limiting case is F = 1, for which case it follows from (3.26) that $C_i = C_i^{eq}$, thus there is no excess air at all. Since $q \geq 1$ and $v \leq 1$, F = 1 can only occur if v = q = 1. This means that there is no hydrostatic pressure excess and no

spontaneous collapse of bubbles (no change of the gas amount). Thus, the concentrations in the water simply remain in atmospheric equilibrium.

The above discussed traditional assumptions reflect the typical case of excess air generation due to an increase of pressure, e.g. due to a rise of the water table, when all gases behave conservatively. If we allow for the presence of non-conservative gases, equation (3.36) is no longer valid and we cannot calculate the values of v and q from those of F and A. Conceptually, however, it remains valid to interpret F in terms of changes in the gas amount (v) and pressure (q), although these factors are now decoupled. In this general case, excess air may also be formed at constant pressure ($q = 1$) if the gas amount is reduced ($v < 1$ and thus $F < 1$) by removal of one or more reactive gases (e.g., O_2 consumption).

On the other hand, the gas amount may increase ($v > 1$) at constant pressure ($q = 1$) by addition of, e.g., biogenic gases. In such a case, $F > 1$ and from eq. (3.26) it follows that the concentrations of dissolved noble gases decrease, i.e., degassing takes place. Of course, degassing may also result from a reduction of pressure ($q < 1$).

Degassing may occur naturally in aquifers. In the capillary fringe, water is sucked up by capillary forces against atmospheric pressure and the effective pressure in this zone is below atmospheric. Pressure reduction may also occur in response to pumping in the vicinity of a well. Addition of gases such as CH_4 or CO_2 is quite common in deep circulating groundwater. Denitrification may add significant amounts of N_2. Degassing is further favored by increases of temperature and salinity of the groundwater.

It is therefore possible that the initially entrapped air bubbles are actually enlarged rather than reduced, or that later on in the evolution of groundwater a secondary gas phase is formed. In this case, gas will be transferred from the dissolved phase into the growing gas bubbles. If this process continues until equilibrium between gas and water is reached (at the same T and S conditions as during the initial equilibration with the atmosphere), the CE-model equation (3.26) with $F > 1$ should correctly describe the final concentrations of dissolved gases.

3.4 Ledo-Paniselian aquifer (Belgium) as a field example of degassing

3.4.1 Study area

The investigation area is located in the Belgian province of Flanders north-west of Ghent (Figure 3.3). In this region, the Eocene Ledo-Paniselian sands form a confined coastal aquifer of substantial extension. The Ledo-Paniselian Aquifer (LPA) has been subject of extensive previous research concerning groundwater flow, hydrogeochemical processes and hydrodynamics (e.g. Van der Kemp et al., 2000). This aquifer extends from the provinces of Eastern and Western Flanders in north-western Belgium across the Belgian-Dutch border to the Dutch province of Zealand and the sea branch of the Western Scheldt.

The LPA is part of an alternating sequence of marine tertiary clay and sand deposits gently dipping towards the north. This sequence is shown in the cross section (A-A ') of Figure 3.4, extending from the unconfined/semi-confined boundary of the Ledo-Paniselian in the south towards the north. In the semi-confined region, the aquifer is overlain by the Bartonian clay. A thin layer of Paniselian clay underlies the aquifer, followed by the Ypresian aquifer, which itself overlies the Ypresian clay. The Ledo-Paniselian aquifer is recharged in topographically higher regions where the aquifer is covered by the Bartonian clay and therefore is semi-confined. The discharge partly takes place in the unconfined area where the Ledo-Paniselian crops out beneath the Quaternary sediments. The remaining part of the recharged groundwater flows to the north or northwest, where the depth of the aquifer increases. In this region, discharge occurs by upward leakage through the confining Bartonian clay, causing flow velocities in the Ledo-Paniselian to diminish gradually.

Samples from a total of 39 wells were collected during three field campaigns in 1997, 1998 and 2001 in a collaboration of the Universities of Ghent, Bern, and ETH Zurich. The aim of the study was to derive a paleotemperature record from dissolved noble gases in groundwater of the LPA (Aeschbach-Hertig et al., 2003). Here, we will focus on the interesting observation of degassing in part of the data set from this study, which we will analyze with the theoretical concepts discussed above.

The Ledo-Paniselian data set contains 10 samples out of a total of 44 samples that show gas undersaturations, rather than the usual excesses over solubility equilibrium. This phenomenon is readily visible in the measured Ne concentrations: For temperatures between 0 and 10 °C, in which range recharge temperatures since the last glaciation can reasonably be expected to lie, the Ne equilibrium concentration ranges between 2.0 and $2.2 \cdot 10^{-7}$ cm^3STP/g. The data are divided into two groups: The majority of the samples (34) have Ne concentrations above equilibrium, ranging between 2.2 and $2.8 \cdot 10^{-7}$ cm^3STP/g, thus exhibiting the typical excess air signature. The remaining 10 samples have Ne concentrations clearly below equilibrium, scattering widely between 0.7 and $1.9 \cdot 10^{-7}$ cm^3STP/g. These Ne concentrations are clear signs of gas loss.

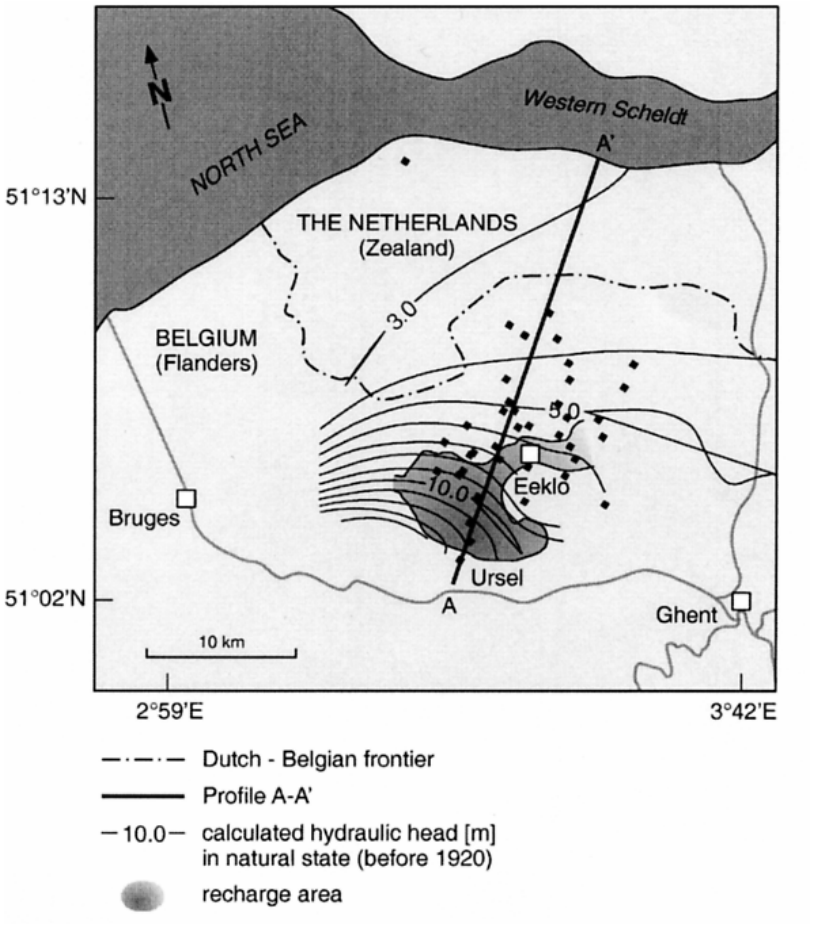

Figure 3.3: Overview of the investigation area with sampling locations, hydraulic head isolines and localization of the recharge area (cross section A-A ')

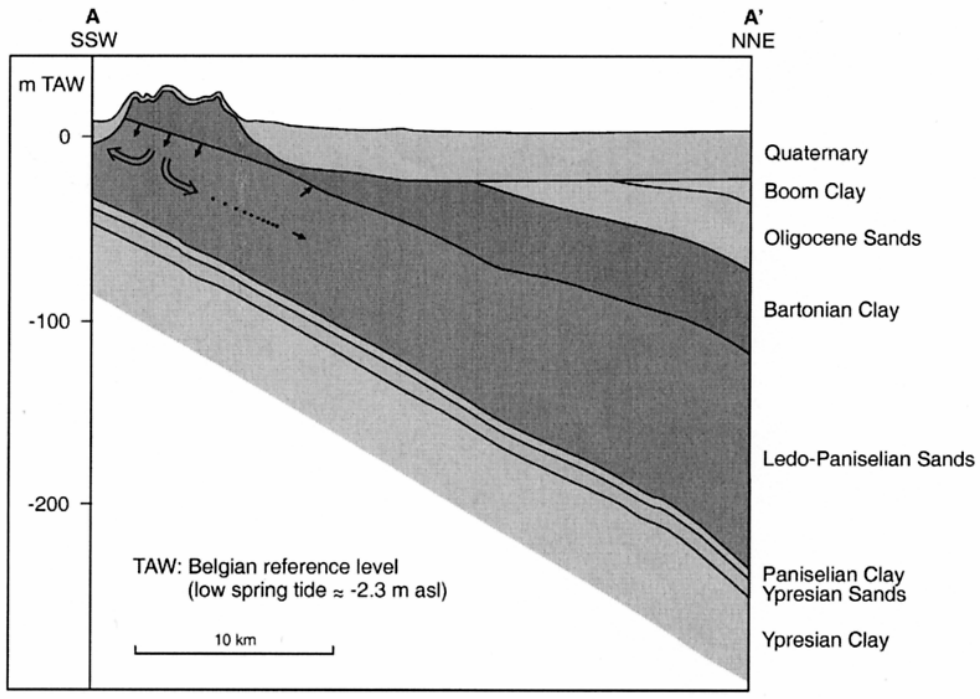

Figure 3.4: Geological cross section through the investigation area (profile A-A ')

It is important to note that the degassing pattern in two wells used in this study was reproduced in two sampling campaigns that were separated by 3 years and conducted by different people. This observation strongly argues for a systematic origin of the degassing, unrelated to the details of the sampling procedure. In this case, it should be possible to explain the observed noble gas abundance patterns by a physical model. We therefore discuss the presently available excess air models (see sections 3.1, 3.2 and 3.3) as potential models to describe degassing.

3.4.2 Evaluation of the noble gas data by inverse modeling

The inverse modeling program described by Aeschbach-Hertig, et al. (1999) was used to find the best fit of the different models to the observed concentrations of each sample. As usual in noble gas studies of groundwater, the excess air models are not applicable to the observed He because of the presence of radiogenic He. Thus, at maximum 3 parameters can reliably be estimated from the four measured atmospheric noble gases Ne, Ar, Kr, and Xe. The parameters T, A, and if applicable F were treated as unknowns, whereas P and S were prescribed. A pressure of P = 0.998 atm was used, corresponding to a mean altitude of the recharge area of 20 m a.s.l, and salinity S was estimated from the electrical conductivity.

The inverse algorithm varies the model parameters in order to minimize χ^2, the sum of the weighted squared deviations between the modeled and measured concentrations:

$$\chi^2 = \sum_i \frac{\left(C_i - C_i^{\mathrm{mod}}\right)^2}{\sigma_i^2} \tag{3.38}$$

where C_i^{mod} are the modeled, C_i the measured concentrations, and σ_i their experimental errors (see section 2.4). The quantity χ^2 can be used to objectively judge the ability of the conceptual models to describe the given data. The model selection is based on the χ^2 -test. The probability p for χ^2 to be equal or higher than the observed best value by chance, i.e. due to random experimental errors, is calculated from the χ^2 -distribution. If this probability is lower than some cut-off value, the model is rejected. Only models with $p \geq 0.01$ are considered valid descriptions of the data. The χ^2-test with this criterion was applied on two levels: first on the level of individual samples, which allowed us to identify irregular samples that cannot be described by any model. Later on application of the χ^2 -test to the entire set of "good" samples yields a more stringent criterion to select the appropriate excess air model, because of the much larger number of degrees of freedom (ν).

In a first step, the 10 samples that show obvious signs of degassing (e.g., in the Ne concentration, see above) were excluded from the analysis, because these samples cannot be described by any of the classical models, i.e., UA-, PR-, and CE-model with $F \leq 1$. The χ^2 -test was then applied to the complete set of the remaining 34 samples, in order to choose the appropriate model. The UA-model fits only 17 of these 34 samples individually within the confidence limit defined above and is clearly not

acceptable for the entire data set. The PR-model fares much better, as only one of the 34 samples does not meet the criterion of $p \geq 0.01$. Yet, applying the χ^2 -test to the whole data set shows that the model does not provide a good description of the entire data set ($\nu = 34$, $\chi^2 = 76$, $p << 0.01$). In contrast, the CE-model not only yields acceptable fits to all 34 samples individually, but also to the complete data set ($\nu = 34$, $\chi^2 = 33.7$, $p = 0.39$). Thus, the CE-model – and only the CE-model – is in perfect agreement with the noble gas concentration data within experimental uncertainty.

As discussed by Peeters et al. (2003), the Ne isotope ratios provide additional and possibly more stringent constraints on the choice between the PR-and CE-models. The reason is that the diffusive re-equilibration assumed by the PR-model should lead to signficant isotope fractionation, whereas the CE-model only predicts a very small (< 0.2 %) isotope shift due to the different solubilities of the two isotopes (Beyerle et al., 2000). Figure 3.5 compares the measured $^{20}Ne/^{22}Ne$ ratios with those predicted from the PR-model (open symbols) and the CE-model (solid symbols). The agreement between data and model prediction is significantly better for the CE-model than for the PR-model. Almost all measured $^{20}Ne/^{22}Ne$ fall in the range between the atmospheric isotopic ratio (Ozima and Podesk, 1983) and the slightly lower isotopic ratio at atmospheric equilibrium (Beyerle et al., 2000), which is the range predicted by the CE-model. The PR-model predicts much lower $^{20}Ne/^{22}Ne$ ratios (up to about 3 % below the atmospheric ratio) which are not observed. Formally, the agreement between model and data can again be quantified by a χ^2 -test, where now the measured Ne ratios are included as an observable in addition to the concentrations of Ne, Ar, Kr, and Xe. Using this data set, the CE-model yields a good fit ($\nu = 68$, $\chi^2 = 94$, $p = 0.02$), whereas the PR-model has to be rejected, ($\nu = 68$, $\chi^2 = 298$, $p << 0.01$). The observed unfractionated Ne isotope ratios clearly rule out strong diffusive fractionation, which would be needed to fit the noble gas concentrations with the PR-model, thus resulting in bad fits.

Now we will try to handle the 10 degassed samples by using the diffusive degassing model (DD-model, equation 3.3) and the CE-model with $F > 1$ (eq. 3.26, 3.31), which are implemented in the inverse fitting program of Peeters et al. (2003), although only in the approximation that temperature and salinity do not change between recharge and degassing. We consider this approximation as justified for a first test of the models. An important observation is that with the usual initial parameter values $A = F = 0$, the CE-model normally does not find the solution with $F > 1$ corresponding to degassing, even for the obviously degassed samples. However, if the parameter optimization routine is started with $A \neq 0$ and $F > 1$, it usually converges to reasonable solutions describing degassing by equilibration with a gas phase. This behavior is due to the fact that for the degassed samples there exist usually at least two local minima of χ^2 in the parameter space of the CE-model, one with $F < 1$ and one with $F > 1$. Starting with $F = 0$, the procedure only finds the first minimum, which is a bad fit with $A = F = 0$ (or even A or $F < 0$, if the parameter range is unrestricted). This finding highlights the necessity to run the inverse fitting procedure with varying initial conditions, in particular in the case of the CE-model, in order to make sure that all minima of χ^2 are found.

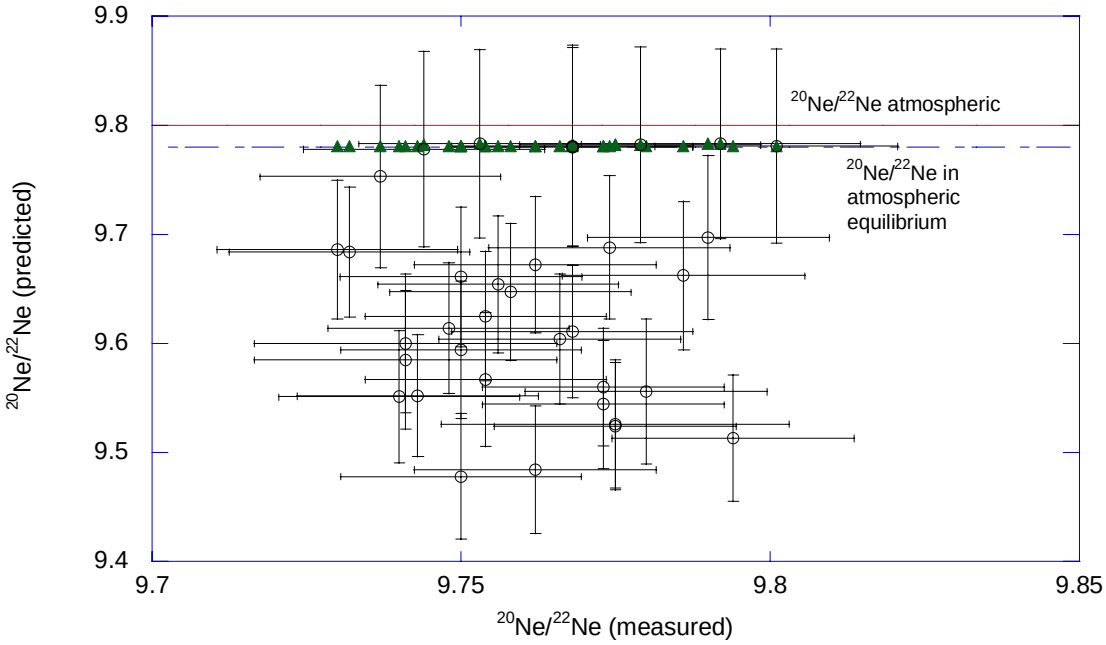

(a)

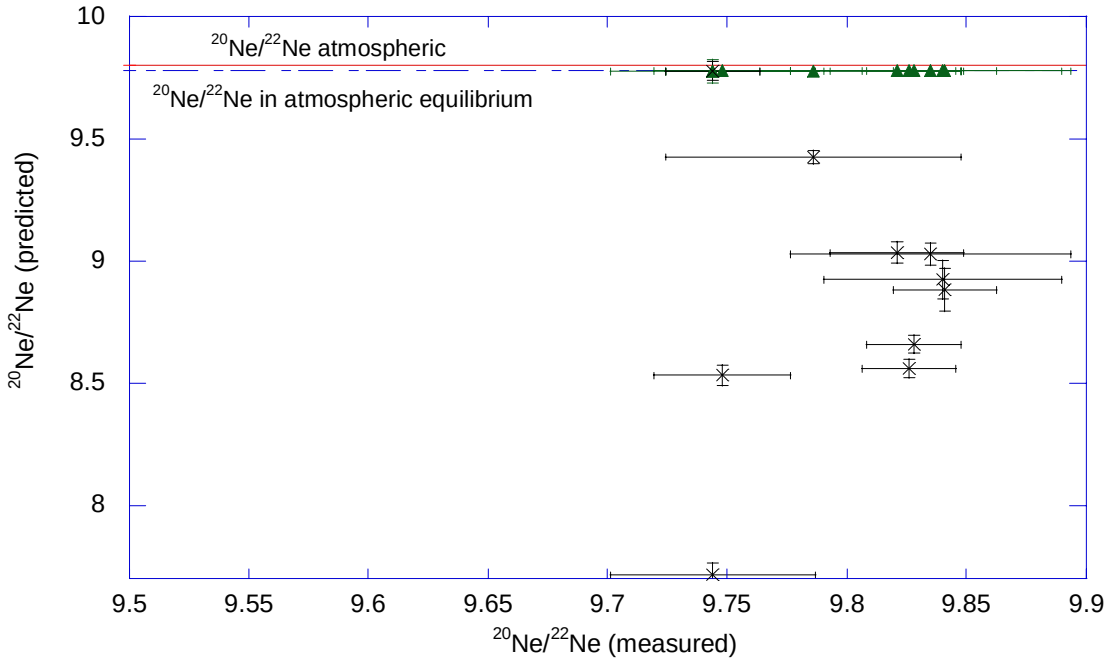

(b)

Figure 3.5: Comparison of measured and predicted $^{20}Ne/^{22}Ne$ ratios. Predictions were calculated from the model parameters describing recharge temperature, excess air or degassing, and fractionation, obtained by inverse fitting of the models to the concentrations of Ne, Ar, Kr and Xe. (a) The 34 undegassed samples from the LPA. Predictions derived with the CE-model are indicated by solid symbols, those from the PR-model by open symbols. (b) The 10 degassed samples from the LPA. The solid symbols represent predictions made by the CE-model, whereas the "x" symbols represent results of the DD-model.

Neither the DD- nor the CE-model provides an adequate description of all 10 degassed samples. Applying the DD-model, only 4 samples meet the criterion of $p \geq 0.01$. The CE-model yields acceptable fits to 5 samples. For two samples, neither model works. A decision between the two models on the basis of the concentration data appears not possible. However, including $^{20}Ne/^{22}Ne$ as an additional constraint in the fitting procedure helps to choose between the two models. Similar to the PR-model, the diffusive process of the DD-model should lead to significant fractionation of the $^{20}Ne/^{22}Ne$ ratio. Strong diffusive loss of Ne should lead to a depletion of the light isotope in the remaining dissolved fraction, even stronger than in the case of the PR-model, (see Figure 3.5b). Consequently, if the $^{20}Ne/^{22}Ne$ ratio is included as an additional constraint in the fitting procedure, the DD-model clearly fails to explain any of the degassed samples. In contrast, inclusion of the Ne isotopes does not significantly affect the performance of the CE-model, which still fits half of the 10 samples. The results of the fitting procedure with the CE-model for the degassed samples are listed in Table 3.1.

sample	χ^2	p [%]	T [°C]	err T [°C]	A [ccSTP/kg]	F	q	v
LPA17	0.9780	32.2686	10.3801	0.5187	0.4413	5.5717	0.9127	5.0854
LPA20	0.1487	69.9755	8.8935	0.9825	30.9087	2.4200	0.5491	1.3289
LPA22	0.1967	65.7414	6.5856	4.3268	120.0780	1.7689	0.6095	1.0782
LPA23	1.9513	16.2442	4.9315	6.2326	183.1840	1.3444	0.7674	1.0316
LPA23b	*18.0059*	*0.0022*	*3.3958*	*4.6268*	*159.6060*	*1.4391*	*0.7258*	*1.0445*
LPA32	5.8099	1.5937	6.9174	4.7454	96.0322	3.4235	0.3403	1.1650
LPA32b	*11.8236*	*0.0585*	*6.7654*	*4.4561*	*99.6961*	*3.2632*	*0.3543*	*1.1560*
LPA33	*38.7658*	*0.0000*	*9.3808*	*7.2238*	*109.3770*	*3.1675*	*0.3578*	*1.1334*
LPA38	*8.4461*	*0.3658*	*3.9638*	*4.3079*	*157.6580*	*1.2446*	*0.8260*	*1.0280*
LPA39	*20.8003*	*0.0005*	*7.6345*	*5.9233*	*157.5530*	*1.1455*	*0.8874*	*1.0165*

Table 3.1: The fitting parameters obtained with the CE-model for the 10 degassed samples from the LPA. Numbers in italic refer to samples which are not fit with the model ($p < 1$ %).

Thus, the CE-model is the best choice for all samples of the Ledo-Paniselian study, although its performance for the degassed samples is not optimal. If degassing is due to equilibration with a gas phase – either atmospheric gases under reduced pressure or a secondary, initially noble gas free gas phase – it appears unlikely that this equilibration occurred in the short time of sampling. This conclusion is consistent with the good reproducibility of the degassing pattern in duplicate samples taken several years apart, which also argues against a sampling artifact. It still remains to be investigated, whether the interaction with a gas phase takes place at the beginning of the flow path (e.g., in the quasi-saturated zone or the capillary fringe) or at its end (e.g., in the depression cone around the well).

3.4.3 Correction of the He concentration in the Ledo-Paniselian aquifer

The CE-model is valid for conservative gases of purely atmospheric origin. It is usually applied to describe the final dissolved concentrations of the noble gases Ne, Ar, Kr, and Xe. For He, the CE-model only yields the component of atmospheric origin. The difference between the total measured He concentration and the modeled atmospheric He concentration is interpreted as radiogenic He (He_{rad}) accumulated during the subsurface residence time of the groundwater. In the case of degassed samples, the question arises whether and how the radiogenic He component may have been affected by the degassing process. In this section we discuss how to calculate the radiogenic He component in the case of degassing.

In contrast to the purely atmospheric noble gases, the time of degassing has important and potentially detectable consequences for He. If degassing happens at the time of infiltration, the initial atmospheric He component will be strongly reduced, and the observed He concentration may be interpreted as almost purely radiogenic He. The radiogenic He component itself will not be affected by the degassing. If degassing happens at the time of sampling, when the groundwater has already accumulated radiogenic He, both atmospheric and radiogenic He will be lost. The true concentration of radiogenic He before degassing must then be calculated by correcting for the lost He, and may be much bigger than the observed He concentration. Although the atmospheric and radiogenic He components have strongly different isotope ratios, the two different pathways are hardly discernible on the basis of the He isotopes, because equilibrium degassing does almost not fractionate the isotopes.

Degassed samples may be recognized by having a more radiogenic isotopic signature at the same total He concentration than undegassed samples. However, whether this signature arises by initial loss of atmospheric He and subsequent addition of radiogenic He, or by addition of a larger radiogenic component followed by loss of both atmospheric and radiogenic He, cannot be distinguished. The only way to distinguish the two pathways is by using additional information on the expected concentration of radiogenic He. Such information may be derived from the undegassed samples. In the following, we discuss the calculation of the radiogenic He for both cases, and finally compare the results with the available data from the undegassed samples.

3.4.3.1 Case 1: Early degassing (at the time of infiltration)

The calculation of the radiogenic He_{rad} is straightforward if the modifications of the gas content predicted by the CE-model (excess air formation or degassing) happen during infiltration, before any addition of non-atmospheric He. In this case, the parameters derived from the inverse modeling of the heavier noble gases can be used to calculate the degassed atmospheric He component from the CE-model equation (eq. 3.26 or 3.31). The radiogenic He excess (He_{rad}) then simply is the difference

between the measured total He and the modeled He, which is the degassed atmospheric He.

3.4.3.2 Case 2: Late degassing (at the time of sampling)

The situation is more complicated if degassing happens by equilibration with a secondary gas phase at the time of sampling, because then both the atmospheric and radiogenic He components are affected. In this case, the CE-model can be interpreted in terms of two separate steps: In the first step, the entrapped air is completely dissolved and unfractionated excess air according to eq. (3.1) is formed. The resulting dissolved concentrations $C_{i,1} = C_i^{eq} + Az_i$ represent the initial concentrations in a secondary degassing step, which is analogous to the special case of the CE-model with no initial gas volume ($V_g^* = 0$, compare equation 3.15), except that it does not start with equilibrated water. The effect of such a secondary degassing is described by a modified version of equation (3.25), with A → 0, B = AF ≠ 0, and $C_{i,1}$ instead of C_i^{eq} as initial concentrations:

$$C_i = C_{i,2} = \frac{C_{i,1}}{1 + B\dfrac{z_i}{C_i^{eq}}} = \frac{C_{i,1}}{1 + \dfrac{B}{rG_i}} \tag{3.39}$$

Inserting B = AF and $C_{i,1} = C_i^{eq} + Az_i$ into this equation yields the usual CE-model (equation 3.31), which shows that, as already mentioned, equation (3.39) is just a special interpretation of the CE-model. The importance of equation (3.39) is that it shows explicitly how the gas concentrations are affected by the secondary degassing step. The dissolved gas concentrations are reduced by a factor

$$k_i = \frac{C_{i,2}}{C_{i,1}} = \frac{C_i}{C_i^{eq} + Az_i} = \left(1 + AF/rG_i\right)^{-1} \tag{3.40}$$

If the first step (complete dissolution of A) happened during infiltration and the second step (degassing into B = AF) happened during or just before sampling, the addition of He_{rad} must have happened in between the two steps. Therefore, the degassing factor of equation (3.40) affects both the atmospheric and the radiogenic He components. The He concentration calculated from the CE-model only describes the effect of degassing on the atmospheric component. The difference between the measured and modeled He concentration is the degassed radiogenic component. Hence, to correct for degassing, the He_{rad} concentration derived in the usual way from the difference between measured and modeled He concentration has to be multiplied by the factor $1/k_{He}$.

It should, however, be noted that the interpretation of the CE-model in this case appears somewhat unrealistic, because it assumes complete dissolution of the entrapped air in the first step. In reality, a smaller fractionated excess air component may have formed during infiltration, and the later degassing may have been weaker.

Such a scenario is not exactly described by the CE-model, but the model may provide a sufficient approximation to yield acceptable fits in some cases. A more exact description of the two step excess air formation – degassing scenario would require additional parameters, which cannot be estimated from only four measured noble gas concentrations. For this reason, such more complex models are not treated here.

3.4.3.3 Comparison of radiogenic He values

Obviously, the result for the radiogenic He concentration depends on the assumed time of degassing. If degassing happened at the time of sampling, the calculated He_{rad} will be larger by a factor of $1/k_{He}$ compared to the case of degassing during infiltration. Therefore, the radiogenic He in the following is calculated for both pathways for the degassed samples from the LPA. Comparing the two estimates of He_{rad} obtained in this way with He_{rad}–values from the undegassed wells might indicate when the degassing took place. The corrected He concentrations and the radiogenic He component for both cases are listed in Table 3.2. The samples in italic are the samples which did not fit well with the CE-model.

sample	He_{meas}	He_{mod}	k_{He}	$He_{corr}^{(2)}$	$He_{rad}^{(1)}$	$He_{rad}^{(2)}$
LPA17	3.92E-08	3.78E-08	7.82E-01	5.01E-08	1.30E-09	1.66E-09
LPA20	1.26E-07	2.20E-08	1.06E-01	1.19E-06	1.04E-07	9.84E-07
LPA22	6.77E-07	2.73E-08	4.04E-02	1.67E-05	6.49E-07	1.61E-05
LPA23	9.80E-07	3.56E-08	3.53E-02	2.77E-05	9.44E-07	2.67E-05
LPA23b	*9.64E-07*	*3.37E-08*	*3.81E-02*	*2.53E-05*	*9.31E-07*	*2.44E-05*
LPA32	4.55E-07	1.46E-08	2.65E-02	1.72E-05	4.40E-07	1.66E-05
LPA32b	*3.78E-07*	*1.52E-08*	*2.67E-02*	*1.42E-05*	*3.63E-07*	*1.36E-05*
LPA33	*1.87E-06*	*1.54E-08*	*2.49E-02*	*7.50E-05*	*1.85E-06*	*7.44E-05*
LPA38	*1.25E-06*	*3.87E-08*	*4.42E-02*	*2.82E-05*	*1.21E-06*	*2.73E-05*
LPA39	*1.39E-06*	*4.10E-08*	*4.70E-02*	*2.95E-05*	*1.35E-06*	*2.86E-05*

Table 3.2: Measured, modeled and degassing-corrected concentrations for helium and the calculated radiogenic He components. (1) refers to the case 1 when the degassing happens at the time of infiltration, in this case He_{rad} is the difference between the measured and modeled He concentrations, (2) refers to the case 2 when degassing happens at the time of sampling, in this case He_{rad} is the difference between the measured and modeled He concentrations multiplied by the factor $1/k_{He}$, which is defined in the text (equation 3.40). The corrected He concentration in this case is the total He concentration just before the final degassing step, which is given by the measured He concentration multiplied by $1/k_{He}$.

Table 3.2 shows that the difference between the two estimates of He_{rad} is very large (more than one order of magnitude) for most samples. The assumption of a late degassing (case 2) of course always yields higher corrected He_{rad} values, which are of the order of 10^{-5} cm^3STP/g for most samples. These high radiogenic He concentrations are not in agreement with the radiogenic He obtained from the undegassed samples. Of those 34 samples, only one has $He_{rad} > 10^{-5}$ cm^3STP/g, which is by far the most downgradient well yielding highly saline and probably very old water.

The conclusion that case 2 yields too high He_{rad} results can be substantiated by relating the calculated radiogenic He concentrations of all samples with the groundwater residence times derived from ^{14}C-measurements performed at the University of Bern (P. Blaser, pers. communication). The He_{rad}-values of the undegassed samples define a linear trend between He_{rad} and ^{14}C-age, as expected as a result of He accumulation over time. The He_{rad}-values from the degassed samples using case 1 (early degassing) lie on this trend within its quite large scatter. Assuming case 2 (late degassing), however, yields He_{rad}-values that lie way above the trend defined by the other samples. A reason for these very high estimates of He_{rad} may be that the assumption of initially complete dissolution of the entrapped air is too extreme. More realistic two-step scenarios would probably lead to less degassing and lower estimates of He_{rad}, but as discussed above such scenarios can not be evaluated with the available data.

We can therefore conclude that the interpretation of the CE-model as an initial complete dissolution followed by a late degassing (case 2) is not applicable for the degassed samples from the Ledo-Paniselian aquifer. A late degassing can however not be ruled out if the possibility of more complex scenarios is taken into account. In any case, the He data are compatible with a scenario where degassing in the LPA happened before the accumulation of substantial amounts of radiogenic He. This indicates that in this aquifer system, the occurrence of degassing in some wells may not be related to the conditions at or near the wells, but rather to the conditions in or near the recharge area during the time of recharge of the respective waters. The wells affected by degassing lie in a part of the aquifer that is also characterized by other anomalies in chemical and isotopic parameters (P. Blaser, pers. communication). These anomalies may all be related to special recharge conditions, but the exact origin of the degassing has not been identified so far.

3.5 Other examples of degassing

The degassing process has also been observed in samples collected from the well GWMC located close to Lake Willersinnweiher, which is a quarry pond in the congested urban area of Ludwigshafen/Rhein, Germany. The samples had been taken during three different campaigns in 2000, 2001 and 2003; and they were collected from the well at three different depths of 4, 13 and 24 m, respectively. The degassing patterns observed in all samples indicate a systematic origin of degassing, which does not take place during the sampling process.

Ne and He were measured for the samples of the first two campaigns, while all noble gases have been measured for samples from the last one. One can easily observe the degassing effect from the Ne and He concentrations (Figure 3.6). All measured Ne concentrations lie clearly below the atmospheric equilibrium concentration for an expected recharge temperature of about 10 °C. The He concentrations lie partly below and partly above the equilibrium, depending on the degree of degassing and on the presence of radiogenic He.

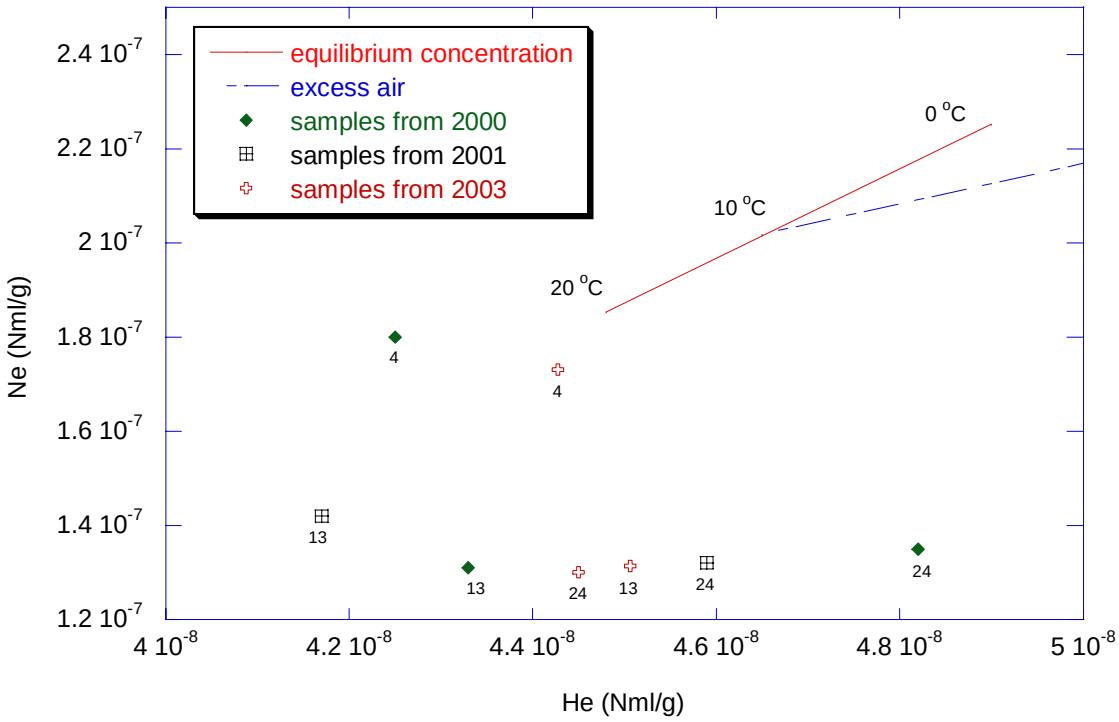

Figure 3.6: He versus Ne for groundwater samples from a well in the vicinity of Willersinnweiher Lake, collected in the year 2000, 2001 and 2003 respectively. The numbers in the plot refer to the depth (in m).

The complete noble gas data sets of the samples from the last campaign (2003) were fitted with the different models and the χ^2 test was applied to check the performance of the models. As expected, neither the CE-model with $F < 1$ nor the PR-model yield acceptable fits for these samples, since these models describe excess air, while the samples are degassed. The diffusive degassing (DD) model provides better, but still not acceptable fits. The best fits are achieved with the CE-model, allowing for $F > 1$. This model yields acceptable fits for the samples from 4 and 13 m depth, but not for the sample from 24 m depth (Table 3.3). The noble gas temperatures obtained with the CE-degassing model are reasonable, lying between 8 and 10 °C.

The CE-model parameters can again be used to estimate the radiogenic He, applying the two scenarios discussed above for the LPA. For comparison, the sample from the nearest well GWMD (sample from 2001 at 21 m depth) may be used, This sample indicates a radiogenic He concentration of about $1.4 \cdot 10^{-8}$ cm^3STP/g. For the 2003-samples, case 1 yields He_{rad}-values of $1.6 \cdot 10^{-8}$ cm^3STP/g at 13 m and $1.5 \cdot 10^{-8}$ cm^3STP/g at 24 m depth, which are in a good agreement with the reference sample. As may have been expected, the He_{rad}-concentration at 4 m depth is somewhat lower ($0.5 \cdot 10^{-8}$ cm^3STP/g). In contrast, case 2 yields much higher, seemingly unrealistic results for He_{rad} (8 to $10 \cdot 10^{-8}$ cm^3STP/g for the two deeper samples). The conclusions made before for the Ledo-Paniselian aquifer thus also apply for the Willersinnweiher samples.

sample	χ^2	p [%]	T [°C]	err T [°C]	A [ccSTP/kg]	F	q	v
GWMC 24	13.54	0.02	7.74	0.7	28.51	1.76	0.7	1.24
GWMC 13	5.83	1.58	8.09	0.59	20.01	1.83	0.72	1.32
GWMC 4	2.46	11.67	9.81	0.48	9.4	1.33	0.91	1.21

Table 3.3: Fit results for degassed samples from well GWMC near Lake Willersinnweiher. The fit has been done by the CE-model assuming F > 1 and using T, A, and F as a free parameters.

In addition to the Willersinnweiher samples, one sample from Egypt and some samples from Oman (compare chapters 5 and 6) are also considered in this section. For these single samples we do not have any evidence that degassing is a consistent feature, it may well be related to sampling artifacts. This is especially true for the Oman samples, which originate from open, sometimes carstic springs in the Oman Mountains.

Sample No. 19 from the southwestern Nile Delta area in Egypt (Table 5.2, chapter 5) seems to have been slightly degassed or to have undergone gas exchange with the atmosphere, possibly during sampling. This can be inferred from the Ne concentration, where the Ne equilibrium concentration ranges between $2.02 \cdot 10^{-7}$ and $1.78 \cdot 10^{-7}$ cm^3STP/g for the temperature range between 15 and 25 ^oC, while the measured Ne for that sample is only $1.74 \cdot 10^{-7}$ cm^3STP/g. This sample can in fact be fitted with no excess air or degassing at all (only T as a fit parameter), indicating that it may simply be re-equilibrated water. The best fit in terms of the deviation between model and data (lowest value of χ^2) is however achieved by the CE-model with F > 1, although this fit does not pass the χ^2-test because of the lower number of degrees of freedom (T, A, and F as fit parameters). The CE-model fit yields a very small value for A and a large value for F, which does not seem to be a very realistic description.

Nearly equilibrated water has also been observed in some samples collected from springs in the mountains of Oman (MA1a and AA1, see Table 6.1, chapter 6). These samples can reasonably well be described with little or no excess air. The inclusion of an additional fractionation or degassing parameter F does not significantly improve the fits. These samples are therefore not suited to investigate the different degassing models. It appears likely that these samples taken from open springs have experienced nearly complete equilibration before sampling.

Strange noble gas abundance patterns possibly indicating degassing have also been observed in some other samples from Oman (HA1c, MA4, and MA5, see Table 6.1, chapter 6). The CE-model with F > 1 does not yield a significant improvement over other models for these samples. They cannot be described with any available model, except for MA5, where the DD-model provides a reasonably good fit. It appears difficult to derive any general results from these few quite special samples.

Degassing of groundwater however seems to occur in many places, although it is certainly much less common than the ubiquitous phenomenon of excess air. Very strong degassing has been observed in some ultra-deep mine groundwaters of South

Africa by Lippmann et al. (2003). Degassing seems to be a quite common feature in the groundwaters of some tropical river delta regions (Bangladesh, Vietnam). Noble gas and ^{3}H-^{3}He studies have been conducted in these areas in connection with arsenic contamination problems, and have repeatedly encountered the problem of degassing (M. Stute, W. Aeschbach-Hertig, pers. Communication). The problem may be related to the occurrence of high amounts of organic material in these areas, leading to very reducing conditions in the subsurface and possibly to the formation of methane, which may lead to the formation of gas bubbles. Degassing has also been observed at industrially contaminated sites, probably for the same reason, i.e. methanogenesis under strongly reducing conditions. Very little has been published about degassed groundwaters so far, probably because the investigators found it difficult to interpret their data.

More research should therefore be done to enhance the performance of the degassing models, which might help to overcome the degassing problem that currently limits the use of gaseous tracers to study groundwater problems in some locations. The CE-model seems to provide a valuable description of many, although not all, degassed samples, indicating that degassing by equilibration with a gas phase may be a realistic process under natural conditions. It is possible that a better explanation of the degassed samples could be reached if different temperatures would be assumed for the initial and final equilibrations, or if more complex multi-step scenarios would be considered. Experiments under controlled conditions might be useful to investigate such more complex processes, because the number of unknown parameters could possibly be reduced.

Chapter 4

4 Groundwater dating by sulfur hexafluoride and CFCs

Sulfur hexafluoride (SF_6) and chlorofluorocarbons (CFCs) are volatile compounds of predominantly anthropogenic origin. Because these compounds are quite stable in the environment, their mixing ratios in the atmosphere have increased as a result of their industrial production and use during the last 4 to 6 decades. This increase combined with the mostly conservative behavior in water makes it possible to use these substances as transient environmental tracers for the dating of young groundwaters. The principle of dating rests on the known time-dependence of the atmospheric mixing ratios and is the same for SF_6 and the various CFCs. CFCs have been used in groundwater research since the early 1990s, but because of various problems they are in recent years increasingly being replaced by SF_6. In this work, both methods were applied, but essentially only SF_6 has produced useful results in the field studies in Egypt and Oman (see chapters 5 and 6). In this chapter, both methods will be discussed, but the main focus will lie on SF_6, for which attempts have been made to improve sampling and evaluation methods.

4.1 Properties of sulfur hexafluoride

Sulfur hexafluoride (SF_6) is a gas that is used in electrical power equipment. It is colorless, odorless, non-flammable and chemically stable. This means that at room temperature it does not react with any other substance. Stability comes from the symmetrical arrangement of the six fluorine atoms around the central sulfur atom. And this stability is just what makes the gas useful in electric equipment. SF_6 is a very good electrical insulator and can effectively extinguish arcs, which makes high and medium voltage apparatus filled with SF_6 highly popular. SF_6 is formed by a chemical reaction between molten sulfur and fluorine. Fluorine is obtained by the electrolysis of hydrofluoric acid (HF). Industrial production of SF_6 began in 1953 for use in high voltage electrical switches, and the annual production has increased from nearly zero to 85.700 t of SF_6 in 1995 (Maiss and Brenninkmeijer, 1998). SF_6 is released to the atmosphere and the tropospheric concentration of SF_6 has increased from a natural steady state value of 0.054 ± 0.009 pptv (parts per trillion by volume) to more than 4 pptv (Busenberg and Plummer, 2000) during the past 40 years. The atmospheric mixing ratio of SF_6 has increased from 0.9 pptv in 1976 (Maiss and Brenninkmeijer, 1998) to about 5 pptv in 2003 and continues to increase at a rate of about 1 pptv in 4 years. The accumulation of SF_6 in the atmosphere is due to:
(1) The long lifetime of SF_6 in the atmosphere, estimated to range from 1935 (Patra et al., 1997) to 3200 (Ravishankara et al., 1993) years. (2) The low solubility of SF_6 in water. (3) The lack of other significant natural sinks (Maiss and Brenninkmeijer, 1998). (4) The apparent high stability in soils (Maiss and Brenninkmeijer, 1998).

SF_6 has been extensively used in many oceanographic studies to determine horizontal and vertical turbulent mixing and air-sea gas exchange (e.g. Watson and Ledwell, 2000); it is also used to study longitudinal dispersion, gas exchange and vertical mixing in lakes and rivers (e.g. Clark et al., 1996; Von Rohden and Ilmberger, 2001).

SF_6 can be used as a dating tool in shallow groundwater if it attains equilibrium with atmospheric SF_6 at the time of recharge and does not contain significant SF_6 from any other sources. The dating range is currently 0-30 years (Busenberg and Plummer, 2000). This application of SF_6 is used in this work and will be discussed in detail in section 4.5.

Sulfur hexafluoride is primarily of anthropogenic origin but also occurs naturally in fluid inclusions in some minerals and igneous rocks, and in some volcanic and igneous fluids. Harnish and Eisenhauer (1998) reported the presence of SF_6 in fluorite and granites, also Busenberg and Plummer (1997) found large concentrations of SF_6 in hot springs from volcanic and igneous areas. These results give a good indication to the existence of a natural source of SF_6 and to the presence of SF_6 in the atmosphere before the industrial production of SF_6. As already mentioned, Busenberg and Plummer (2000) estimated the natural background atmospheric mixing ratio of SF_6 to be 0.054 ± 0.009 pptv.

4.2 The solubility of SF_6 in water

The solubility of SF_6 in water samples and the effect of temperature on solubility must be known to determine the equilibrium concentration of SF_6 in water samples. The solubility of SF_6 in fresh water has been measured by several authors like Friedman (1954), Ashton et al. (1968), Wilhelm et al. (1977) and Cosgrove and Walkley (1981). The effect of salinity has been studied by Morrison and Johnstone (1955); they indicated a 25% reduction in solubility, while Wanninkhof et al. (1991) recommended approximately a 30% reduction in solubility of SF_6 in seawater with a salinity of 35‰, they performed SF_6 solubility measurements in seawater at only one temperature (~22 ^oC) and in freshwater at temperatures from about 8-22 ^oC. They combined these studies with measurements in water and seawater and developed an equation describing the solubility of SF_6 as a function of temperature and salinity. The most recent and possibly most precise determination of the solubility of SF_6 has been performed by Bullister et al. (2002) for fresh and sea water over the temperature range of 0.5 °C to 40 °C.

The comparison of the different solubilities reported in the literature is complicated by the fact that many different forms and units of solubility are used. In the following, it is briefly discussed how these different forms can be converted to become comparable. As a reference form of solubility we use the dimensionless Henry coefficient H, or its inverse, the Ostwald solubility α. These forms of solubility occur as coefficients in Henry's law if the concentrations in both phases are given in units of mol/L, as in equations (2.5) and (3.5):

$$C_g = H \cdot C_w \quad \text{or} \quad C_w = \alpha \cdot C_g \quad \text{with} \quad \alpha = 1/H \tag{4.1}$$

We drop the index i for the different gases here and in the following, as we always refer to SF_6 in this section. Wanninkhof (1992) used the Bunsen solubility β to express the solubility of SF_6. The Bunsen coefficient is defined as the STP-volume of the dissolved gas (STP: T_0 = 0 °C, P_0 = 1 atm) per unit volume of water if the gas pressure is equal to P_0 = 1 atm. As all forms of solubility, β is a function of temperature and salinity, and was given by Wanninkhof (1992) as follows:

$$\beta(T,S) = \exp(75701 \cdot \ln(T) + 25060 \cdot \frac{1}{T} - 520602 - 0.0117 \cdot S) \tag{4.2}$$

where β is the Bunsen coefficient in [cm^3STP cm_w^{-3}], T is the temperature in Kelvin, and S is the salinity in ‰. The Ostwald solubility can be calculated from the Bunsen solubility β according to the following equation:

$$\alpha = \beta \cdot \frac{T}{T_0} \tag{4.3}$$

Bullister et al. (2002) performed laboratory measurements of the solubility of SF_6 in which volumes of water and sea water held at constant temperature in glass chambers were equilibrated with a gas mixture containing SF_6 and CFC-12 at ppt levels in nitrogen. Small-volume water samples were analyzed by electron capture gas chromatography. Bullister et al. (2002) referred to the alternative form of Henry's law, where the gas phase concentration is expressed as a partial pressure (see equations 2.6 and 3.18), and used an equation introduced by Warner and Weiss (1985) to describe the SF_6 solubility in terms of moist air equilibrium concentrations (compare eq. 3.22):

$$C^{eq}(T,S,P) = K'(T,S) \cdot (P - e) \cdot z \tag{4.3}$$

where K' is the partial pressure equilibrium constant (the inverse of the Henry coefficient H' in equations 3.18 or 3.22), P is the total atmospheric pressure, e is the saturation water vapor partial pressure, and z is the dry air mole fraction of the gas (SF_6 in our case). The method of least squares has been used to fit equations of the type used in previous solubility studies (e.g., Weiss, 1970, 1971) to describe K' as a function of temperature and salinity (see Appendix 2).

Warner and Weiss (1985) for CFCs and Bullister et al. (2002) for SF_6 defined a solubility function F = K'(P-e) to express equation (4.3). Since the function F explicitly contains the pressure dependence, these authors only gave expressions to calculate the values of F for P = P_0 = 1 atm. They also noted that their expressions for K' and F are only valid for total pressures near 1 atm and z << 1 to avoid corrections for non-ideality of the gas. However, in the range of environmental atmospheric pressures, K' is in very good approximation independent of pressure. We prefer to define a pressure-independent moist air solubility function G at the fixed reference pressure P_0, which is identical to the reported values of F (see also equation 3.28):

$$G(T,S) \equiv \frac{C^{eq}(T,S,P_0)}{z} = \frac{P_0 - e}{H'(T,S)} = K'(T,S)\cdot(P_0 - e) \qquad (4.4)$$

The pressure dependence of the moist air equilibrium concentration C_i^{eq} can then explicitly be given as follows (also see equation 3.29):

$$C^{eq}(T,S,P) = \frac{P - e}{P_0 - e} G(T,S) z \equiv rG(T,S) z \qquad (4.5)$$

with the dry gas pressure ratio

$$r \equiv \frac{P - e}{P_0 - e} \qquad (4.6)$$

The equation and constants which are used to calculate G according to Bullister et al. (2002) are given in Appendix 2.

By using the ideal gas law the solubility coefficient K' in its volumetric form (in mol L^{-1} atm^{-1}) can be converted to the Ostwald solubility α as follows:

$$\alpha = RTK' \qquad (4.7)$$

The comparison between different SF_6 solubilities in terms of dimensionless Ostwald coefficients (Figure 4.1) shows a good agreement between the solubilities of Bullister and Wanninkhof for fresh water over a temperature range of 10-30 °C, but they differ by nearly 10 % at 0 °C and by nearly 9 % at 40 °C. Also the agreement between the solubilities of Bullister and Wilhelm for fresh water is relatively good over the temperature range 8-25 °C, but they differ by nearly 3.5 % at 0 °C and by 3.5-10 % in the range of 26-40 °C. For sea water, the Bullister and Wanninkhof solubilities differ by 5-7 % at 0 °C and at temperatures over 20 °C. These disagreements at the higher and lower ends of the temperature range were discussed by Bullister et al. (2002). They mentioned that these disagreements are somewhat greater than the estimates for the accuracies of the solubility functions (~2 % in their study and ~5 % in Wanninkhof, 1992). Part of the reason for these differences may be the limited temperature range of the fresh water (~8-20 °C) and sea water (~22 °C) measurements in the Wanninkhof (1992) study, and the less accurate fit of the solubility functions at significantly higher and lower temperatures.

Figure 4.1 furthermore shows that the temperature dependence of the SF_6 solubility is very strong in the rang of environmental temperatures. This is an important problem for application of SF_6 in groundwater, because accurate estimates of the recharge temperature are necessary to be able to calculate the equilibrium concentrations with sufficient precision.

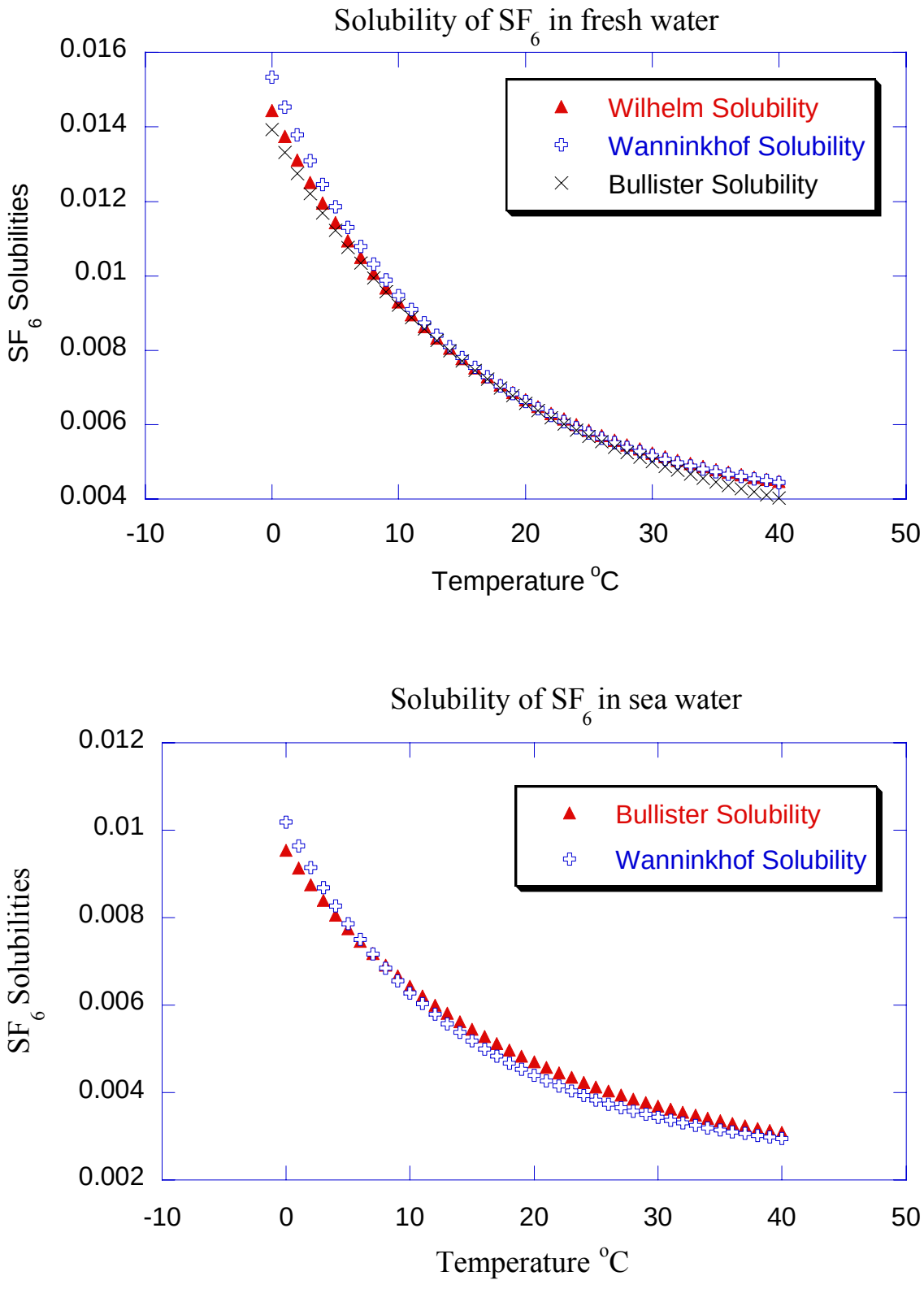

Figure 4.1: The solubility of SF_6 in fresh water and sea water

4.3 Atmospheric history of SF_6

The potential of SF_6 as a useful tracer in atmospheric and marine studies was recognized by Lovelock (1971), who made the first atmospheric measurements. The first attempt to reconstruct the atmospheric history from an oceanic depth profile has been done by Watson and Liddicoat (1985). The atmospheric growth history of SF_6 has been described by several authors e.g. Ko et al. (1993), Maiss and Levin (1994), Law et al. (1994), Maiss et al. (1996) and Geller et al. (1997). Maiss and Brenninkmeijer (1998) recognized the presence of a natural background concentration of atmospheric SF_6, i.e. they noticed that the concentration extrapolated back to the year of 1970 did not equal zero, as was assumed in their earlier work (Maiss et al., 1996). They also calculated the pre-1970 atmospheric history of the tracer from production data, their estimated natural background, and atmospheric measurements. The history of the atmospheric mixing ratio of SF_6 according to Maiss and Brenninkmeijer (1998) is shown in Figure 4.2.

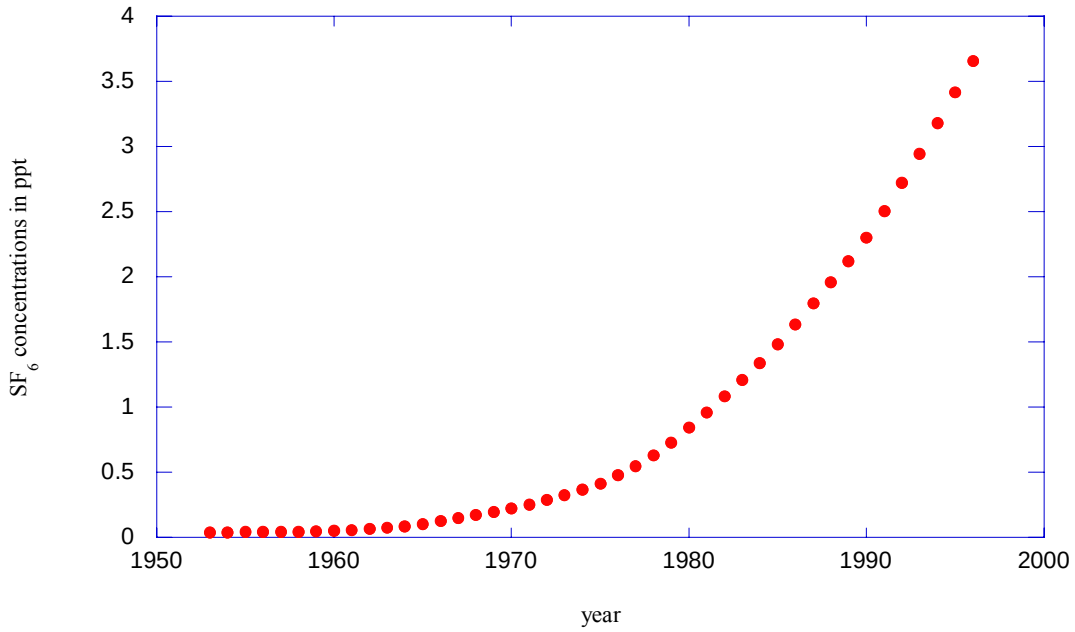

Figure 4.2: The atmospheric concentrations of SF_6 as estimated by Maiss and Brenninkmeijer (1998), they calculated the pre-1970 atmospheric history of SF_6 from production data.

Busenberg and Plummer (2000) compared the Northern Hemisphere growth curve calculated from the equation given by Geller et al. (1997) and the Northern Hemisphere growth curve calculated from the equation of Maiss and Brenninkmeijer (1998) with more than 250 measurements of SF_6 in air from various parts of the USA. They found that the atmospheric history of SF_6 was slightly revised using the natural background of 0.054 pptv, and that the Northern Hemisphere growth curve calculated from the equation of Maiss and Brenninkmeijer (1998) gave a slightly better fit to the North American air data and was thus used to date US groundwater. The Northern Hemisphere growth curve calculated from the equation of Maiss and Brenninkmeijer (1998) is also used in this work to date groundwater of the southwestern Nile Delta, Egypt, and the Oman Mountains (see chapters 5 and 6).

4.4 Sampling, extraction, and measurement of SF_6 samples

Samples of SF_6 have been collected by two different methods. The usual method at the Institute of Environmental Physics in Heidelberg uses special glass sampling bottles (Figure 4.3). These sampling bottles with know volumes between 0.5 and 1 L are prepared in the laboratory by flushing and filling all bottles with ultrapure nitrogen, and are then closed with some overpressure to prevent air contamination during transport. Just before taking the water sample, the bottles are evacuated to a pressure of 0.2 - 0.5 atm, depending on the concentrations expected. The filling starts through valve V1, the bottle upside down, creating an absolute pressure of about 1100–1300 mbar in the remaining N2-headspace. Due to the pressure drop within the bottle at the beginning of the filling, the strong degassing of the sample water helps to reach the equilibrium.

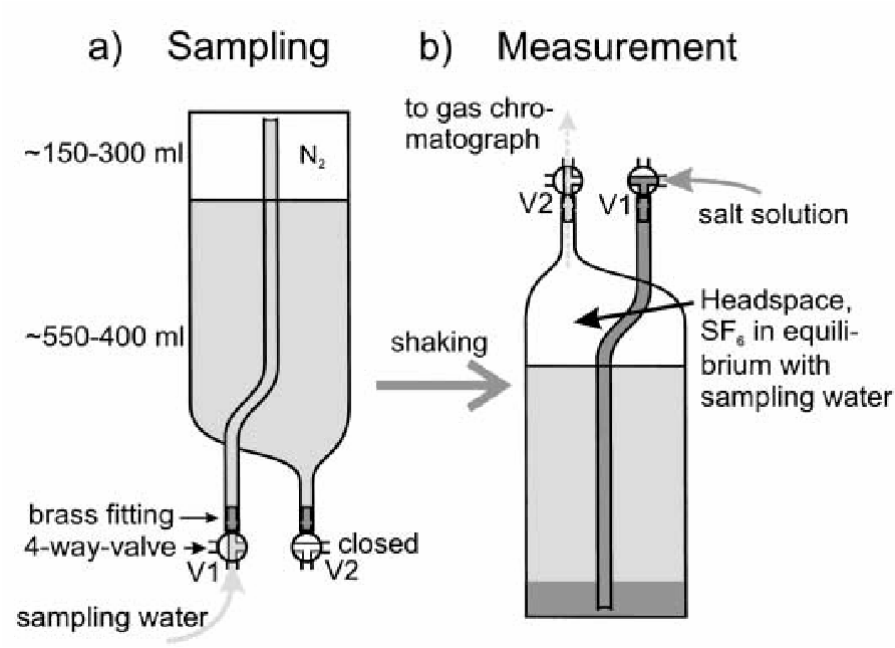

Figure 4.3: Sampling bottles (Von Rohden and Ilmberger, 2001)

These sampling bottles are adapted to fit seamlessly with the following laboratory measurements of SF_6 concentrations in the headspace gas using the method reported by Wanninkhof et al. (1991). In the closed bottle (Figure 4.3), the water sample is shaken under controlled pressure and temperature conditions to achieve SF_6 equilibration between water and the nitrogen headspace. A gas chromatographic system (Shimadzu GC-8AIE) with an electron capture detector (ECD) specifically designed for SF_6 by Maiss (1992) is used for the headspace measurements. After gravimetrical determination of the sample water and consequently the gas volumes, a SF_6 mass balance is applied to calculate the original sample concentration C_w from the measured headspace concentration C_h', assuming solubility equilibrium between the water and gas volumes at the time of the analysis:

$$C_w = C'_h\left(\frac{V_h}{V_w} + \alpha(T,S)\right) \qquad \left[\frac{fMol}{l}\right] \qquad (4.8)$$

where V_h and V_w are the volumes of headspace and water, respectively and α is the SF_6 solubility.

Alternatively, samples of SF_6 can also be collected in 500 ml stainless steel cylinders (Whitey, 304L-HDF4-500, Arbor Inc) equipped with two plug valves (Nupro, SS-4P4T1, Arbor Inc). The cylinder can be connected with the wells or pump by using any material including plastic, rubber, or metal tubing, provided that all connections are airtight and will not come loose when back pressure is applied during closing of the stainless steel cylinder. Clear plastic tubing (Tygon) is preferred because one can visually observe whether air bubbles are present in the water line. Squeezing and bending the hoses or knocking against the cylinder can remove the bubbles that tend to stick at connections or inside the stainless steel cylinder. After filling the stainless steel cylinder with water samples, the two plug valves are closed, sealing off the sample gas-tight. Because the sampling cylinders are pressurisable, no care has to be taken about expansion of the water due to warming.

Advantages of the stainless steel cylinders over the usual glass bottles are their ease of use in the field, their robustness, and the fact that no special preparations are necessary. The main disadvantage is that samples collected in this way can not directly be analyzed with the existing system. For measuring the SF_6 concentration in the water samples the water has to be transferred from the stainless steel cylinders to the 500 ml glass sampling bottles. The sampling bottles must be evacuated and flushed with ultrapure nitrogen, and then closed with some overpressure to avoid any contamination. Before the water transfer the bottles are evacuated to about 0.2 atm pressure. The success of the water transfer process (Figure 4.4) mainly depends on transferring the water samples from stainless steel cylinders without any contact with the atmosphere. To achieve this, all tubes of the connection must be evacuated. Salt water prepared in the laboratory has been used to push the sample water from the cylinder to the sampling bottle. Mixing between water sample and the salt water can be recognized by adding a red color to the salt water. After the transfer process the SF_6 concentration in the water samples can be measured as described above for the headspace bottles. The transfer process is summarized in the following steps:

(1) Salty, colored water is filled in a 1L glass sampling bottle (bottle A), keeping a small headspace inside.
(2) Connect V2 at bottle A with a pure nitrogen gas bottle and V1 with the stainless steel cylinder using a tygon hose with a three-ways valve at both ends.
(3) Connect a second glass sampling bottle (bottle B) with the stainless steel cylinder.
(4) Evacuate all tubes of the connection.
(5) Let the salt water move in the tygon hose by opening V1 at bottle A, and let pure nitrogen enter the bottle A, creating an over pressure by opening V2.

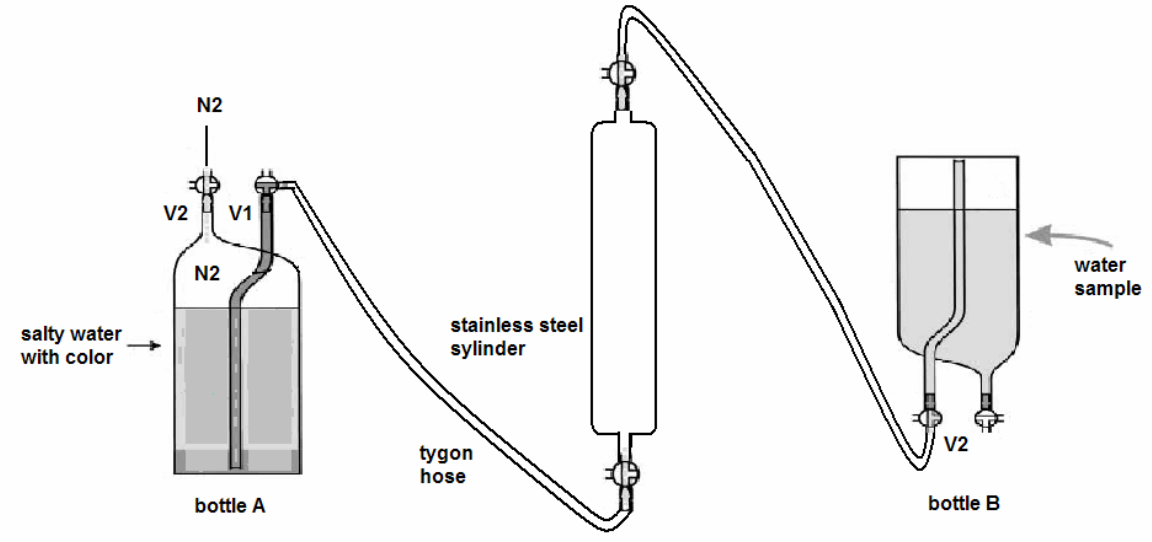

Figure 4.4: Transfer of a water sample from a stainless steel cylinder to a glass bottle

(6) Open the three-ways valve at the second end, which connects to the cylinder to flush the tube and remove all the bubbles that tend to stick at the inner wall of the tube, and then close the three-ways valve.
(7) Open the bottom plug valve of the cylinder and then open the upper valve slowly.
(8) Open V2 on bottle B to fill it with the water sample.
(9) After finishing the transfer process, close V2 at bottle B, and the plug valves of the cylinder.

All tubes of the connection must be cleaned and dried before transferring a new water sample from another cylinder.

To test the reliability of the water transfer procedure, samples have been collected from a single location in Willersinnweiher Lake, which is a small quarry pond in the congested urban area of Ludwigshafen/Rhein, Germany. Eight samples were collected in normal glass bottles (Figure 4.3), and six samples were collected in stainless steel cylinders. All samples were measured in the limnology laboratory of the Institute of Environmental Physics in Heidelberg, using the techniques described above. The measured concentrations of samples collected in glass bottles are considered as reference values. Figure 4.5 shows that there are no big concentration differences between the samples collected in glass bottles, the results of these samples are reproducible within a small error of about 2%. In contrast, the concentrations of the samples collected in stainless steel cylinders exhibit large differences. Two of the six samples were lost during the transfer, for reasons described below. Only two of the four analyzed samples give nearly the same concentration, which agrees well with the mean value obtained from the glass bottles. The other two samples show two different behaviors: One of them has a too high concentration, while the second has a too low concentration. These deviations can be explained as follows:

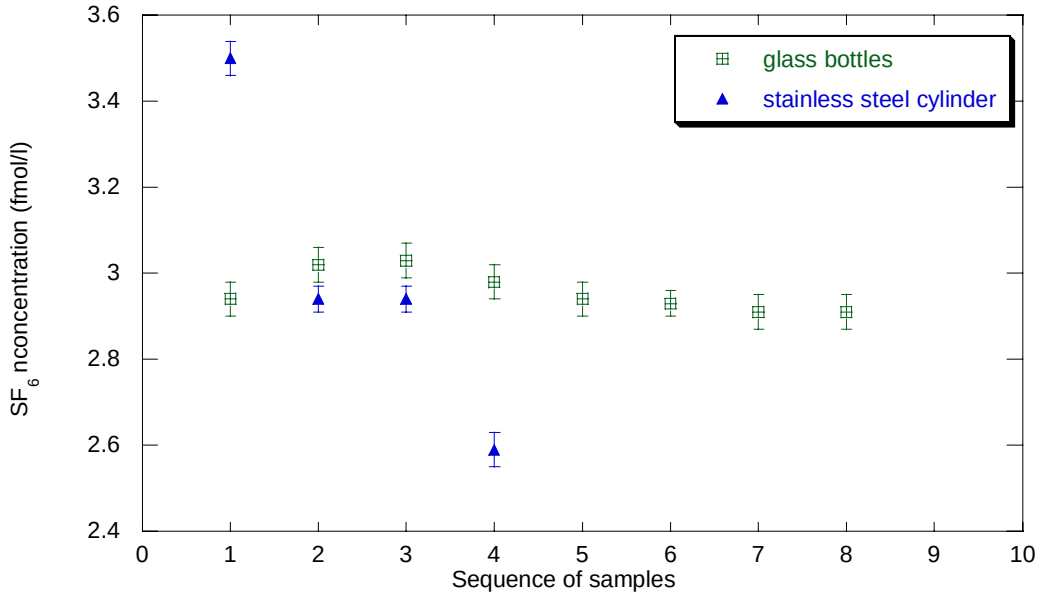

Figure 4.5: SF_6 concentration of samples collected by two different methods

The sample with the high concentration might have been contaminated during the transfer procedure by air bubbles sticking at the inner wall of the tygon hose, which connects bottle A with the stainless steel cylinder. During the movement of the salt water through the hose these bubbles, if not removed during step 6 of the above procedure, may be flushed into the steel cylinder and finally enter the glass bottle B. Air contamination may also originate from incomplete evacuation of the connecting lines or from leaky connections.

The sample with the low concentration might be explained by degassing during the transfer of the water sample from the stainless steel cylinder to the glass bottle B. Gas bubbles can form during this step, which tend to stick at the inner wall of the hose and must be removed to enter the bottle B. Sometimes these bubbles can not be avoided and result in measured concentrations lower than the actual concentration of the water samples.

One more precaution must be considered during the transfer: The over-pressure created by the nitrogen in bottle A must be controlled, otherwise it leads to strong mixing between the salt water and the sample water in the stainless steel cylinder. The color added to the salt water is very useful to detect this effect, visible by the color of the mixed water in the tubing between the cylinder and bottle B. This effect took place in two of the six samples, which thus became useless and were not analyzed.

The apparently correct and nearly identical results of two samples indicate that if the effects discussed above can be avoided, the measured concentrations should be unaltered and reproducible with the same precision as the reference glass bottle samples. Obviously, the failure rate of the transfer procedure needs to be reduced dramatically in order to render its combination with sampling in stainless steel cylinders a reliable method of SF_6 sampling and analysis.

The method discussed here was further tested by Klement (2005), along with other ways of sampling and sample preparation for the measurement. This study showed that although the salt water transfer seems to work in principle, it has a high potential of problems due to improper handling and requires a rather large and cumbersome effort. An alternative transfer method, where the sample water is directly pushed into an evacuated glass bottle by pure nitrogen gas, i.e., without the intervening salt water, appeared to be simpler and more reliable.

4.5 Dating young groundwater by SF_6

Young groundwater can be dated by SF_6 because of the following facts:

(1) The concentration of SF_6 increases in the atmosphere with a high rate (nearly 7 % per year).
(2) The historical concentration of SF_6 in the atmosphere is known (Maiss and Brenninkmeijer, 1998)
(3) SF_6 has an apparent stability in soils (Maiss and Brenninkmeijer, 1998), it appears to be resistant to biodegradation and does not significantly sorb onto organic matter (Wilson and Macky, 1996). The low reactivity of SF_6 is not due to thermodynamic stability but because of kinetic factors (Busenberg and Plummer, 2000). SF_6 has a high inertness, especially to hydrolysis because of the octahedral coordination of sulfur, the complete saturation of sulfur, the steric hindrance, the lack of polarity of the molecule and the high S-F bond strength (Cotton and Wilkinson, 1972).
(4) SF_6 does not readily sorb into rubber and polymers; therefore groundwater is less likely to be contaminated with SF_6 from contact with these materials during sampling than in the case of CFCs (Busenberg and Plummer, 2000).

The measured concentration of SF_6 can be attributed to several components and effects according to the following mass balance equation:

$$C_{SF_6}^{meas} = C_{SF_6}^{eq} + C_{SF_6}^{exc} + C_{SF_6}^{terr} + C_{SF_6}^{cont} - C_{SF_6}^{loss} \tag{4.9}$$

Where $C_{SF_6}^{meas}$ is the measured SF_6 concentration, $C_{SF_6}^{eq}$ is SF_6 concentration in solubility equilibrium with the atmosphere, which is a function of temperature, pressure and salinity (see eq. 4.5) and also of time (through the increase of the atmospheric mixing ratio z_{SF_6}), $C_{SF_6}^{exc}$ is the supersaturation of SF_6 derived from the dissolution of air bubbles as a result of fluctuation of the water table (excess air), $C_{SF_6}^{terr}$ is the natural (terrigenic) concentration of SF_6, $C_{SF_6}^{cont}$ is the concentration added to groundwater from any anthropogenic source (contamination), and $C_{SF_6}^{loss}$ is the removed SF_6 by sorption, biodegradation, matrix diffusion, degassing, or any other removal process.

The estimation of the groundwater residence time by SF_6 relies on the time-dependent increase of the atmospheric mixing ratio z_{SF_6} and consequently of the equilibrium concentration $C_{SF_6}^{eq}$. One therefore needs to determine this equilibrium component from

the measured total SF_6 concentration by correcting for all other contributions. The excess air term plays a very important role in this correction, because almost all groundwaters are apparently supersaturated with air at the time of recharge. The amount of excess air can be influenced by many factors such as climate, lithology, recharge temperature and mean annual precipitation (Aeschbach-Hertig et al., 1999, 2002). Excess air concentrations range usually from nearly zero to 3 cm^3STP/kg (Wilson and McNeill, 1997) but the concentrations can become as high as 18 cm^3STP/kg when the recharge happens during times of flooding in a semi arid climate (Glynn and Busenberg, 1996). The presence of excess air in the water samples means that the SF_6 concentration of the groundwater sample will be higher than the air-water equilibrium concentration and if the presence of excess air is not considered in the calculation of the residence time by SF_6, then the calculated age will be too young.

In the typical case, when there is no significant contribution of SF_6 originating from natural or any anthropogenic sources and also no loss of SF_6, then the last three terms in equation (4.9) can be neglected. Further assuming that excess air is due to complete dissolution of atmospheric air (UA-model, equation 2.17), the mass balance equation can be written in the form

$$C_{SF_6}^{meas} = C_{SF_6}^{eq} + C_{SF_6}^{exc} = C_{SF_6}^{eq} + A \cdot z_{SF_6} \tag{4.10}$$

where A is the excess air concentration and z_{SF_6} is the atmospheric mixing ratio of SF_6 in dry air.

Equation (4.10) can easily be solved for the equilibrium component if the excess air concentration A is known (e.g. from noble gas measurements), and if the atmospheric mixing ratio of SF_6 in dry air z_{SF_6} is known. Unfortunately this latter value is not known, because it depends on the unknown time of infiltration. Busenberg and Plummer (2000) proposed an iterative procedure to determine z_{SF_6} such that it is consistent with the age (recharge time) determined from the equilibrium component. In this procedure, the excess air correction is made with an initial value of z_{SF_6}, which is then revised based on the calculated corrected age and used for a new correction, and so on, until the procedure converges. Although this procedure is fairly simple, there is a more direct way to perform the excess air correction. The key to the solution of this problem is the notion that for any conservative gas i both C_i^{eq} and C_i^{exc} are linear functions of z_i. Therefore the ratio C_i^{exc} / C_i^{eq} is independent of z_i and can be calculated for SF_6 or any other gases if it is known for one (e.g. Ne). This is demonstrated in the following for the typical case where the SF_6 excess is estimated from that of Ne (which is often used to characterize the excess air component). The equilibrium concentration in equation (4.10) can be expressed by Henry's law in the form of equation (4.5):

$$C_{SF_6}^{eq} = rG_{SF_6} z_{SF_6} \tag{4.11}$$

then equation (4.10) can be written as:

$$C_{SF_6}^{meas} = C_{SF_6}^{eq} + C_{SF_6}^{exc} = rG_{SF_6} z_{SF_6} + Az_{SF_6} = \left(rG_{SF_6} + A\right) z_{SF_6} \tag{4.12}$$

The ratio $C_{SF_6}^{exc} / C_{SF_6}^{eq}$ for SF_6 can thus be written in the following form

$$\frac{C_{SF_6}^{exc}}{C_{SF_6}^{eq}} = \frac{A}{rG_{SF_6}} \tag{4.13}$$

This ratio can also be written for Ne (or any other gas):

$$\frac{C_{Ne}^{exc}}{C_{Ne}^{eq}} = \frac{A}{rG_{Ne}} \tag{4.14}$$

By combining equations 4.13 and 4.14 we obtain a relationship between the ratios C_i^{exc} / C_i^{eq} for SF_6 and for Ne:

$$\frac{C_{SF_6}^{exc}}{C_{SF_6}^{eq}} = \frac{C_{Ne}^{exc}}{C_{Ne}^{eq}} \frac{G_{Ne}}{G_{SF_6}} \tag{4.15}$$

The amount of excess air is often reported as a relative Ne excess ΔNe in %, which is equal to $\frac{C_{Ne}^{exc}}{C_{Ne}^{eq}} \cdot 100$, so that equation 4.15 can be written in the form (also using equation 4.10 to eliminate $C_{SF_6}^{exc}$):

$$\left(\frac{C_{SF_6}^{meas}}{C_{SF_6}^{eq}} - 1 \right) = \frac{\Delta Ne}{100} \cdot \frac{G_{Ne}}{G_{SF_6}} \tag{4.16}$$

The equilibrium concentration of SF_6 can thus be calculated from the amount of excess air by using the last equation which can also be written in the form

$$C_{SF_6}^{eq} = \frac{C_{SF_6}^{meas}}{1 + \frac{\Delta Ne}{100} \cdot \frac{G_{Ne}}{G_{SF_6}}} \tag{4.17}$$

Of course, equation (4.17) is also valid for any other pair of conservative gases.

So far, the simplifying assumption of unfractionated excess air has been made. However, the above considerations can easily be generalized to the case of excess air according to the CE-model. In this case, the excess air component of any conservative gas i can be written as follows (see equation 3.31):

$$C_i^{exc} = \frac{\left(1 - F\right) Az_i}{1 + AF / rG_i} \tag{4.18}$$

The ratio of the excess air and equilibrium components is then given by (compare equation 4.13 for the case of unfractionated excess air):

$$\frac{C_i^{exc}}{C_i^{eq}} = \frac{(1-F)A}{rG_i + AF} \tag{4.19}$$

This ratio is again independent of the atmospheric mixing ratio z_i and only differs between the gases because of their different solubility functions G_i. The relationship between the ratios C_i^{exc}/C_i^{eq} for SF_6 and for Ne now becomes (compare equation 4.15):

$$\frac{C_{SF_6}^{exc}}{C_{SF_6}^{eq}} = \frac{C_{Ne}^{exc}}{C_{Ne}^{eq}} \frac{rG_{Ne} + AF}{rG_{SF_6} + AF} = \frac{C_{Ne}^{exc}}{C_{Ne}^{eq}} \frac{G_{Ne} + AF/r}{G_{SF_6} + AF/r} \tag{4.20}$$

The factor relating the relative excesses of the two gases is now not simply given by the ratios of the solubilities, but is modified by the term AF/r. If this term is small compared to the solubilities (e.g. small values of A or F), the factor approaches the ratio of the solubilities, as in the case of unfractionated excess air (equation 4.15). If the term is large compared to the solubilities (large or strongly fractionated excess air), the factor approaches unity, which means that the relative excesses of the two gases are equal. This is the limiting case that can be interpreted as a pressure effect as already discussed in section 3.3.3 (equation 3.33).

Equation (4.20) can be used to calculate the equilibrium component of SF_6 from the relative Ne excess ΔNe for the general case of fractionated excess air according to the CE-model. In analogy to equation (4.17) one obtains:

$$C_{SF_6}^{eq} = \frac{C_{SF_6}^{meas}}{1 + \frac{\Delta Ne}{100} \cdot \frac{G_{Ne} + AF/r}{G_{SF_6} + AF/r}} \tag{4.21}$$

In order to determine the age of a groundwater sample, the equilibrium concentration of SF_6 calculated from equation (4.21) or (4.17) is related to the time dependent atmospheric mixing ratio $z_{SF6}(t)$ by using equations (4.3) or (4.11):

$$C_{SF_6}^{eq}(T,S,P,t) = r(P)\,G_{SF_6}(T,S)\,z_{SF_6}(t) = K'_{SF_6}(T,S)\cdot(P-e)\cdot z_{SF_6}(t) \tag{4.22}$$

Of course the equilibrium conditions T, S, and P need to be known to calculate $z_{SF6}(t)$ from this relationship. These parameters, and in addition the excess air parameters A and F, also need to be known to evaluate equations (4.21) or (4.17). In principle, the only reliable way to obtain this information is from model fits to measured noble gas concentrations. In this work, SF_6 samples were always combined with noble gas samples, so that this complete information was available. In many other studies, this is not the case. At least one conservative gas, preferably Ne, should however be measured in order to be able to perform an approximative excess air correction. In this

case, the equilibrium conditions T, S, and P have to be estimated and unfractionated excess air has to be assumed. Then, equations (4.17) and (4.22) can be evaluated.

The value of z_{SF_6} obtained from equation (4.22) is finally compared to the atmospheric history of SF_6 (see section 4.3) to determine the time of equilibration and thus the groundwater age or residence time, which is defined as the time that has passed since this last contact with the atmosphere.

4.6 Dating groundwater by chlorofluorocarbons (CFCs)

Chlorofluorocarbons (CFC-12, CFC-11 and CFC-13) are stable and synthetic anthropogenic organic compounds, they are nonflammable, noncorrosive, nonexplosive, very low in toxicity, and nonreactive with other chemical species. They are man-made volatile organic compounds widely used as refrigerants and occurring in many manufactured goods. The atmospheric concentration of CFCs has been increasing since their creation in the 1940s. Atmospheric concentrations have been measured for approximately 30 years and concentrations before 1960 are estimated from manufacturing records. Recently, concentrations of CFCs have leveled off and in the case of CFC-11 and CFC-113 have begun to decrease somewhat due to reduced production, atmospheric loss (by reaction) and transfer of CFCs from the atmosphere to the oceans. Figure 4.6 shows the atmospheric history of the concentrations of CFCs, also in comparison with that of SF_6. The fact that the SF_6 concentration still rises rapidly is a major advantage of SF_6 over the CFCs for tracer applications aimed at dating very young waters.

CFCs have emerged as useful age-dating tracers for young ground water (Thompson and Hayes, 1979; Plummer et al., 1993). For atmospheric tracers, the age of ground water is defined as the time since the water was in contact with the atmosphere. Conceptually, recharge to the saturated zone is in chemical equilibrium with the atmosphere at the water table, and below in the saturated zone that concentration is maintained. Hence, if the atmospheric concentration changes in time, then different concentrations in ground water presumably correspond to different recharge times, and different ages.

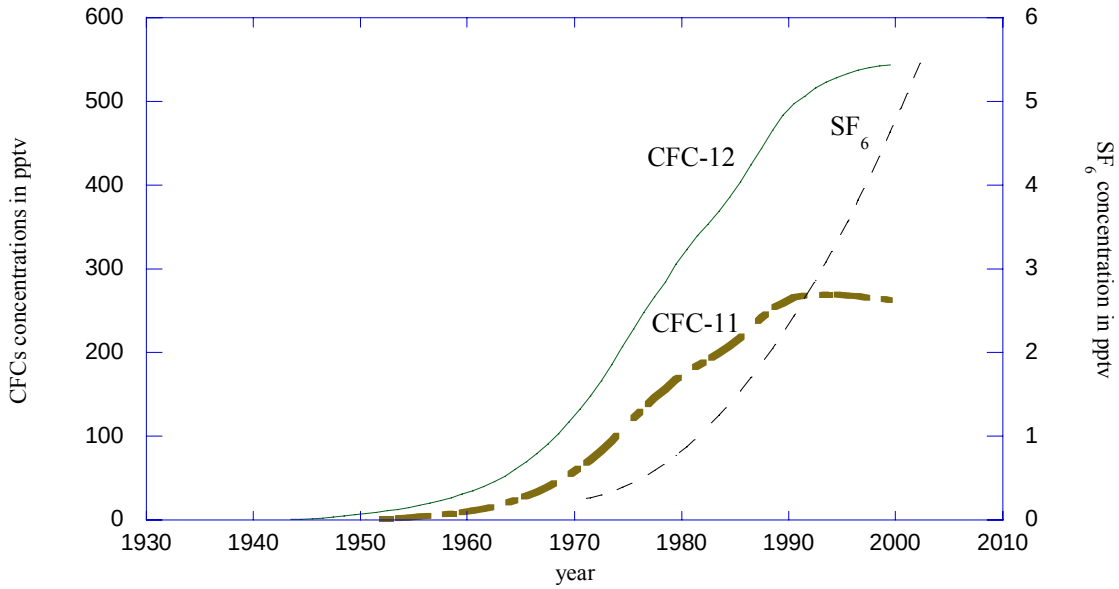

Figure 4.6: Concentrations of CFCs and SF_6 in the atmosphere, CFCs have started to decline in 1990 due to a global ban, while SF_6 is accumulating rapidly and is a promising alternative tracer to CFCs.

The concepts of groundwater dating by CFCs are completely analogous to those discussed above for SF_6. By measuring CFC concentrations in groundwater and determining or estimating the recharge temperature of the groundwater, a CFC-model age can be assigned to the sample. Apparent CFC ages are obtained by converting measured CFC concentrations in groundwater to equivalent air concentrations using known solubility relationships (Warner and Weiss, 1985) and the recharge temperature. Corrections for excess air are made if appropriate (Busenberg and Plummer, 1992). The equilibrium concentrations are compared with the atmospheric concentration curve (Figure 4.6) to obtain an apparent CFC age. Because all these steps have been discussed above in detail for the case of SF_6, the following discussion of CFCs mainly focuses on the aspects that are specific for CFCs.

An advantage of CFCs is that their input began comparatively early, thus dating may reach back until the 1940s in the case of CFC-11 and CFC-12. On the other hand, the recent stop of the atmospheric growth severely limits the ability to date very young water. However, the ability to date groundwater that entered the saturated zone prior to the 1990s will probably not change for several decades.

Another advantage of CFCs is that in addition to the use of individual CFC compounds to date groundwater, the ratios of atmospheric CFC concentrations can also be used for groundwater dating. Figure 4.7 shows a reconstruction of the ratios of CFC-11/CFC-12 and CFC-113/CFC-12 in remote North American air. The ratio of CFC-11/CFC-12 in air increased dramatically from the late 1940s to about 1977, and that of CFC-113/CFC-12 had a modest increase during the 1980s.

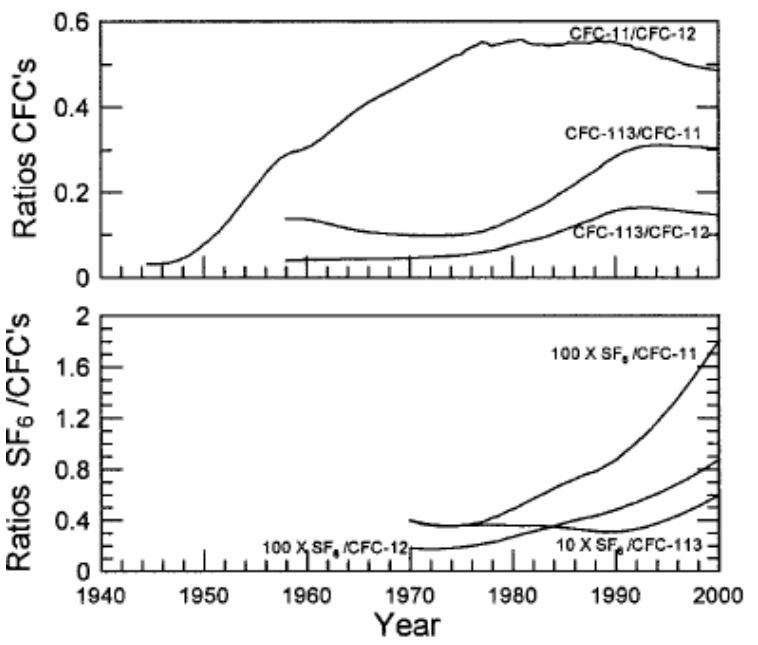

Figure 4.7: Ratio of the partial pressures of CFCs and the ratio of the partial pressures of SF_6 to CFCs in North American air as a function of time (Busenberg and Plummer, 2000)

The solubilities of CFC-11 and CFC-12 in water and sea water have been determined by Warner and Weiss in 1985 for the temperature range of 0 to 40 °C and salinities between 0 and 40 per mil. The solubilities were reported in the same form as later used by Bullister et al. (2002) for SF_6 and as has been discussed above (see equations 4.3 to 4.7 and Appendix 3). An important difference compared to SF_6 is that the solubilities of the CFCs are much larger, by more than an order of magnitude. As a consequence, the CFCs are much less sensitive to air contamination during sampling or analysis, as well as to the presence of excess air. In many cases, the excess air correction can be neglected without introducing significant errors.

In addition to excess air formation, however, there are a number of processes that affect the CFC concentrations in groundwater and thus the apparent CFC ages, e.g. the effect of recharge temperature, the effect of the thickness of the unsaturated zone, the effect of contamination, and the effect of microbial activity. These effects have been discussed in details by Plummer and Busenberg (1999). In the following we will focus only in two effects that might affect our groundwater samples, these are:

(1) The effect of the thickness of the unsaturated zone

The apparent CFC age is based on the assumption of equilibrium of infiltration water with tropospheric air at the time of recharge. This assumption is approximately true for unsaturated zone thickness less than 10 m but with increasing thickness of the unsaturated zone, the gas transport through the unsaturated zone plays a larger role in the interpretation of the apparent CFC age. The presence of a very thick unsaturated zone can substantially modify the concentrations of CFC-11 and CFC-12 and their ratios in the soil air, resulting in erroneous apparent CFC recharge ages. Increasing thickness of the unsaturated zones leads to the occurrence of lag times which affect

the calculated apparent CFC ages. Cook and Solomon (1995) presented theoretical calculations of the lag times for apparent CFC-11, CFC-12 and CFC-113 ages for water recharged through thick unsaturated zones of 0 - 40 m. They found that lag times were mostly dependent on gas solubility, gas diffusion coefficient, and soil water content. The extent to which unsaturated zone gas transport processes affect the apparent CFC age depends also on the predominant recharge mechanism, and physical and hydraulic properties of the unsaturated zone. Figure 4.8 shows the lag times for water recharged through an unsaturated zone of 0 - 40 m thickness. This figure also shows that a similar effect has to be expected for SF_6.

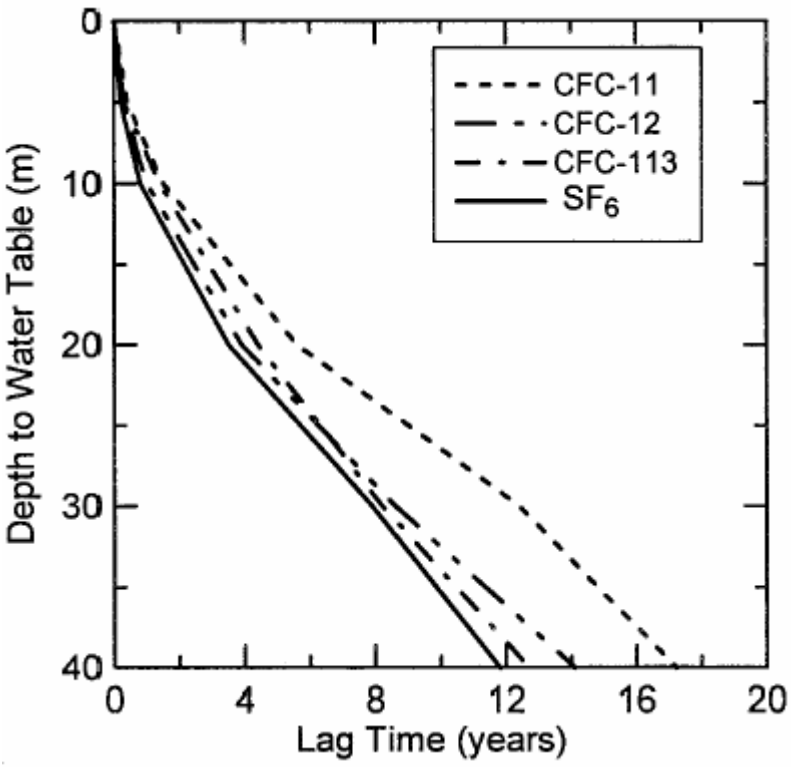

Figure 4.8: the lag times for water recharged through unsaturated zone of 0 - 40 m thickness. The thickness of unsaturated zone has a similar effect on SF_6. (Busenberg and Plummer, 2000)

(2) The effect of groundwater contamination

An important restriction of the use of CFCs as a dating tool of groundwater comes from the occurrence of non-atmospheric sources, that can lead to concentrations in groundwater that are greater than the value for equilibrium with tropospheric or even urban air. Groundwater from urban and industrial areas is often contaminated with CFCs. The addition of CFC contamination to groundwater can usually be attributed to anthropogenic point sources such as discharge from septic tanks, leaking sewer lines, leakage from underground storage tanks, discharge or injection of industrial wastes, and recharge from rivers carrying effluent from sewage treatment plants (Plummer and Busenberg, 1999). Beyerle et al. (1999) showed that dating groundwater in the Linsental aquifer (Switzerland) was impossible because of contamination. The expected CFC concentrations of the groundwater in the Linsental aquifer were in the range of 800 to 1500 pg/kg for CFC-11 and of 300 to 500 pg/kg for CFC-12.

However, the measured CFC concentrations in the Linsental aquifer varied from 1000 up to 4100 pg/kg for CFC-11 and from 320 up to 730 pg/kg for CFC-12. In chapter 6 the effect of contamination is found to also limit the use of CFC to date Oman groundwater. In this case, the contamination might come from sampling for CFCs under very difficult conditions.

Chapter 5

5 A multi-tracer study of groundwater in reclamation areas south-west of the Nile Delta, Egypt

5.1 Introduction

The high and rapidly growing population density and the constant rate of inflow of Nile river water in Egypt is a great challenge to the Egyptians. To solve this problem, Egypt adopted aggressive policies to develop new agricultural communities outside the overpopulated Nile Delta and Nile valley. Such newly developed so-called reclamation areas depend almost exclusively on groundwater as water resource. For the long-term sustainability of these developments it is of central importance to understand the processes and rates of recharge of the groundwater resources.

The reclamation area under investigation in this study is located near the south western Nile Delta (Figure 5.1). It is mainly depending on groundwater, and several studies have been performed to investigate groundwater in this area. In this study, several different environmental tracer methods are applied, namely SF_6, and ^3H-^3He are used to date the shallow groundwater, whereas noble gases and stable isotopes are used to obtain information on the conditions during recharge and to study groundwater mixing (see Cook and Herczeg, 2000, for reviews of the applied tracer methods). The main goal of this work is to determine the main recharge resources and the recharge rate, which will be important to plan for the future of this area.

5.2 Study area

The investigation area is located southwest of the Nile delta; between about 30° 00′ to 30° 30′ N and 30° 10′ to 31° 05′ E, in the arid province of Egypt, within about 100 km west-northwest of Cairo. Its climate is characterized by a long hot summer and a short warm winter, the maximum air temperature is reached in August and lies typically at about 36 ^oC, whereas the minimum air temperature of about 6 ^oC is observed in February. Monthly mean temperatures in Cairo vary between about 14 °C in January/February and 28 °C in July/August. The mean annual rainfall increases from 30 mm at Wadi El Natrun to 80 mm at El Tahrir. The relative humidity is generally higher in the summer season than in winter, the highest annual relative humidity is 69.2 % at El Tahrir and the lowest recorded value is 53.7 % at Wadi El Natrun. The area also characterized by a high evaporation rate, e.g. about 13.8 mm/day in June.

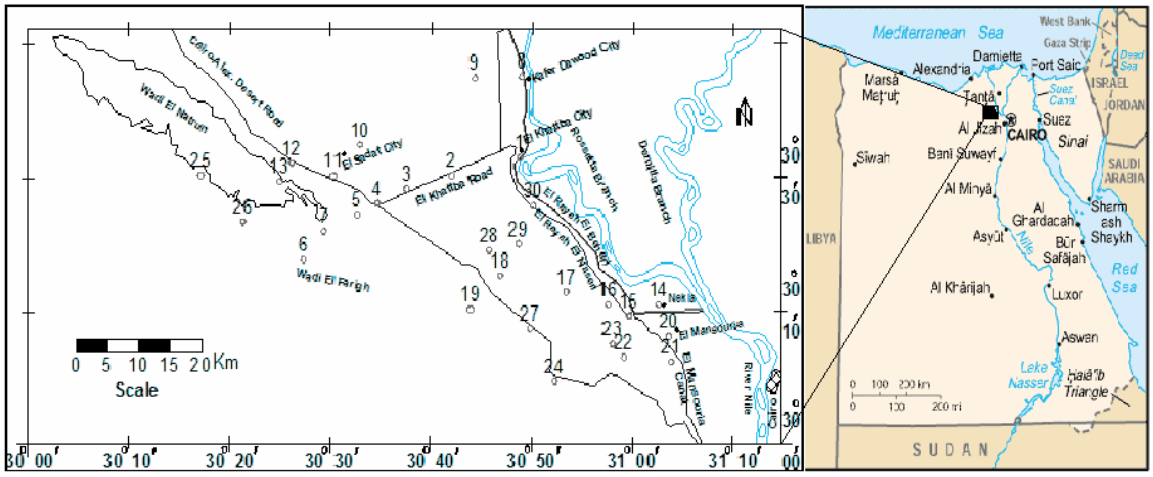

Figure 5.1: Map of the investigation area. The right panel shows the location southwest of the Nile Delta and northwest of Cairo. The left panel shows the area in detail, with the sampled wells indicated by circles and well numbers. The area extends from the border of the Nile Delta close to the Rosetta branch of the Nile River to the southwest out into the desert, where reclamation areas are developing, in particular along the Cairo – Alexandria Desert Road.

5.2.1 Geomorphological features

The investigation area southwest of the Nile Delta is characterized by a low relief and a mild topography with pronounced depressions, e.g. Wadi El Natrun (-23 m) and Wadi El Farigh (-4 m). These depressions act as prominent discharge areas for groundwater movement in the whole area.

In the study area the land surface is slightly undulated and generally slopes towards the Nile Delta. A gradual slope to the North is also a remarkable feature. The surface water canals, as represented by El Rayah El-Behary and El Rayah El- Nasiry have levels of the order 13-15 m above sea level. The investigation area shows different geomorphological units, which can be discriminated into the alluvial plains and the structural plains (Figure 5.2).

The alluvial plains can be differentiated into young and old alluvial plains. The young alluvial plain is mostly occupied by cultivated lands, it represents the flood plain of the Nile Delta and it is composed of Nile silt, clay and sand, which was deposited during the recent time. This plain is generally flat and its elevation varies between 12 and 14 m above sea level in our study area, where it is restricted to a narrow stretch along the Rosetta branch of the Nile River. The old alluvial plain lies south of the young alluvial plain and occupies most of the area extending between the Rosetta branch on the eastern side and Wadi El Natrun in the western side. It is characterized by slight undulation with several low-lying hills e.g. Garet El Nagar, Khashm El Kalb, etc., and it is underlain by sand and gravel deposits.

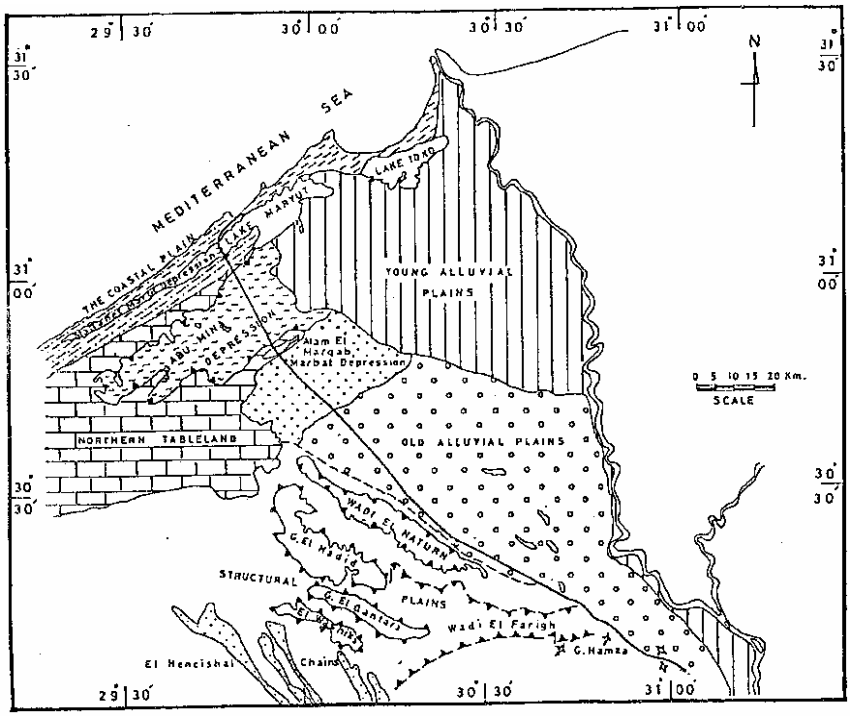

Figure 5.2: Geomorphological map of the investigated area

5.2.2 Groundwater system

The water-bearing formations in the investigation area are classified into five aquifers: The Recent, Pleistocene, Pliocene, Miocene and Oligocene aquifers (Figure 5.3). These aquifers are hydraulically connected and considered as one hydrological unit. The Recent and Pleistocene aquifers are sometimes considered as one unit and referred to as the Quaternary aquifer. In this work, samples were collected along four different transects in the direction of flow, which is generally from northeast to southwest (Figure 5.4). The location of the transects and cross sections along them are shown in Figure 5.5. This figure also shows how the aquifers are connected to each other.

5.2.2.1 The Recent aquifer

The Recent aquifer is only detected in the Wadi El Natrun depression and its sediments are mainly composed of sandy deposits with calcareous intercalations of aeolian fillings in the low area of the Wadi El Natrun depression. The Recent aquifer sediments have a thickness of 8 m to 10 m and the transmissivity measured by Shafei (1972) is about 230 m^2/day, when the discharge rate was about 75 m^3/hr. The previous studies supposed that the Recent aquifer is mainly recharged from the Pleistocene aquifer (section 5.2.2.2), outcropping to the east of Wadi El Natrun. This is because the Recent aquifer is lower than the Pleistocene aquifer. The Recent aquifer is also recharged from the Miocene aquifer southeast of Wadi El Natrun. Also the Pliocene aquifer and rain water may participate in recharging the Recent aquifer.

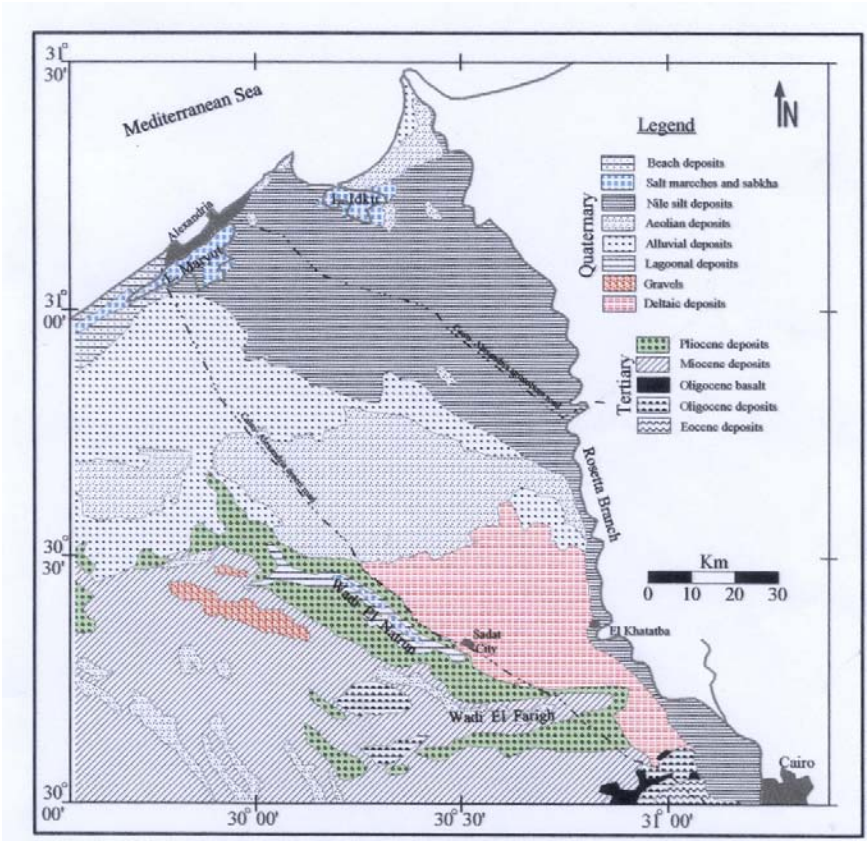

Figure 5.3: Distribution of different aquifers in the investigated area. The Quaternary refers to the deposits of the Recent and Pleistocene aquifer

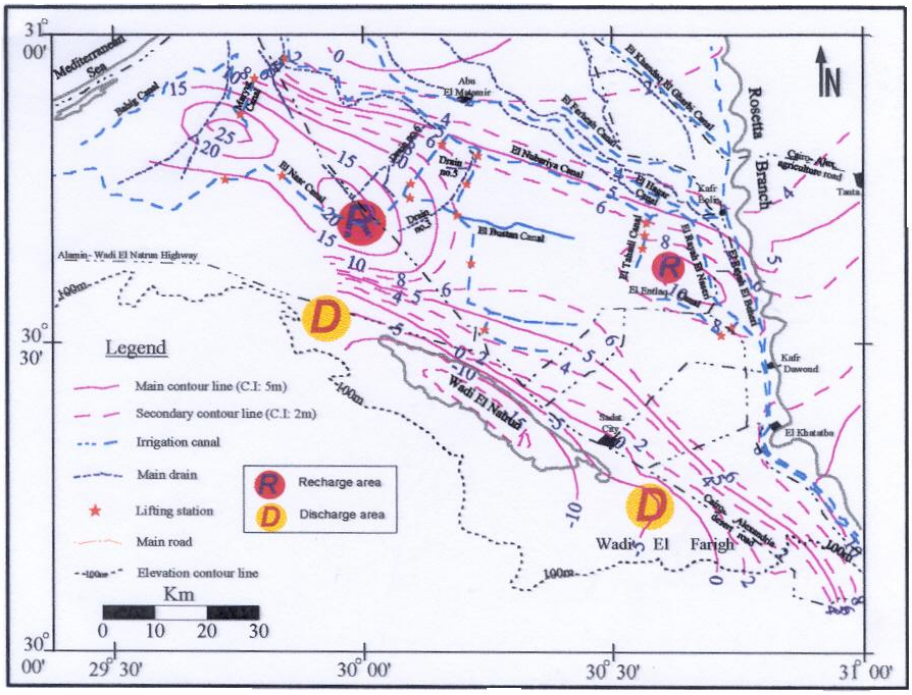

Figure 5.4: Contour map of hydraulic head in the study region. Groundwater flow direction is at right angles to the contours of the water level. The area investigated in this study covers the southern part of this map, where the groundwater flow is generally from northeast to southwest towards Wadi El-Natrun.

The Recent aquifer is discharging into the western lakes (salty lakes); this is because the absolute level of the groundwater in the aquifer (generally between -16.5 m and -9.40 m) is higher than the water level of the salty lakes (ranges between -22 m and -16 m). The Recent groundwater is also discharged through the withdrawal of water from trenches for irrigation.

5.2.2.2 The Pleistocene

The Pleistocene aquifer occupies the major part of the investigation area and it is essentially composed of fluviatile graded sand and gravel intercalated with thin clay lenses. The hydraulic conductivity of the Pleistocene aquifer ranges from a few meters per day to nearly 60 m/day, the transmissivity has a value from about 1300 m^2/day to 11500 m^2/day (Gomaa, 1995). The variation in transmissivity may be attributed to the lateral facies changes due to the presence of the clay lenses intercalation.

The Pleistocene aquifer is bounded by the Rosetta branch in the east and Wadi El Natrun in the west, and extends from El Khatatba road at the south to the Mediterranean Sea at the north. The sediments of this aquifer have a variable thickness, from about 80 m near Wadi El Natrun to 1000 m along the Mediterranean coastal line. The saturated thickness of the Pleistocene aquifer is about 100 m in the southern part and it has its maximum values in the northern part. The base of this aquifer is composed of a clay layer (about 100 m thick) related to the Pliocene time.

The Pleistocene aquifer is mainly recharged from the Nile water, infiltration of irrigation water and from the adjacent canals. The discharge from this aquifer can happen naturally or artificially. Natural discharge occurs mainly through the Rosetta branch. The artificial discharge occurs through the agricultural drains found in the area and through a few hundreds of productive wells that occur in the area, mainly around the Cairo-Alexandria Desert Road. The extracted water from these wells is about 1600 million m^3/yr (Gomaa, 1995).

Gomaa (1995) showed that the groundwater flow in this aquifer is generally from east to west and locally from southeast towards northwest as well as from northeast towards the Wadi El Natrun depression. Such local trends of groundwater flow are mainly attributed to the over exploitation of groundwater to irrigate the newly reclaimed lands.

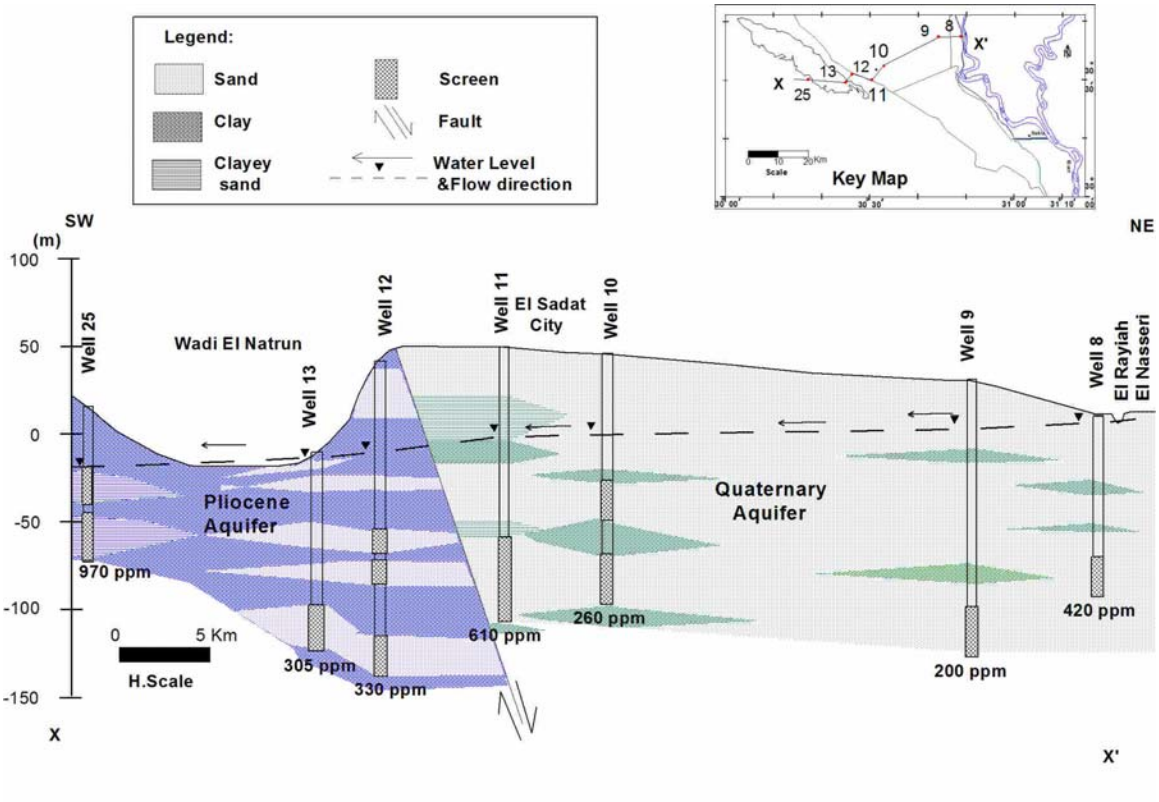

(a) Cross section X-X`

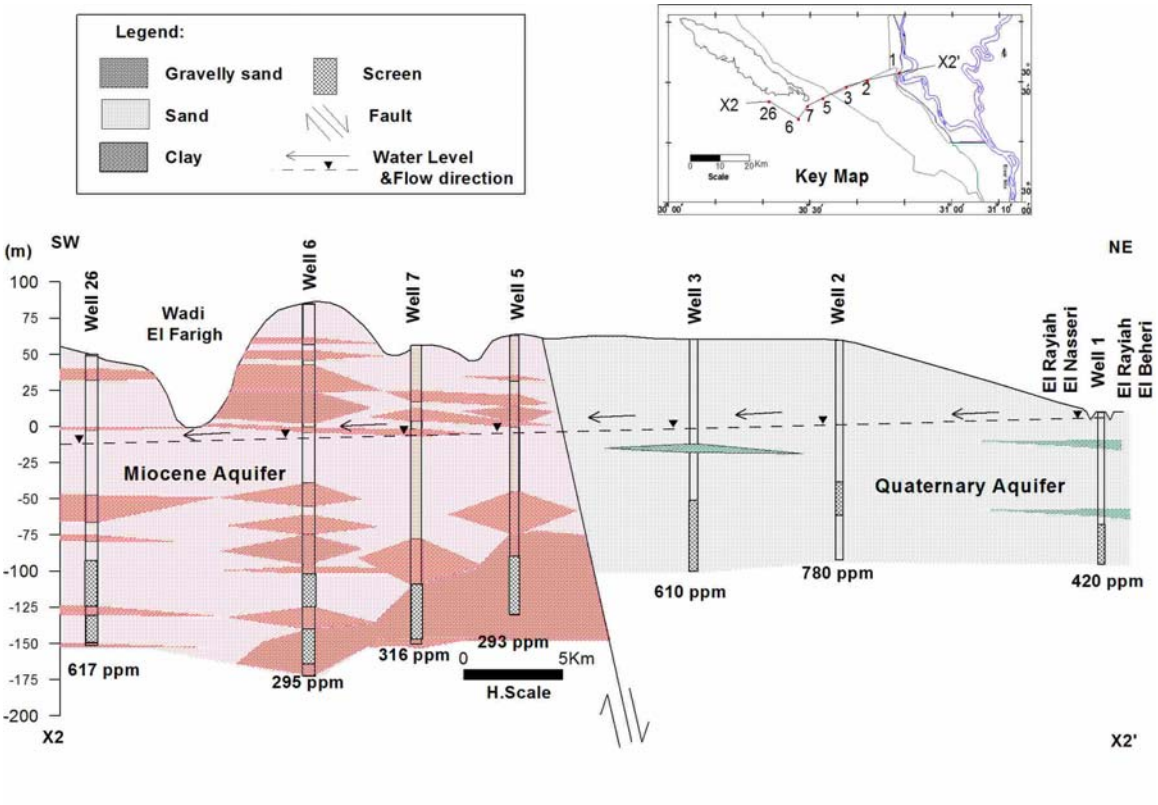

(b) Cross section X2-X2´

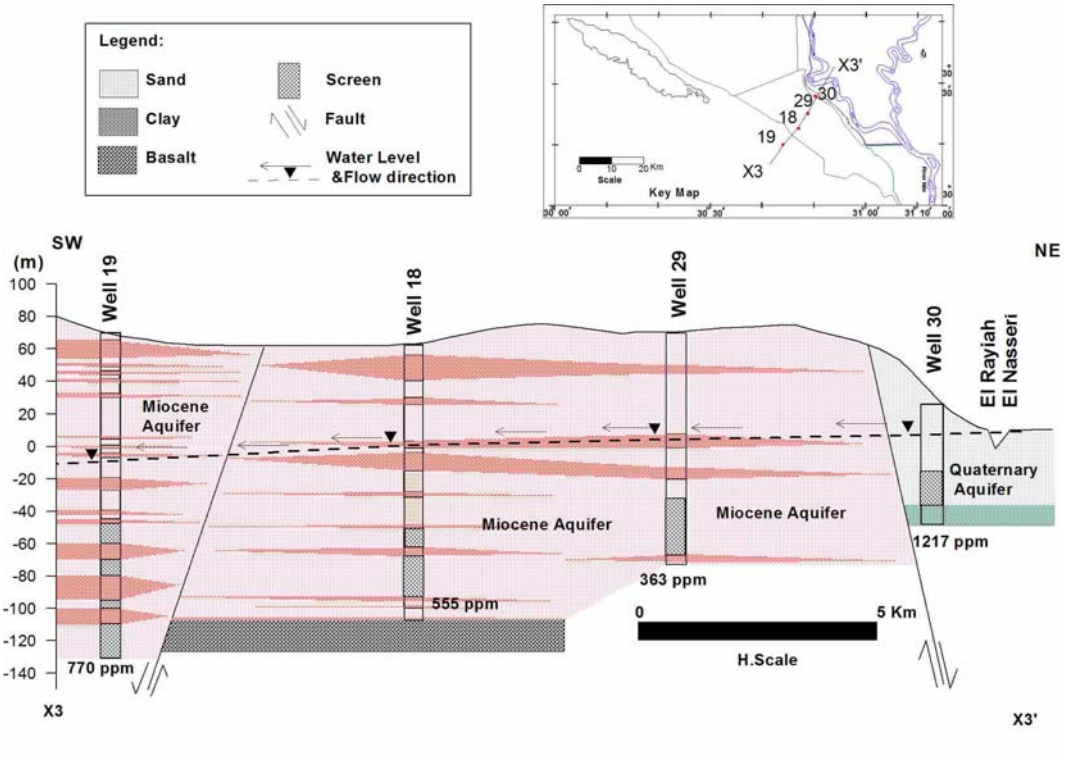

(c) Cross section X3-X3´

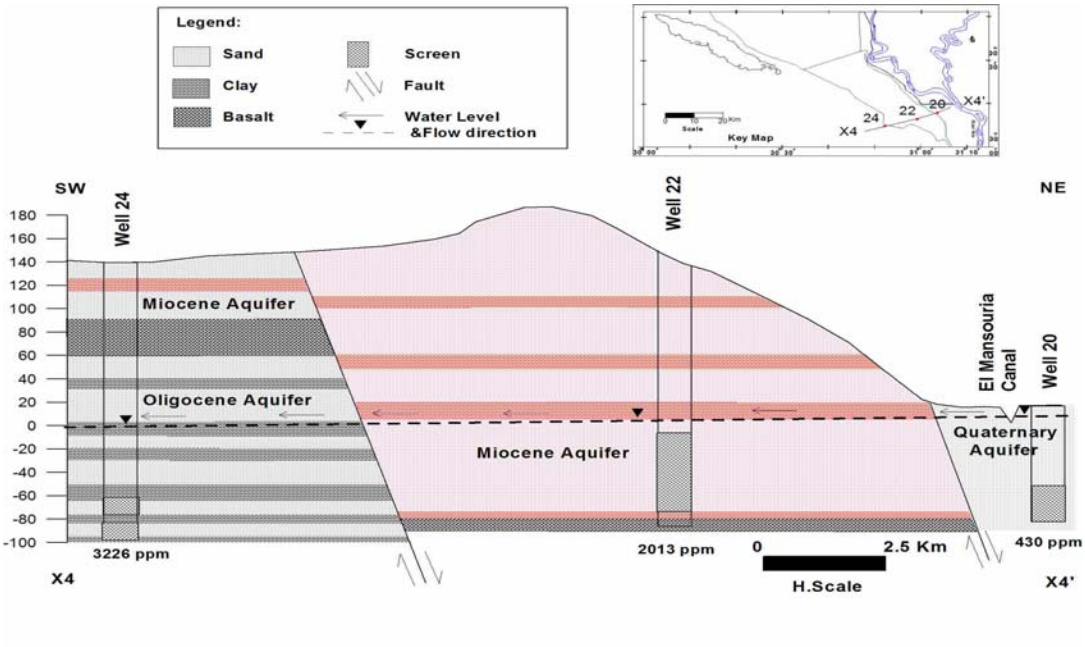

(d) Cross section X4-X4´

Figure 5.5: The hydrological cross sections of four different transects. Locations of the wells in the transects are shown in the inset at the upper right in each panel.

5.2.2.3 The Pliocene aquifer

The Pliocene aquifer is mainly restricted to the Wadi El Natrun depression, its sediments are composed of clay facies with interbeds of water bearing sandy layers. The thickness of the aquifer deposits is about 140 m at Wadi El Natrun, with a saturated thickness of about 90 m. The depth of the base of this aquifer increases from west to east and from south to north. The hydraulic parameters of the Pliocene aquifer, as determined by Gomaa (1995), are as follows: The hydraulic conductivity is about 10 m/day, the transmissivity ranges between 330 and 500 m^2/day.

Previous studies expected that there is a hydraulic connection between the Pliocene and Pleistocene aquifers, explaining why the groundwater level in the two aquifers is mostly the same. Because of this, the Pleistocene aquifer is considered as one of the main sources of recharge to the Pliocene aquifer, also because there is a lateral flow towards Wadi El Natrun depression, which acts as a natural discharge area. The Pliocene aquifer is also recharged from the irrigation water in the newly reclaimed areas in the study area. The Pliocene aquifer is also hydraulically connected to the Miocene aquifer (section 5.2.2.4), through faults occurring in the study area, so that the Pliocene aquifer is also recharged from the underlying Miocene aquifer. The Pliocene aquifer is also recharged by local rain storms. The total annual recharge to the Pliocene aquifer is estimated to approximately 60 million m^3/year (Fekry, 1993).

The discharge from the Pliocene aquifer can happen naturally through spring flow, and through seeping to the Recent aquifer as well as to the salty lakes. The discharge can also happen artificially through the productive wells used for agricultural and domestic purposes.

5.2.2.4 The Miocene aquifer

The Miocene sediments are represented by the Moghra Formation, and are mainly composed of sand, sandstone and clay interbeds with vertebrate remains and silicified wood (Said, 1962). These sediments are occasionally overlain by Quaternary deposits and are underlain by the Oligocene basaltic sheet. The total thickness of the Miocene sediments is varying from 75 m in the northeastern portion to about 250 m at Wadi El Natrun, regionally this thickness increases in northwest direction (El Ghazawi and Attwa, 1994).

The saturated thickness of the Miocene aquifer is controlled by the prevailing structural conditions in the area. The maximum saturated thickness attains about 169 m, and thins out in the northeastern direction to reach about 27 m at the Khasm El Kalb area (El Ghazawi and Attwa, 1994). According to El Ghazawi and Attwa (1994), the faults that are found in the area are responsible for elevating the Oligocene basaltic sheet and the underlying clay beds in the northeastern side. This leads to a very steep hydraulic gradient near the intake front adjacent to the Rosetta branch,

which may reduce the direct recharge from the Rosetta branch to the lower Miocene. The general hydraulic head gradient is from the southeast to the northwest and varies from 4.6 cm/km to 32 cm/km. This means that the regional groundwater flow is directed towards the west and northwest.

The eastern and southeastern boundaries of the Miocene aquifer are hydraulically connected with the underlying Oligocene aquifer (section 5.2.2.5), where the basaltic sheets are highly elevated (+70 m) (El Ghazawi and Attwa, 1994).

The recharge of the Miocene aquifer takes place from the Pleistocene aquifer in the southeastern part of the study area. The recent amount of recharge was estimated by the general company for Research and Groundwater (REGWA, 1990) and it is varying between 50 and 100 million m^3/year. The other sources of recharge to the Miocene aquifer are the occasional rain storms (about 25,000 m^3/year) and the upward leakage from the deep Nubian sandstone aquifer, so that the water of the Miocene aquifer is considered as a mixture of paleowater and recent water.

The discharge of the Miocene aquifer takes place through the production wells around the Cairo-Alexandria desert road and the sporadic wells in Wadi El Farigh. Also the Miocene groundwater is discharged through the Pliocene aquifer at the southern portion of Wadi El Natrun, where the two aquifers are hydraulically connected (Gomaa, 1995).

5.2.2.5 The Oligocene aquifer

The Oligocene sediments are mainly composed of sands and gravels with clay interbeds and are overlain by basaltic sheets, which differ widely in their occurrences and levels. The Oligocene sandstone in the study area is overlain by dissected basaltic sheets belonging to the Gebel Qatrani volcanic rocks of upper Oligocene to lower Miocene age (Abdel Rahman, 1996). The Oligocene aquifer is characterized by confined conditions, where its piezometric level lies at about 3 m above sea level. The saturated thickness is more than 60 m (El Ghazawi and Attwa, 1994).

The Oligocene aquifer is characterized by a relatively high water salinity, which indicates that there is no recharge from the Nile or from the Pleistocene aquifer. The recharge may originate from the rainwater of the recent and the previous periods, which dissolved salts during the circulation of the water through the Oligocene fluvio-marine deposits (Abdel Baky, 1983). The Oligocene aquifer is hydraulically connected with the lower Miocene aquifer, This leads to a mixing of groundwater of both aquifers resulting in an increase in the lower Miocene water salinity on the one side and a decrease in the Oligocene water salinity on the other side.

5.2.3 Geochemistry and water quality

Water quality with respect to salinity is one of the main constraints for using groundwater as irrigation water in the study area. The irrigation water infiltrates into the shallow aquifer where its salinity is increased, i.e. its usefullness as irrigation water is deteriorated. Consequently, the intensity of deterioration is important because downward percolation of salts may seriously affect the groundwater quality in the shallow aquifer.

The total dissolved solids (TDS) in groundwater can be measured in the zone of saturation where the water has percolated to the water table through the unsaturated zone and has undergone reactions between water and rock. The TDS values that have been measured in the investigation area differ among the investigated aquifers. In other words, the TDS in the shallow aquifer horizons may differ considerably from that of the deeper ones. There are also local anomalies in TDS concentrations the reason for that may be the effect of overpumping, which may increase the water salinity in one of the aquifer horizons rather than the others.

In general, quality variations are more likely to occur in shallow than deeper aquifers since temporal changes in recharge and discharge may create corresponding fluctuations in water salinity (Ibrahim, 2000). The increase of TDS that has been observed parts of the investigation area may be explained by the overpumping due to excessive irrigation or due to inherited salts within the aquifer deposits.

The latter reason explains the deterioration in the water quality in the deep horizons e.g. well 24 (Figure 5.1), located in the Oligocene aquifer, which is characterized by the highest salinity (section 5.2.2.5). The deterioration in the water quality in the shallow aquifer may be explained by the former reason, e.g. the wells 21, 22 and 30 (Figure 5.1), which are located near the surface water (at distances of about 1, 6.5 and 1.6 km, respectively) have a higher TDS compared to the other wells in the same area (Table 5.1). The average value of the pumping rate of each well is 100 m^3 h^{-1} in the El-Khatatba area and the average number of operating hours is 12 hours per day (Ibrahim, 2000). The pumping rate depends on the types of the cultivated crops, e.g. at the farms that cultivate banana trees it is actually at the average about 200 m^3 h^{-1} per well and the wells work for at least 18 hours a day. The high rates of pumping in the cultivated areas lead to some serious problems e.g. (1) the groundwater levels dropped during the last decade (2) the induced infiltration is highly accelerated towards the areas of overpumping (e.g. banana farms) (3) the groundwater salinity is seriously increased in the overpumped areas as a result of the mismanagement of the farms.

In the following the hydrochemistry of the different aquifers will be discussed to specify the type of groundwater according to the concentration of the major ions in groundwater samples.

The Recent aquifer is characterized by two different sequences of major ions, these are:

(i) $Na^{+} > Ca^{++}$ $(Mg^{++}) > Mg^{++}(Ca^{++})$ and $Cl^{-} > SO_4^{--}$ $(HCO_3^{-}) > HCO_3^{-}$ (SO_4^{--})
(ii) $Na^{+} > Ca^{++} > Mg^{++}$ and $SO_4^{--} > Cl^{-} > HCO_3^{-}$

Consequently, the chemical water types are sodium chloride and sodium sulfate, which reflect the influence of Wadi El Natrun's salt lakes due to the effect of overpumping (Gomaa, 1995).

The Pleistocene aquifer, which is mainly composed of coarse sand and gravels intercalated with clay lenses is characterized by increasing salinity from east to west along the direction of groundwater flow. The total salinity of groundwater varies from 236 mg/l near Wadi El Natrun to about 4000 mg/l close to the El Nasr canal, reflecting fresh to brackish water(Gomaa, 1995).

The Pleistocene groundwater is classified into three main categories according to the ion dominancy for ions and cations, these are:

(i) $Na^{+} > Ca^{++}$ $(Mg^{++}) > Mg^{++}$ (Ca^{++}) and $HCO_3^{-} > SO_4^{--}(Cl^{-}) > Cl^{-}(SO4^{--})$
(ii) $Na^{+} > Ca^{++} > Mg^{++}$ and $SO_4^{--} > Cl^{-} > HCO_3^{-}$
(iii) $Na^{+} > Ca^{++}$ $(Mg^{++}) > Mg^{++}(Ca^{++})$ and $Cl^{-} > SO_4^{--}$ $(HCO_3^{-}) > HCO_3^{-}$ (SO_4^{--})

The first sequence reflects the sodium bicarbonate fresh water; this type of water is recorded in the eastern portion of Wadi El Natrun. The second sequence has sodium sulphate water type reflecting the effects of drainage water on the Pleistocene groundwater. The third sequence shows the sodium chloride water type, this type of water is mainly recorded in the local areas of brackish water, which reflects the impact of lithofacies as well as overpumping (Gomaa, 1995).

The Pliocene aquifer sediments are mainly composed of sand intercalated with clay. The groundwater of the Pliocene aquifer is slightly alkaline to alkaline, where the pH values range from 7.5 to 8.9. The total salinity varies from 260 mg/L in the southern part of Wadi El Natrun (Beni Salama area) to about 6400 mg/L in the west central part of Wadi El Natrun, reflecting fresh to brackish water. High groundwater salinities are due to the presence of clay beds of great thickness of lagoonal and marine origin with high content of salts, the salt lakes and marches, the high rate of evaporation, and the low groundwater recharge from the irrigation canals in the east and north.

Four water types exist in the Pliocene aquifer, namely: the $NaHCO_3$, Na_2SO_4, $MgCl_2$ and $CaCl_2$ water type. The first type represents 50 % of the samples and occupies the southern part of Wadi El Natrun, the second type represent 33 % of the samples; the third and fourth types are limited only to high salinity samples (17 %).

The $NaHCO_3$ water type reflects fresh water of meteoric origin. The Na_2SO_4 water type reflects the effect of the dissolution and leaching processes of evaporite deposits

in salt marches around the salt lakes rich in sulphate by the meteoric water percolation. The presence of $MgCl_2$ and $CaCl_2$ water types might reveal the leaching of the evaporite deposits in salt marches around the salt lakes rich in chloride minerals by the percolation of meteoric water.

The Miocene aquifer sediments are mainly composed of coarse sand and clay lenses intercalation. In view of the hydrogeology, this aquifer is proved as mentioned before to be hydraulically connected with the Quaternary aquifer to the east as well as northeast, the Pliocene aquifer to the northwest and Oligocene aquifer to the south. So, the quality of Miocene groundwater is essentially influenced by Miocene lithofacies (clay lenses), groundwater of the deeper aquifer (Oligocene), and paleowater which is mixed with old Nile fresh water trapped in the Miocene sediments, when the old Nile Delta branch was directed towards the Wadi El Farigh area.

The groundwater of the Miocene aquifer is slightly alkaline to alkaline, with pH values ranging from 7.2 to 8.85. The total salinity of the Miocene aquifer varies from 150 mg/L in the western part of Wadi El Farigh to about 5000 mg/L in the southwest of Wadi El Natrun, reflecting fresh to brackish water. Local anomalies in water salinity are detected at the area east of the Cairo-Alexandria desert road, west of the El Rayah El Nasiry canal, and southwest of the Wadi El Natrun due to the high pumping rates, the presence of shallow clay lenses within the water bearing layers especially west of El Rayiah El Nasiry, and the low groundwater recharge from the irrigation canals in the east.

The ionic dominancy of the Miocene aquifer reflects eleven different sequences; these are:

(i) $Na^+ > Ca^{++} > Mg^{++}$ and $HCO_3^- > Cl^- > SO_4^{--}$.
(ii) $Na^+ > Ca^{++} > Mg^{++}$ and $HCO_3^- > SO_4^{--} > Cl^-$.
(iii) $Na^+ > Mg^{++} > Ca^{++}$ and $HCO_3^- > SO_4^{--} > Cl^-$.

The above patterns reflect the sodium-bicarbonate fresh water of meteoric origin; such water type is similar to that of the Nile water.

(iv) $Ca^{++} > Mg^{++} > Na^+$ and $HCO_3^- > SO_4^{--} > Cl^-$.

This sequence shows a calcium–bicarbonate water type, which is mainly attributed to the dissolution of the cement material (calcium carbonate) (Gomaa, 1995).

(v) $Na^+ > Ca^{++} > Mg^{++}$ and $Cl^- > SO_4^{--} > HCO_3^-$.
(vi) $Na^+ > Ca^{++} > Mg^{++}$ and $Cl^- > HCO_3^- > SO_4^{--}$.
(vii) $Na^+ > Mg^{++} > Ca^{++}$ and $Cl^- > HCO_3^- > SO_4^{--}$.
(viii) $Na^+ > Mg^{++} > Ca^{++}$ and $Cl^- > SO_4^{--} > HCO_3^-$.

The above patterns show the sodium–chloride water type. This type of water is mainly recorded in the local areas of high salinity, it reflects the mixing process of meteoric water with marine water through the faults and fractures and the impacts of lithofacies and over pumping.

(ix) $Ca^{++} > Na^{+} > Mg^{++}$ and $Cl^{-} > HCO_3^{-} > SO_4^{--}$.
(x) $Ca^{++} > Mg^{++} > Na^{+}$ and $Cl^{-} > SO_4^{--} > HCO_3^{-}$.
(xi) $Ca^{++} > Na^{+} > Mg^{++}$ and $Cl^{-} > SO_4^{--} > HCO_3^{-}$.

The above patterns show the calcium–chloride water type, which is limited in occurrence and characterized by the presence of salts of permanent hardness, where the salt combinations are NaCl, $MgCl_2$, $CaCl_2$, $CaSO_4$, and $Ca(HCO_3)_2$. The presence of $MgCl_2$ and $CaCl_2$ water types reveals the leaching actions of the original marine water between rock pores by the meteoric water percolation, or is due to old marine water discharges along fault planes and mixing with water of meteoric origin.

The Oligocene aquifer sediments are mainly composed of sand intercalated with clay. The groundwater is alkaline, with pH values ranging from 7.8 to 8.3. The total salinity of the Oligocene aquifer varies from 560 mg/L in the Gebel Khashm El Kalb area to about 2400 mg/L in the southern portion of the study area, reflecting fresh to brackish water. High salinities are due to the presence of clay beds of great thickness of lagoonal and marine origin with high content of salt where the recharge of the Oligocene aquifer originated from the paleo-rainwater, which dissolved salts during the circulation through the Oligocene fluviomarine deposits. The low water salinities in the Gebel Khashim El Kalb area are due to the mixing of Miocene fresh water with the Oligocene saline water.

According to the ion dominancy in the groundwater of the Oligocene aquifer, only one sequence is recorded. This is:

$$Cl^{-} > SO_4^{--} > HCO_3^{-} \text{ and } Na^{+} > Ca^{++} (Mg^{++}) > Mg^{++} (Ca^{++})$$

Such a pattern shows the sodium – chloride water type pertaining to the ultimate phase of metasomatism. This type of water mainly reflects the mixing process of meteoric water with marine water through the faults and fractures and the impacts of lithofacies.

Well. No	Well Name	Aquifer	Distance from surface water [km]	Depth to water [m]	EC [ms/cm]	TDS [ppm]
1	El-Katatba station	Pleistocene	-0.2	3.5	0.481	320
2	Mabruka farm	Pleistocene	10.5	60	1.338	780
3	El-Katatba Company	Pleistocene	17.5	58.83	0.316	190
4	Teba	Pleistocene	22	64.61	-	-
5	Dr. Kamal	Miocene	26	68.64	0.601	360
6	Amr Syna	Miocene	37	75	0.516	310
7	El Manara	Miocene	31.5	70	0.476	300
8	Kafer Dawood west	Pleistocene	0.2	3.5	0.696	420
9	Al Shoraa	Pleistocene	7.8	25	0.315	200
10	Sadat R	Pleistocene	26.5	44	0.445	260
11	2000 Fedan 12	Pleistocene	31	50	1.005	610
12	Hanfy	Pliocene	37.5	50	0.487	330
13	Beni Salama	Pliocene	40	2.5	0.505	310
14	Nekla Station	Pleistocene	-0.05	3.5	0.597	370
15	Roshedy	Pleistocene	1.6	10	0.947	560
16	Nabil	Miocene	4	65	0.520	310
17	Sherif	Miocene	7	93	0.607	360
18	El Waha	Miocene	13.2	58	0.922	570
19	Misila	Miocene	19.5	75	1.253	750
20	El Mansouria	Pleistocene	-0.05	9	0.770	430
21	Giza station	Pleistocene	1	8	1.230	710
22	Biko	Miocene	6.5	122	2.980	1380
23	Intergroup	Miocene	6.8	148	0.954	560
24	Soady	Oligocene	17	140	5.750	2800
25	El Kauser	Pliocene	52.5	30	1.398	970
26	El Ham	Miocene	44	82	1.109	640
27	Helal	Miocene	14.8	102	0.771	460
28	Ismail	Miocene	12	103	0.486	280
29	El Hussain	Miocene	7.2	75	0.557	350
30	Said	Pleistocene	1.6	24	1.941	1100

Table 5.1: Well data and salt contents. Distance is measured in southwestern direction from the artificial canals (El Rayah El Nasiry & El Rayah El Behary), negative values refer to the wells on the eastern side of these canals.

5.3 Methods

Samples of groundwater from 30 wells in the area south west of the Nile Delta were collected in one sampling campaign in August 2003 (see Table 5.1 for a list of sampled wells). The groundwater samples were taken for stable isotope, noble gas, tritium, ^{14}C, and SF_6 analysis. The sampling and measurement of SF_6 samples have been described in section 4.4, while the measurements of tritium, stable isotopes and noble gases will be described in the following.

5.3.1 Tritium

Tritium samples were taken in 1 L glass bottles and were analyzed radiometrically using low-level gas proportional counters. Hydrogen gas was formed by chemical reduction of the water by reaction with Mg in an oven at 560 °C. The resulting H_2-gas was mixed with argon and methane and introduced to a gas proportional counter tube of a volume of 1.1 L. No enrichment of tritium was performed. This procedure yields a precision and detection limit of about 1.5 TU. More details on the methods used for tritium analysis have been described by Grothe (1992).

5.3.2 Stable isotopes

Stable isotope samples were collected in 50 ml glass bottles and have been analyzed at the laboratory of the Institute of Environmental Physics in Heidelberg with a Finnigan MAT 252 mass spectrometer. For oxygen isotope analyses, 5-ml water samples were equilibrated with a CO_2 standard gas in an Isoprep automated, online-equilibration bench for 6 hours. The equilibrated CO_2 sample was then directly inlet into the MAT 252 mass spectrometer and analyzed for $\delta^{18}O$ of CO_2. For hydrogen isotope analyses 2 µL of water were reduced to hydrogen gas by reaction with hot chromium in a reaction furnace kept at 850 ^oC for 30 min. At this temperature the chromium reacts quantitatively with H_2O, thus producing H_2 with an isotopic composition equal to that of the water. The H_2 gas was subsequently analyzed on the MAT 252 mass spectrometer. Further details on the techniques used for stable isotope analysis can be found in Neubert (1998).

5.3.3 Noble gases

The water samples for noble gas analysis are collected in copper tubes containing about 40 cc of water and fitted with stainless steel pinch-off clamps at each end. The copper tube is fixed in an aluminum channel holding the stainless steel pinch-off clamps. The water is transferred from the well head into the copper tube through a tight combination of PVC-tubing, avoiding any contact with the air. The entire system

is kept under pressure to avoid degassing, and the tubing is carefully checked for the presence of air bubbles.

The noble gas measurements have been done by the mass spectrometric system described by Beyerle et al. (2000). The samples were quantitatively degassed on a vacuum line by water vapor transport through a capillary onto liquid nitrogen cooled cold traps. Splits of the light noble gas fraction (He and Ne) were analyzed in two different sector field mass spectrometers, a non-commercial small radius machine for the analysis of the amounts of ^{4}He and ^{20}Ne, and the $^{20}Ne/^{22}Ne$ ratio, and a Micromass MM5400 for the determination of the $^{3}He/^{4}He$ ratio. After He and Ne analysis, the extracted water vapor (less than 0.5 g) and all other condensable gases were released from the cold traps by heating to 180°C. After passing through a molecular sieve (3 Å pore diameter) to remove the water vapor, the gas was expanded to a 2 L reservoir. A split of 0.7 cm^3 was taken, passed through a series of getters to remove the reactive gases, and then admitted to the mass spectrometer for simultaneous analysis of Ar, Kr, and Xe. Ar was detected on the Faraday cup, Kr and Xe with an electron multiplier.

Calibration is regularly performed with aliquots of an air standard, which are known with an accuracy of about 0.3%. This systematic source of error is of minor importance compared to statistical fluctuations of the instrument sensitivity, which typically are on the order of 1% (Aeschbach-Hertig, 1999). The statistical errors are estimated from the standard deviation of the calibrations within a measurement run, and cross-checked by regular measurements of aliquots of an internal freshwater standard. The average errors for the measurements of the samples from this study were 0.69 % for He, 1.26 % for Ne, 0.64 % for Ar, 1.22 % for Kr, and 1.49 % for Xe.

5.4 Results and discussion

5.4.1 Stable isotopes

Stable isotopes, mainly of oxygen (^{16}O and ^{18}O) and hydrogen (^{2}H or D) have a wide field of application in groundwater studies, e.g. tracing the origin of the water and evaluating the extent of mixing of groundwater with other resources. The isotopic composition of water is expressed in per mil (‰) deviation from the SMOW standard. These deviations are written δD for deuterium and $\delta^{18}O$ for ^{18}O, Water with less ^{18}O than SMOW has a negative $\delta^{18}O$; water with more ^{18}O than SMOW has a positive $\delta^{18}O$. The same is true for deuterium. Oxygen and hydrogen stable isotopes are highly effective naturally occurring tracers of mixing of different water sources because oxygen and hydrogen constitute and move with water molecules. For instance, surface water that has been enriched in $\delta^{18}O$ and δD because of evaporation has a different isotopic signature than groundwater, which can be used to evaluate the extent of mixing between the two components. Stable isotope measurements can provide very useful quantitative information about recharge patterns and interactions between ground water and surface water. In the following we will discuss the result of

stable isotopes analysis for the samples collected from the investigation area south west of the Nile Delta.

The δD and δO^{18} values show a systematic change with distance from the surface water as shown in Figure 5.6 (also see Table 5.2). The delta values in the groundwater wells near the surface water are enriched in heavy isotopes, whereas the farthest wells are depleted in the heavy isotopes. Intermediate values are observed between these two extremes, this may be explained by mixing between old water that is present in the aquifers and the young water that infiltrates from the surface water. This interpretation is supported by linear mixing trends observed for the stable isotopes in Figure 5.7. Two mixing lines can be distinguished, the first line (AB) between paleowater with δD = -84 ‰ and δO^{18} = -10 ‰ and Nile water before the completion of the Aswan High Dam with δD = 4.3 ‰ and δO^{18} = -0.60 ‰, the second line (AC) between paleowater and the Nile water after the completion of the Aswan High Dam with δD = 28.7 ‰ and δO^{18} = 3.5 ‰. The endmembers of these lines are taken from Dahab et al. (1999). Most of the values obtained from the wells of this study lie on the line AB, indicating that most of the water infiltrated before the completion of the dam in 1969. Only groundwater within the Nile Delta and close to surface water features clearly reflects the recent change in isotopic content of Nile water. The change in isotopic content of Nile water is due to the accumulation of Nile water behind the Aswan high Dam, where a high evaporation rate causes an isotopic enrichment in the present day Nile water compared to the one which was present before the completion of the dam (Dahab et al., 1999). The hypothesis of groundwater recharge from Nile water is supported by plotting the precipitation data (GNIP database, IAEA/WMO 2004)) from Alexandria and Sedi Barany located to the northwest of the study area in Figure 5.7. The δD and $\delta^{18}O$ values of precipitation were observed to be significantly lighter (more negative) than those of the Nile waters, which are enriched in the heavy isotopes due to the effect of evaporation. Thus, significant recharge from precipitation can be ruled out, while the recharge from the Nile water is supported.

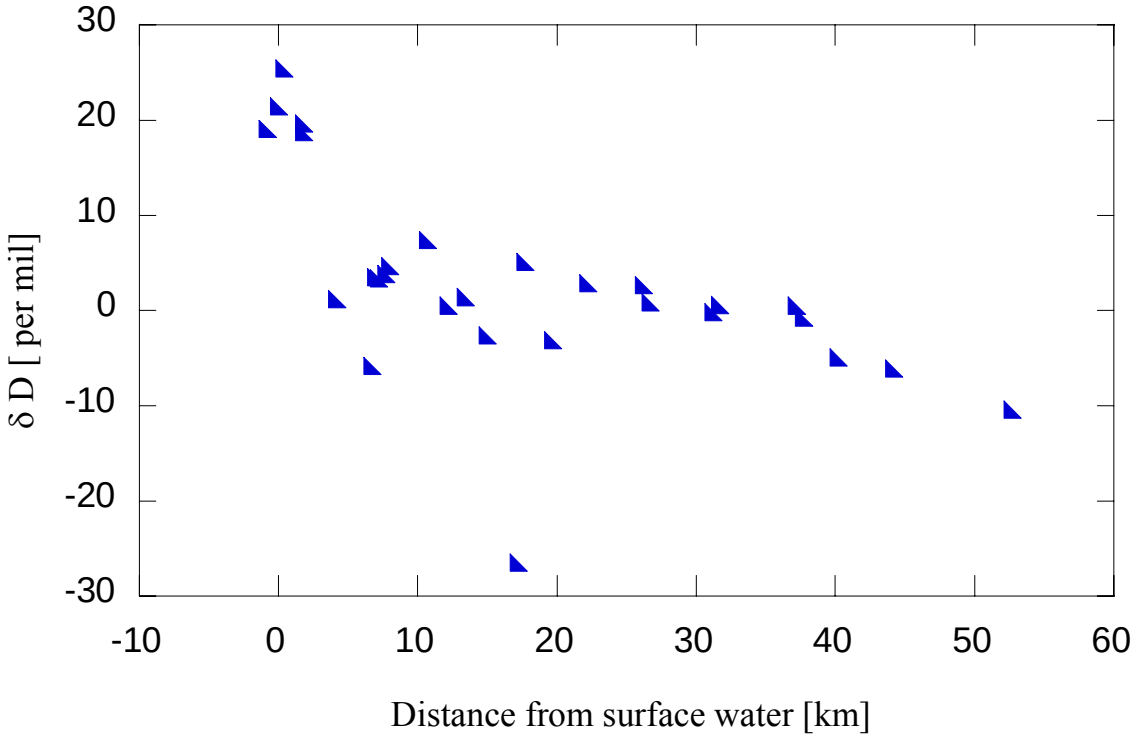

(a)

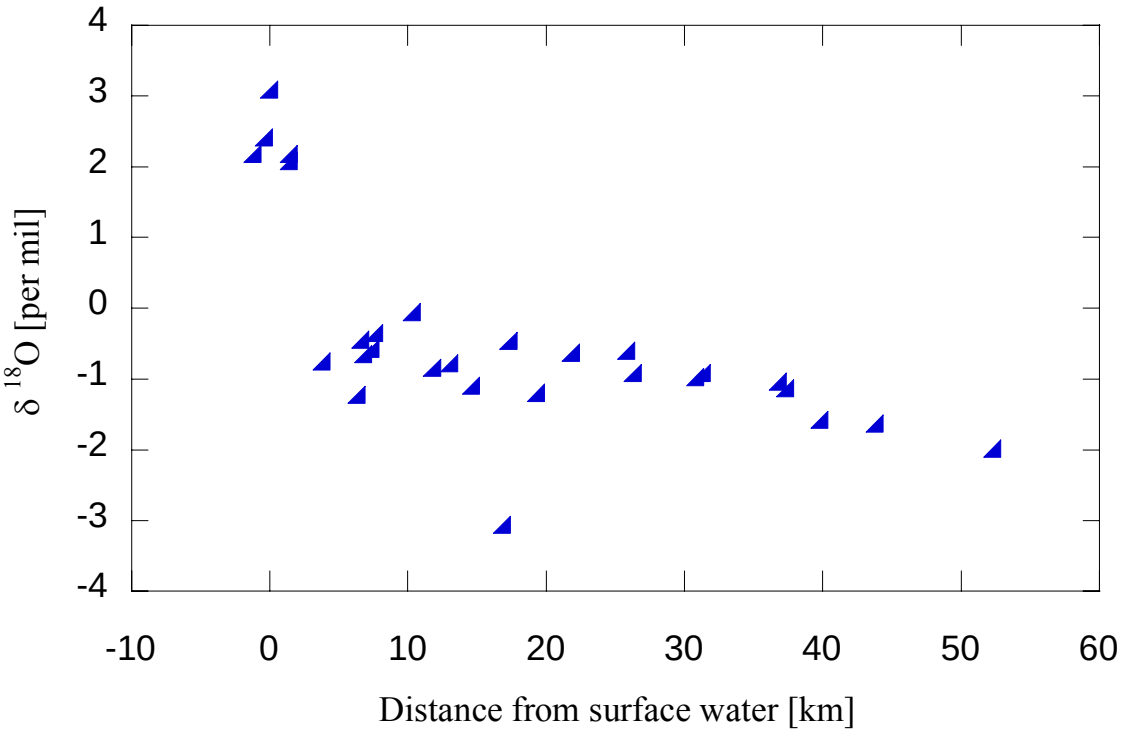

(b)

Figure 5.6: The δD and δO^{18} values against the distance from the surface water

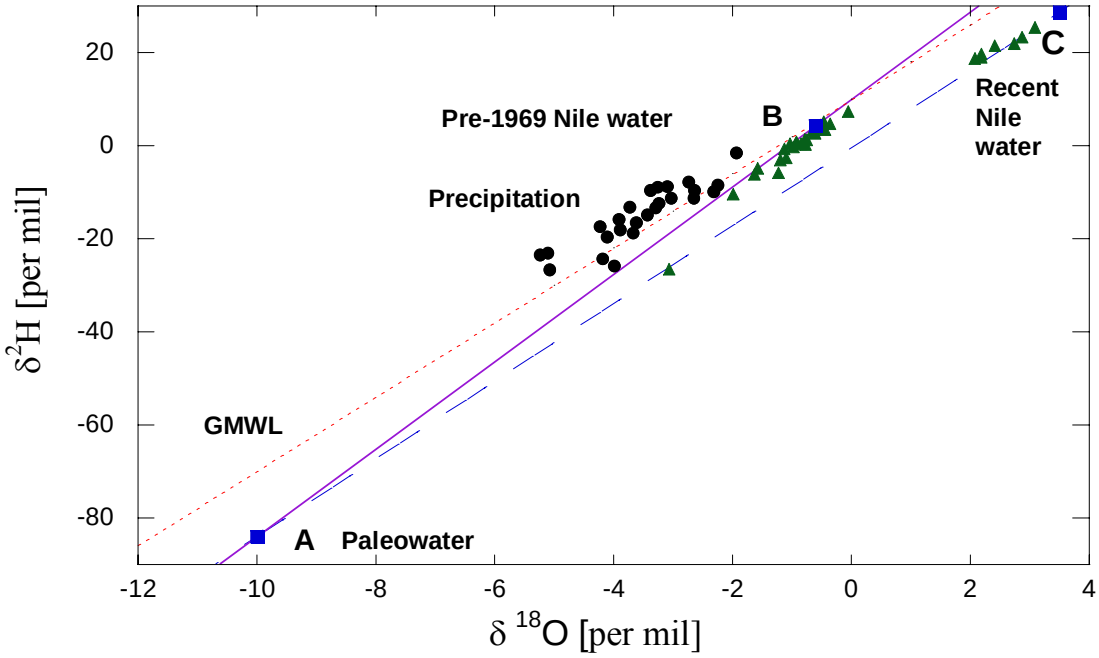

Figure 5.7: Mixing trend lines in stable isotope data. A, B, and C indicate expected end members as defined by Dahab et al. (1999), triangles represent data from the wells. Circles represent precipitation data from Alexandria and Sedi Barany northwest of the study area. The dotted line is the global meteoric water line.

5.4.2 Noble gases

The analysis of all stable noble gases (He, Ne, Ar, Kr, Xe) in the groundwater samples from Egypt allows us to accurately determine not only noble gas temperatures (NGTs), but also the atmospheric (excess air) and non-atmospheric (radiogenic He) excess components present in the water. The knowledge of these components is of crucial importance for the calculation of groundwater residence times from the ^{3}He and SF_6 data (see section 5.4.3). Therefore, we first discuss the noble gas results (Table 5.2) and their use to calculate noble gas temperatures and excess air.

The inverse fitting procedure to determine recharge temperature and excess air parameters, as described by Aeschbach-Hertig et al. (1999) and Peeters et al. (2003) was applied to the data set of this study. The physical processes responsible for the dissolution of atmospheric noble gases in our study area can be adequately described by the CE-model for excess air (Aeschbach-Hertig et al., 2000). The NGTs in the study area show no systematic variation and scatter around 23.7 ± 1.4 °C, slightly higher than the mean annual air temperature of 21.7 °C (at Cairo). All groundwater samples contain appreciable amounts of excess air. The amount of excess air in the groundwater, expressed by the relative Ne excess, varies between 9 and 75 % ΔNe (with the exception of one possibly degassed sample). It is necessary to assume a fractionation of the excess air in order to achieve reasonable fits between modeled and

observed noble gas concentrations for most samples. Although the PR-model of excess air fractionation brings a significant improvement of the fits, the CE-model performs clearly better. Only the CE-model achieves good fits not only to all samples individually, but also to the complete data set (number of samples = numbers of degrees of freedom = 28, sum of $\chi^2 = 39.97$, p = 6.7 %).

The relation between the measured He and Ne concentrations shows that most of the samples lie on or near the line of excess air (Figure 5.8). Due to the presence of excess air fractionation, the samples might actually be expected to lie slightly to the left of the unfractionated excess air line shown in Figure 5.8, but this is not observed. Rather, in most samples He is slightly enriched relative to Ne, which is indicative of a small non-atmospheric He component, most probably of radiogenic origin. Three samples (no. 22, 24 and 25) exhibit large contributions of radiogenic ^{4}He. These samples also have high salinity values, indicating admixing of old fluids from deep or low-permeable layers.

Well 24 originates from the Oligocene aquifer, which is thought to have been recharged by paleo-rainwater (section 5.2.3). The water from this aquifer is characterized by the highest radiogenic He and salinity values of our samples, indicating that it is likely the oldest groundwater in the study area. Well 25 is the farthest well from the surface water (about 52 km) and its water probably formed long ago, so that it accumulated a high salinity and high radiogenic He. Although well 22 is located in the Miocene aquifer and not far from the surface water (about 6.5 km), it is also characterized by high radiogenic helium and high salinity. Well 22 lies on the same transect as well 24, not far from a fault that separates the Miocene from the Oligocene aquifer (Figure 5.5d). We think that the salinity and He anomaly of well 22 may be related to this fault, by two possible mechanisms:

(i) The overpumping in the area might change the direction of flow to be locally from west to east and attract water from the Oligocene aquifer. The nearby fault might enhance the mixing of water between the Oligocene and Miocene aquifers, causing an increase in salinity and radiogenic helium in the latter. To test this assumption, more samples should be taken from wells between our wells 22 and 24 and analyzed for noble gases.

(ii) Helium is not only produced in situ (in the aquifer) but in the entire crust. This helium of deep crustal origin might migrate upward into the groundwater flow system along the nearby fault, affecting not only the Oligocene aquifer but also the Miocene aquifer. However, the migration of He enhanced by the fault hardly explains the high salinity, for which still over-pumping might be invoked as an explanation, possibly via leaching of salts from clay lenses.

Well. No	Well Name	$\delta^{18}O$ (‰)	$\delta^{2}H$ (‰)	He (ccSTP/g)	err He (ccSTP/g)	Ne (ccSTP/g)	err Ne (ccSTP/g)	Ar (ccSTP/g)	err Ar (ccSTP/g)	Kr (ccSTP/g)	err Kr (ccSTP/g)	Xe (ccSTP/g)	err Xe (ccSTP/g)	$^{3}He/^{4}He$	$^{4}He_{rad}$ (ccSTP/g)	NGT (°C)
1	El-Khatatba Station	2.42	21.5	5.31E-08	2.8E-10	2.14E-07	1.6E-09	3.13E-04	8.5E-07	6.62E-08	3.3E-10	8.84E-09	7.1E-11	1.41E-06	0	23.48±0.34
2	Mabruka	-0.05	7.40	5.87E-08	4.1E-10	2.30E-07	2.6E-09	3.29E-04	1.4E-06	6.88E-08	4.1E-10	9.17E-09	1.1E-10	1.42E-06	1.08E-09	22.68±0.50
3	El-Khatatba comp.	-0.46	5.10	6.40E-08	4.4E-10	2.58E-07	2.9E-09	3.50E-04	1.5E-06	7.10E-08	4.1E-10	9.32E-09	1.2E-10	1.41E-06	0	23.68±0.63
4	Teba	-0.63	2.90	n.s.												
5	Dr. Kamal	-0.60	2.70	5.90E-08	3.1E-10	2.22E-07	1.7E-09	3.15E-04	8.7E-07	6.65E-08	3.2E-10	8.75E-09	8.7E-11	1.37E-06	3.10E-09	23.86±0.39
6	Amr Syma	-1.03	0.50	5.98E-08	3.2E-10	2.28E-07	1.7E-09	3.26E-04	8.9E-07	6.84E-08	3.4E-10	8.98E-09	8.5E-11	1.37E-06	2.65E-09	23.32±0.41
7	El Manava	-0.92	0.60	6.28E-08	3.3E-10	2.33E-07	1.8E-09	3.20E-04	8.7E-07	6.53E-08	3.8E-10	8.21E-09	8.1E-11	1.38E-06	3.68E-09	27.49±0.62
8	Kfr Dawod West	3.09	25.40	4.84E-08	3.4E-10	1.99E-07	2.2E-09	3.18E-04	1.5E-06	6.89E-08	4.1E-10	9.39E-09	9.1E-11	1.74E-06	0	21.06±0.49
9	Al-Shoraa	-0.35	4.70	7.00E-08	3.7E-10	2.74E-07	2.1E-09	3.83E-04	1.1E-06	7.79E-08	3.9E-10	9.60E-09	1.1E-10	1.51E-06	1.44E-09	24.44±1.01
10	Sadat R	-0.92	0.90	7.14E-08	4.9E-10	2.70E-07	3.0E-09	3.67E-04	1.6E-06	7.47E-08	4.2E-10	9.39E-09	1.0E-10	1.36E-06	3.67E-09	23.65±0.70
11	2000 Feddans 12	-0.97	-0.20	5.61E-08	3.9E-10	2.23E-07	2.5E-09	3.36E-04	1.5E-06	7.01E-08	4.2E-10	8.99E-09	8.0E-11	1.38E-06	5.97E-10	25.66±2.38
12	Hanfy	-1.13	-0.70	6.90E-08	4.8E-10	2.55E-07	2.8E-09	3.47E-04	1.5E-06	7.13E-08	4.3E-10	9.18E-09	8.9E-11	1.32E-06	4.66E-09	23.40±0.52
13	Beni Salama	-1.57	-4.90	7.49E-08	4.0E-10	2.45E-07	1.8E-09	3.42E-04	9.3E-07	6.99E-08	3.8E-10	9.08E-09	8.4E-11	1.20E-06	1.35E-08	24.18±0.52
14	Nekla station	2.19	19.10	6.24E-08	4.4E-10	2.51E-07	2.8E-09	3.44E-04	1.5E-06	7.25E-08	4.7E-10	9.55E-09	1.2E-10	1.92E-06	0	21.07±0.48
15	Roshedy	2.08	18.80	5.82E-08	4.0E-10	2.29E-07	2.6E-09	3.37E-04	1.5E-06	7.12E-08	4.2E-10	9.55E-09	8.9E-11	1.77E-06	1.25E-09	21.24±0.45
16	Nabil	-0.75	1.20	6.18E-08	4.4E-10	2.44E-07	2.7E-09	3.65E-04	1.7E-06	7.49E-08	4.4E-10	9.53E-09	8.8E-11	1.40E-06	1.01E-09	24.95±2.10
17	Sherif	-0.65	3.40	5.77E-08	3.1E-10	2.35E-07	1.8E-09	3.39E-04	9.2E-07	7.02E-08	3.7E-10	9.20E-09	8.3E-11	1.42E-06	0	23.32±0.50
18	El-Waha	-0.78	1.40	5.58E-08	3.9E-10	2.13E-07	2.4E-09	3.10E-04	1.4E-06	6.59E-08	3.9E-10	8.67E-09	8.2E-11	1.30E-06	2.56E-09	23.90±0.44
19	Misila	-1.19	-3.10	4.36E-08	3.1E-10	1.74E-07	2.0E-09	2.92E-04	1.3E-06	6.35E-08	3.8E-10	8.42E-09	7.6E-11	1.32E-06	0	no fit
20	El Mansouria	2.74	22.00	n.s.												
21	Giza	2.88	23.40	5.23E-08	2.8E-10	2.04E-07	1.5E-09	3.00E-04	8.3E-07	6.43E-08	3.4E-10	8.52E-09	8.3E-11	1.52E-06	8.96E-10	24.06±0.35
22	Biko	-1.22	-5.80	1.48E-07	1.0E-09	2.09E-07	2.3E-09	3.08E-04	1.4E-06	6.58E-08	3.9E-10	8.70E-09	8.1E-11	5.51E-07	9.55E-08	23.44±0.43
23	Intergroup	-0.44	3.50	6.44E-08	4.6E-10	2.37E-07	2.7E-09	3.55E-04	1.6E-06	7.36E-08	4.3E-10	9.47E-09	9.2E-11	1.31E-06	5.56E-09	23.87±1.36
24	Soady	-3.06	-26.50	2.64E-07	1.4E-09	3.08E-07	2.3E-09	3.64E-04	1.0E-06	7.16E-08	3.6E-10	9.07E-09	9.0E-11	3.82E-07	1.85E-07	24.47±0.45
25	El Kauser	-1.98	-10.40	1.07E-07	5.7E-10	2.14E-07	1.6E-09	3.06E-04	8.4E-07	6.39E-08	3.1E-10	8.35E-09	9.8E-11	7.54E-07	5.31E-08	25.47±0.50
26	El Ham	-1.63	-6.10	6.63E-08	4.6E-10	2.41E-07	2.7E-09	3.50E-04	1.5E-06	7.26E-08	4.5E-10	9.33E-09	9.6E-11	1.27E-06	6.39E-09	23.27±0.77
27	Helal	-1.09	-2.60	6.56E-08	4.5E-10	2.41E-07	2.7E-09	3.41E-04	1.5E-06	7.13E-08	4.0E-10	9.11E-09	1.0E-10	1.28E-06	5.31E-09	23.32±0.63
28	Ismail	-0.84	0.50	6.42E-08	4.4E-10	2.49E-07	2.8E-09	3.49E-04	1.5E-06	7.20E-08	4.1E-10	9.35E-09	8.7E-11	1.40E-06	1.91E-09	22.95±0.55
29	El Hussain	-0.57	3.90	5.77E-08	3.1E-10	2.31E-07	1.7E-09	3.34E-04	9.2E-07	6.89E-08	3.3E-10	8.95E-09	8.4E-11	1.43E-06	0	24.82±0.65
30	Said	2.19	19.70	5.02E-08	3.5E-10	2.00E-07	2.2E-09	3.07E-04	1.3E-06	6.61E-08	3.8E-10	9.03E-09	9.5E-11	1.66E-06	4.75E-10	22.26±0.40

Table 5.2: Stable isotopes and noble gas data. n.s. (no sample) means that there is no noble gas sample from the well.

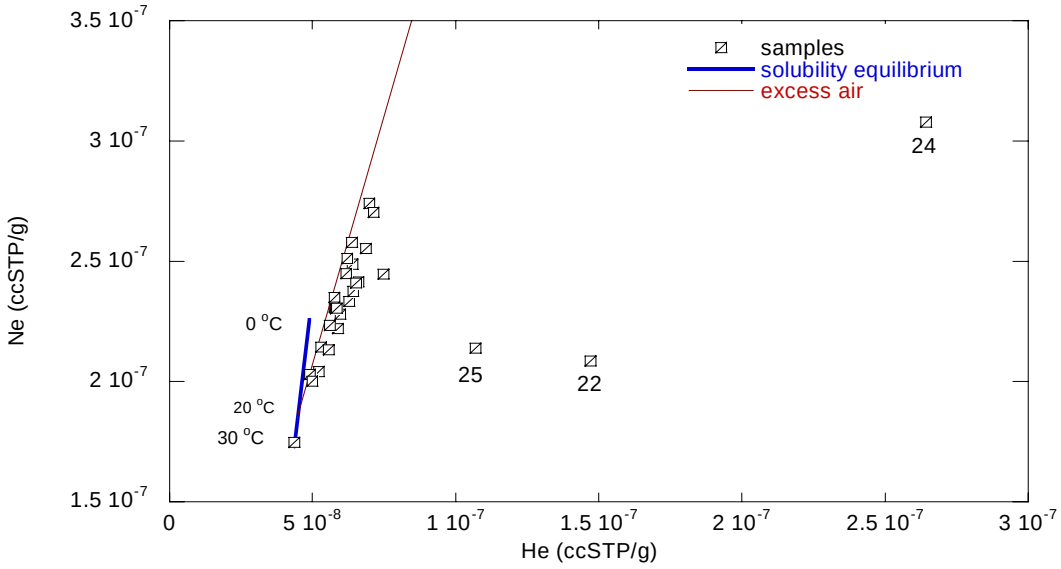

Figure 5.8: He versus Ne concentration of the groundwater samples from the study area

While a plot of Ne versus He (Figure 5.8) is suitable to discuss the effects of excess air and radiogenic He, a similar plot of Xe versus Ne is useful to visualize the effects of temperature and excess air (Figure 5.9). Xe reacts most sensitively to temperature, whereas Ne reflects mainly the presence of excess air. The data show that not only Ne concentrations vary strongly due to different amounts of excess air, but also Xe shows some variation, related to the recharge temperature. Note that because of the presence of excess air fractionation, the temperatures indicated by the lines referring to unfractionated excess air in Figure 5.9 are slightly too low. When fractionation is considered, the lines become somewhat steeper, as indicated in Figure 5.9 by the dotted line referring to the mean NGT and the mean excess air fractionation. Compared to this reference, most samples fall into a quite narrow temperature range close to the mean NGT (23.7 °C), but some samples yield significantly lower or higher temperatures. The best estimates of NGTs obtained by the inverse procedure using all noble gas data are listed in Table 5.2.

Although the coolest NGTs tend to occur close to the surface water, and the warmest at relatively large distance, there is no clear correlation between NGT and distance, radiogenic He, or stable isotopes. For example, Figure 5.10 shows the relationship between NGT and $\delta^{18}O$. Only a weak trend to lower NGTs at higher $\delta^{18}O$ is visible. Whereas the two groups of pre- and post 1969 groundwaters are clearly separated in the stable isotopes, their NGT ranges overlap strongly, although the younger waters with positive $\delta^{18}O$ tend to have cooler NGTs.

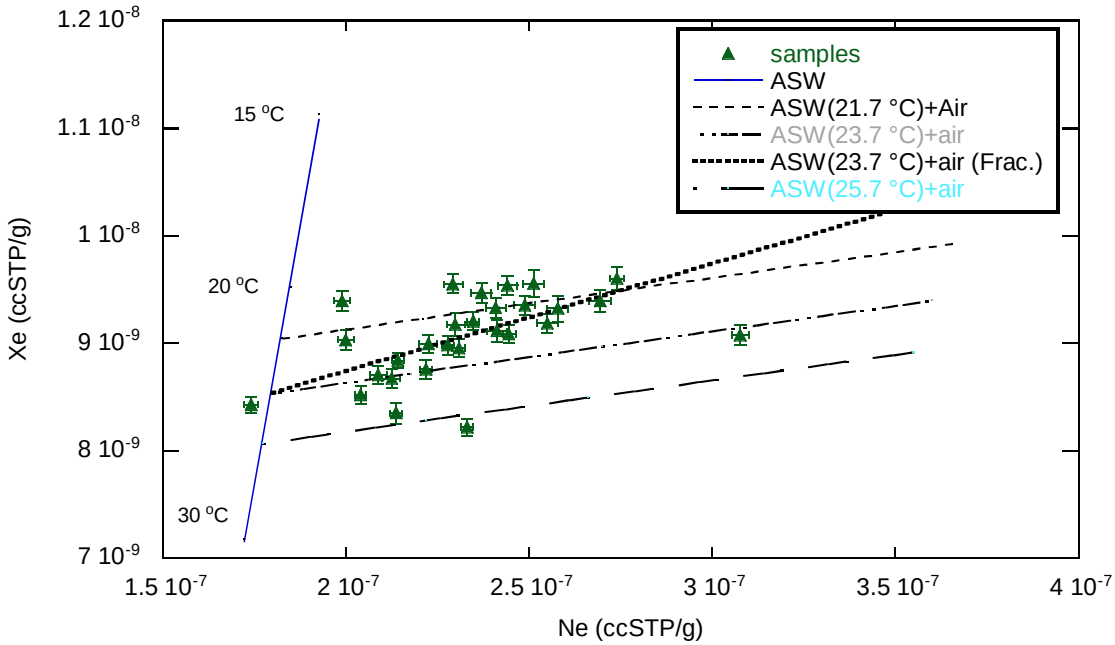

Figure 5.9: Ne versus Xe concentration in the samples from the study area. The ASW-line indicates values in solubility equilibrium for a range of temperatures. The broken, nearly horizontal lines indicate the effect of unfractionated excess air, which mainly is addition of excess Ne, shown for different recharge temperatures (the mean annual air temperature of 21.7 °C, the mean NGT of 23.7 °C, and for 25. 7°C). Note that actual lines representing fractionated excess air would be somewhat steeper (but different for each sample), therefore leading to higher noble gas temperatures. As an example, the case of the mean NGT and mean fractionation is indicated by the dotted line.

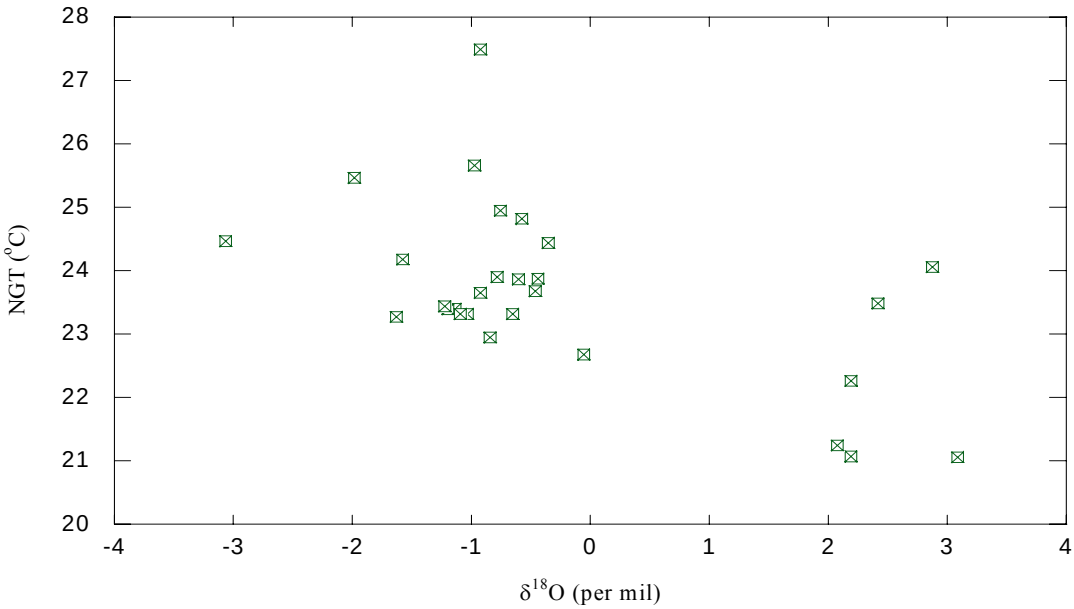

Figure 5.10: NGT versus $\delta^{18}O$ in the samples from the study area.

In summary, the NGTs do not seem to indicate clear paleoclimatic variations in this study. The lack of strong temperature variations (except for a few samples) might indicate that all samples are of Holocene age, i.e. from a period of relatively stable climatic conditions. The deviations of NGTs in some wells may be related to other variations in recharge conditions, e.g. the difference between direct recharge from surface water and recharge from precipitation.

5.4.3 ^{3}H-^{3}He and SF_6 groundwater ages

Only the wells located very close to the surface water have significant ^{3}H concentrations between 1.65 and 11.40 TU, allowing a reliable ^{3}H-^{3}He dating. These values are comparable to the ^{3}H concentration in present day precipitation in the region, which can roughly be estimated based on the few recent data available from the Global Network on Isotopes in Precipitation (GNIP) to be on the order of 5 TU. More important than precipitation data may be the tritium concentrations in the Nile River, for which we have no recent data. Obviously, the scarce data to reconstruct the tritium input history does not allow us to derive precise groundwater ages from tritium. The only firm statement that can be made is that the wells which contain significant ^{3}H concentrations contain at least a component of water that infiltrated after the tritium bomb peak in the early 1960s.

More precise estimates of groundwater residence times can be gained if ^{3}H and its decay product $^3He_{tri}$ are combined to calculate ^{3}H-^{3}He ages according to Eqs. (2.26) and (2.27). For water samples in which ^{3}H was not detected, the ages are assumed to be greater than 40 years. The tritiogenic ^{3}He was calculated using the following assumptions: (1) during recharge the water temperature was equal to the calculated noble gas temperature (NGT), (2) in case of a radiogenic ^{4}He component, the ^{3}He/^{4}He ratio of $2 \cdot 10^{-8}$ was used to correct for the radiogenic ^{3}He. Two different approaches to calculate the excess air contribution to ^{3}He were carried out. In the first, the excess air parameters obtained from the fit to all noble gases were used to calculate the He components. The second approach is essentially the classical method based on the Ne concentrations only (eq. 2.28), i.e. by multiplying the Ne excess by the He/Ne ratio of the excess air, but modified by using the information on excess air fractionation. Instead of the atmospheric He/Ne ratio, a slightly lower ratio representing fractionated excess air derived from the fitting procedure was used in equation (2.28). The two approaches yield very similar results, those obtained by the second procedure are listed in Table 5.3.

A reason to prefer the calculation of ^{3}H-^{3}He ages based on He and Ne data only is that the errors obtained in this calculation are slightly smaller and easier to interpret than if the information from all noble gases is used. The error in the calculated age is mainly caused by errors of the ^{3}H, the ^{3}He/^{4}He ratio and the concentrations of He and Ne. Furthermore, if no radiogenic He component is present in a given sample, the calculation of the ^{3}He components can be entirely based on the He data, instead of using Ne to estimate the atmospheric components. This simplified excess air

correction (eq. 2.30) leads to smaller errors in age because the $^3He/^4He$ ratio is measured with a better precision than the $^3He/Ne$ ratio. This approach was used for three samples where the parameters obtained from the heavy noble gases yield a slightly (not significant) negative result for radiogenic He, even when excess air fractionation is assumed.

Well. No	Well Name	^3H (TU)	SF_6 (fmol/l)	^3H-^3He age (yr)	SF_6 age (yr)
1	El-Khatatba Station	8.40±1.40	1.61±0.02	1.74±0.50	1.96±0.37
2	Mabruka	n.d.	0.21±0.01		25.83±0.57
5	Dr. Kamal	n.d.	0.17±0.02		26.73±0.68
6	Amr Syma	n.d.	0.16±0.02		27.30±0.69
7	El Manava	1.70±1.30	1.29±0.02	14.68±7.82	5.07±0.31
8	Kfr Dawod West	10.30±1.40	1.26±0.02	9.63±1.04	4.81±0.42
10	Sadat R	3.00±1.30	0.10±0.01	8.22±3.52	31.89±1.14
11	2000 Feddans 12	n.d.	0.19±0.02		25.11±0.62
14	Nekla station	4.60±1.60	0.21±0.02	24.73±4.65	26.98±0.61
15	Roshedy	4.80±1.10	1.05±0.02	20.19±2.83	10.17±0.35
19	Misila	n.d.	0.08±0.02		29.97±1.63
21	Giza	11.40±1.30		4.93±0.66	
22	Biko	n.d.	0.11±0.02		29.34±1.08
23	Intergroup	2.37±1.38	0.11±0.02	8.46±4.52	30.22±1.31
27	Helal	1.90±1.35	0.06±0.02	4.84±4.62	
29	El Hussain	n.d.	0.10±0.02		30.29±1.26

Table 5.3: ^3H-^3He and SF_6 ages for samples that have significant ^3H and SF_6 concentrations. n.d. (not detectable) means that tritium concentrations are near or below the detection limit of the measurement and consequently the ^3H-^3He ages can not be estimated for these samples

The ^3H-^3He ages of the groundwater samples show a distinct variation. Most of the wells that are located near the surface water have young ages between 2 and 24 years (Figure 5.11), these samples are the samples which lie on the mixing line (AC) defined by the stable isotope data (Figure 5.7), referring to infiltration after the completion of the Aswan High Dam. Theses ages show that the wells nearest to the surface water are recharged by water derived from the river (i.e., directly from river branches or via canals or irrigation). These samples are characterized by high tritium concentrations (about 5 to 11 TU) and are all located within 1.6 km from the surface water. A few wells (no. 7, 10 and 23) located further away from the surface water exhibit low but detectable tritium concentrations. Of these wells, no. 23 is located at a distance of only 6.8 km from the surface water, whereas the other two are about 30 km away from the delta. The remaining samples are old water (> 40 yr) and three of them (no. 22, 24 and 25) are very old water, characterized by a high radiogenic component and by high salinity.

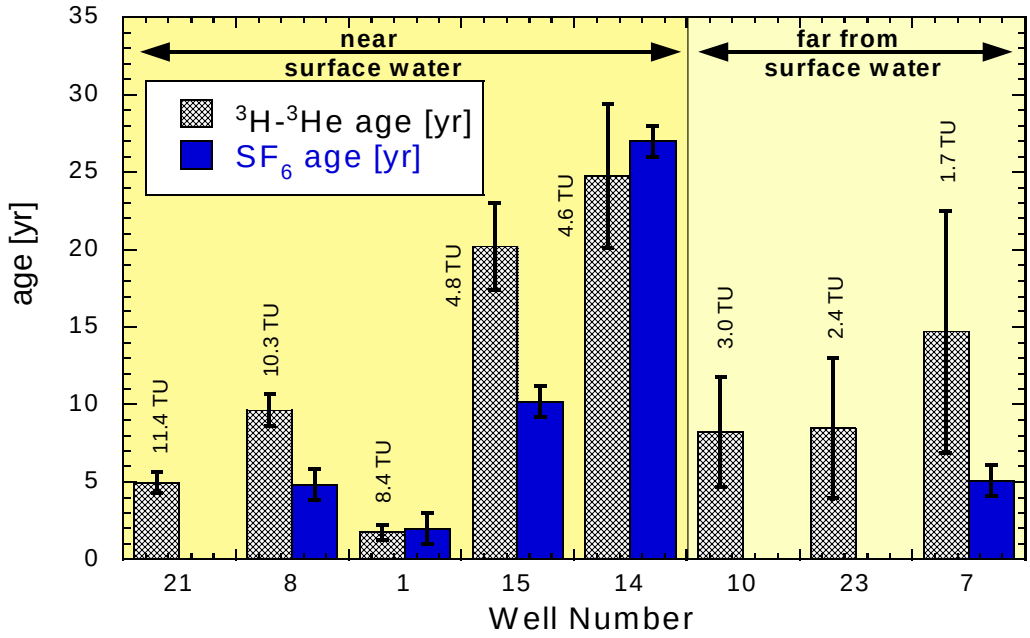

Figure 5.11: ^{3}H-^{3}He and SF$_6$ ages of groundwater samples

The tritium detected in well no. 23 probably indicates admixing of a young, surface water derived component, which tentatively can be dated by the ^{3}H-^{3}He method to an age of 8.5 ± 4.5 yr. The tritium in the more distant wells no. 7 and no. 10 is more difficult to interpret. It may also be attributed to local admixing of a young component, but this would have to be derived from precipitation and penetrate quickly through the deep unsaturated zone, so in reality there is no real explanation to the presence of significant ^{3}H concentrations in these wells. For example, well no. 7 lies on a transect between the wells no. 5 and no. 6 (Figure 5.1), which both contain no tritium. The most plausible but speculative explanation for this phenomenon is related to the orographic condition of this area. The area of well 7 has an elevation between 0 and 50 m above sea level, while well 5 and well 6 are located in areas characterized by 50-100 m in elevation (Figure 5.5b), so that the area of well 7 may be considered as a collection area for precipitation and consequently infiltration of water in this area may be higher than near the other two wells. The apparent ^{3}H-^{3}He age of the young groundwater component present in well no. 7 is 14.7 ± 7.8 yr. Well 10 has a tritium concentration of 3 TU, and the apparent age is 8.2 ± 3.5 yr, again there is no clear interpretation of the presence of tritium in this well.

Another remarkable well is well no. 30, which although located near the surface water (at a distance of about 1.6 km), has no significant tritium concentration and hence of course no ^{3}H-^{3}He age. It is also characterized by a rather high salinity (1100 ppm, Table 5.1), but it has only low radiogenic He (Table 5.2). A possible reason for the absence of young water in this well might be the strong pumping in the area, which has led to a local lowering of water table and changes in the groundwater flow pattern that could have resulted in attracting older, more saline water from deeper layers or clay lenses.

The measured SF_6 concentrations and ages derived after excess air correction (compare chapter 4, section 4.5) are listed in Table 5.3. The results of the SF_6-analyses indicate that the wells that are located close to the artificial irrigation canals (El-Rayah El-Nasiry and El-Rayah El-Behary) have young ages between 2 and 25 years (Figure 5.11), which confirms that the wells nearest to the surface water are directly recharged by water derived from the river. Among these young wells, the ^3H-^3He and SF_6 ages for wells no. 1 and 14 are in good agreement (Figure 5.11, Table 5.3), while there is disagreement between them for wells no. 8 and 15. The SF_6 ages for these two wells are less than the ^3H-^3He ages, this might be explained by a small contamination during sampling, which would lead to an underestimation of SF_6 ages.

SF_6 is very sensitive to air contamination, and the sampling procedure that was applied using glass bottles that were pre-filled with N_2 and partly evacuated in the field (chapter 4, section 4.4) may be more prone to contamination both during sampling and transport than the copper tube method used for He. Duplicate samples were taken from most wells, and several samples could clearly be identified as leaky and were excluded from the interpretation. The remaining samples still exhibited a slight overpressure in the N_2-headspace before analysis, indicating that no air contamination should have taken place during storage and transport. However, a slight air contamination during sampling cannot be entirely excluded.

Most of the wells that are located further away from the irrigation area around the artificial canals have very low, although detectable, SF_6 concentrations. Only one well at large distance (no. 7) has a significant SF_6 concentration. As discussed above, this well also contains some tritium and may be influenced by local recharge, although this remains highly uncertain. The apparent SF_6 age at this well is about 5 yr, much lower than the ^3H-^3He age of about 15 yr, which actually argues against the hypothesis of local recharge, because the deep unsaturated zone should lead to a lag in SF_6 transport to the water table and therefore an older SF_6 age compared to ^3H-^3He (Cook and Solomon, 1995). The unexpectedly high SF_6 concentration and low apparent age is therefore most likely due to SF_6 contamination of this sample.

The SF_6 concentrations in the remaining samples lie near to but usually significantly above the analytical detection limit of about 0.02 fmol/l. These concentrations of dissolved SF_6 translate to atmospheric mixing ratios at solubility equilibrium on the order of 0.2 ppt, typically somewhat above the expected natural background of 0.054 ppt (Busenberg and Plummer, 2000). They are comparable to the reconstructed atmospheric concentrations at around 1970, which Busenberg and Plummer (2000) regarded as the practical dating limit of the method. At this low concentration level, the analytical error corresponds to a dating uncertainty of less than ± 2 years. For waters younger than about 15 yr, which have much higher SF_6 concentrations, the analytical errors result in dating uncertainties of less than ± 0.5 years.

The apparent SF_6 ages (Table 5.3) calculated from the samples at larger distance are all (except well no. 7) higher than 25 years, and frequently larger than the practical limit of 33 yr (i.e. older than 1970). Even though some of the lower age results are

slightly below the detection limit of the method, we do not trust these ages very much, mainly because of the possibility of slight air contamination affecting the samples. An exception may be the wells no. 5 and 6, which reproducibly yielded small but significant SF_6 concentrations that appear unlikely to be due to air contamination. Other possible explanation for traces of SF_6 in these wells, where old water is expected based on tritium and distance from the surface water, might be the presence of natural SF_6 formed in rocks that contain fluoride (Harnisch and Eisenhauer, 1998) or small admixing of a younger water component. In the latter case, one would also expect to detect low levels of tritium in these wells. The detection limit of about 1.5 TU achieved by the radiometric measurement is not sufficient to rule out small concentrations of tritium in the samples. To investigate this possibility, tritium would have to be measured by the more precise ^3He ingrowth technique based on noble gas mass spectrometry, as it was initially planned but not be carried out yet due to technical problems.

5.5 Summary and conclusions

The new reclamation area southwest of the Nile delta seems to be recharged mainly from Nile water. Most of the rechare process took place before the completion of the Aswan High Dam in 1969 as indicated by stable isotope data and corroborated by the absence of the transient tracers tritium and SF_6 in most wells. The few samples that lie on the stable isotope mixing line between paleo-groundwater and recent river water, indicating recharge by Nile water after the completion of the Aswan High Dam, are from wells located very close to the surface water. These samples are also characterized by significant ^3H and SF_6 concentrations, yielding young ages smaller than 25 years.

While the isotopic signature of the groundwater in the reclaimed areas indicates that it originates from the Nile River and therefore is a renewable resource, the absence of recent recharge shows that the groundwater renewal is a slow process. The exact timescale of water flow from the surface water to the reclamation areas in the southwest of the delta still needs to be determined by ^{14}C-dating, as the dating range of the methods discussed above proved to be insufficient. Dating of the groundwater along our transects should be useful to determine the flow velocities in the area and to estimate the total groundwater renewal rate. Although it may be that changes in the hydraulic gradients due to pumping in the reclaimed areas may increase the water flow into the region in the future, knowledge of the groundwater inflow in the past will be an important cornerstone of any policy of sustainable management of the groundwater resource. Our results show that at present recharge is slow and therefore only a limited amount of groundwater is available for pumping in a sustainable resource management regime. Numerical groundwater modeling, preferably making use of the age information from tracer studies, will be needed to make quantitative predictions on the groundwater flow regime in the future for different pumping scenarios.

Chapter 6

6 Environmental tracer study of groundwater in the Oman Mountains

6.1 Introduction

The Sultanate of Oman, which covers an area of about 309.5 thousand km^2 (Figure 6.1) is located at the south-eastern tip of the Arabic Peninsula, bordering the Republic of Yemen in the south, the United Arab Emirates (UAE) in the north and Saudi Arabia in the west. To the south-east it is bounded by the Arabian Sea and to the north-east by the Gulf of Oman.

Figure 6.1: Map of the Sultanate of Oman (Oman maps, Perry-Castaneda Library Map Collection, University of Texas, USA)

Most of the sultanate's area (about 80%) is covered by extensive, relatively flat sand and gravel plains. A chain of mountains extends only in the northern region of the Sultanate, the highest peak of which, Jabal Shams, rises to more than 3000 m above sea level (Lüdeling, 2004). The Oman Mountain range, which structurally forms a giant anticline, subdivides the northern part of Oman and the eastern part of the UAE into the Batinah Plain on the coast, the mountain area and the interior plains (Lüdeling, 2004). The eastern Batinah coastal plain northwest of the capital city Muscat is the most densely populated, cultivated and industrialized area of the Sultanate of Oman. Most of the water demand in this area is supplied by groundwater, making the alluvial aquifer beneath the Batinah plain one of the most important aquifers in the Sultanate (Weyhenmeyer et al., 2002).

In this work we will study groundwater in the Oman Mountains where several oases are found and the citizens in these oases depend mainly on groundwater for drinking and for agricultural purposes. The major goal of this research project is a better understanding of the groundwater system, especially the identification of the dominant recharge areas, the source of recharge, and estimation of the groundwater residence and renewal times. Stable isotopes ($\delta^{18}O$ and δD) are applied to identify recharge areas and recharge sources while ^{3}H, noble gases, SF_6, and CFCs are used to estimate groundwater residence times.

This study was initiated by and conducted in collaboration with the Institute of Crop Science of the University of Kassel. The research group of Prof. Dr. Andreas Bürkert at this institute studies ecological crop production and agricultural ecosystems in the tropics and subtropics. Their primary motivation to investigate the age of the spring water in the oases of the Oman Mountains was to determine how these scattered settlements could survive for thousands of years in a very arid environment, where precipitation occurs only sporadically and several consecutive years without any groundwater recharge are not unusual. In addition, the dating of the spring water would help to estimate the size of the groundwater reservoirs and thereby to determine the natural limits of a sustainable development of these locations.

6.2 Site description and hydrogeologic setting

6.2.1 Study area

This work was conducted to investigate groundwater in several locations in the central part of the Oman Mountains (Figure 6.2). The Balad Seet oasis is situated at the foot of the northern part of a steep cliff where a 1000 m thick layer of highly permeable carbonates (dolomites and limestones) rests over red-greyish-green silt and clay stones of the Muadin Formation, which had been deposited during Pre-Permian times. The springs at this location are considered to have a large catchment area, where a rain event of 50 mm stabilized the spring outflows, which is in the range of 580 $m^3\ d^{-1}$ to 760 $m^3\ d^{-1}$ (Horst et al., 2002). The oases of Hat and Misfat Al Abreen are located in the vicinity of Balad Seet and have similar hydrogeological features.

The oasis of Maqta, Ismaiah and Umq Bir are located in Wadi Khabbah in the Al-Hajar Asha'sharqi range. Around Maqta dark colored, often fractured ophiolitic rocks, mainly harzburgites, dominate. The groundwater circulates in the fractures of these rocks or in the loose sediments of the wadis. The outflows of springs in this location are about 190 m^3 d^{-1} (Horst et al., 2002).

Another two locations have been studied, the location Nakhl, which lies at the foot of the north-western edge of the Hajar Mountains below the Jabal Akhdar, and Al Ain, which is situated several kilometers south east of the Balad Seet oasis.

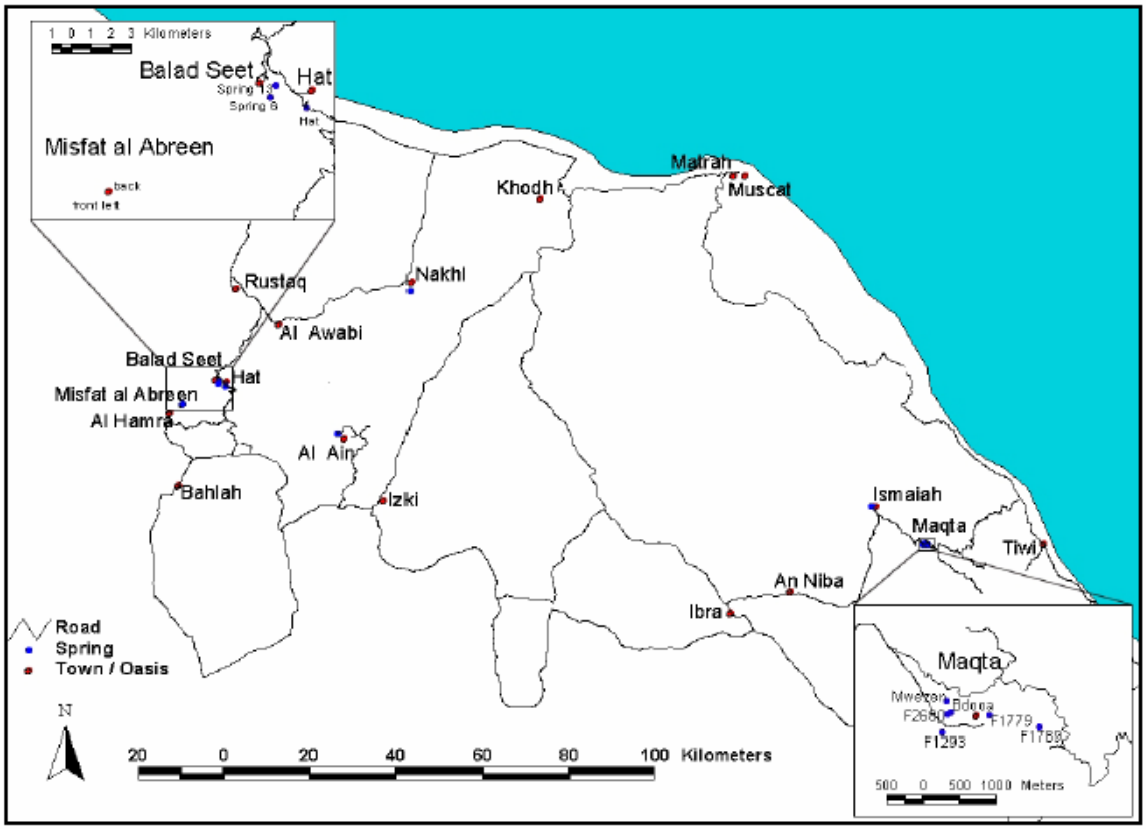

Figure 6.2: Locations where samples were taken. Insets show the areas around the oases of Balad Seet and Maqta in more detail, which were studied most intensively (Lüdeling, 2004).

6.2.2 Geology

The geological structure of Oman is reflected in the main morphologic–hydrogeologic zones of Oman, which are:

(1) the Oman Mountains, (2) the western foreland of the Oman Mountains composed prevailingly of extensive gravel fans, (3) the eastern coastal plain Al Batinah on the Golf of Oman, (4) the sand seas of Rub al Khali extending from Saudi Arabia into the west of Oman, and (5) the mountain and plateau landscapes of Najd and Dhofar which are bordered in the south by the Arabian Sea

The geology of the Oman Mountains has been described by several authors such as Glennie et al. (1974), Robertson et al. (1990) and Hanna (1990) who divided the central Oman Mountains into an internal and external zone, the internal zone comprises Jabal Akhdar, Jabal Nakhl and Saih Hatat. The major structural domains of this zone are the anticlines of Jabal Akhdar, Jabal Nakhl and Saih Hatat, exposing the whole tectonostratigraphic sequence of the Northern Oman Mountains from the pre-Permian basement rocks, Permian to Cretaceous shelf carbonates, Hawasina rocks, Semail ophiolite to the late Cretaceous to Tertiary carbonates. The rock units of the study area are conveniently divided into five major geological units, which will be explained briefly in the following:

The Pre-Permian basement is mainly exposed in the core of the Jabal Akhdar anticline, where erosion has created several topographically low bowls. Rocks of the pre-Permian are considered as the oldest rocks in Oman. The basement consists of several types of crystalline rocks and ancient sediments, most of the basement sediments seem to be of terrestrial nature, which make these rocks unsuitable for water storage (Lüdeling, 2004). The absence of springs with significant discharge and the occurrence of many springs e.g. Al Ain, Hat and Balad Seet (Figure 6.3) along the contact between the pre-Permian and the overlying dolomites of the Hajar Supergroup indicate a low permeability and restricted aquifer capabilities of these rocks.

The Hajar Supergroup is exposed on the southern flank of the Jabal Akhdar, where it actually forms the southern limb of the Jabal Akhdar anticline. The sediments of the Hajar Supergroup mainly consist of massive limestones and some dolomites that were deposited in a shallow marine environment on the Arabian continental shelf. The majority of the Hajar Supergroup is divided into four subdivisions (groups): Akhdar, Sahtan, Kahmah and Wasia. In some locations, all these groups together arise to a thickness of up 3000 m. The limestones of the Hajar Supergroup represent the main bedrock aquifer in the study area. The aquifer is extremely heterogeneous and anisotropic due to the extensive fracture network and karstic features. The water is stored in caves, clefts and crevices, where the Hajar Supergroup contains some of the largest caves in the world and appears to have a porous structure throughout. The Hajar Supergroup aquifer is recharged by rainfall on the Jabal Akhdar, which infiltrates either directly into small fractures and cavities or causes a surface runoff, which infiltrates into the alluvium in the deeply incised gorges within the Jabal Akhdar Mountains.

The Hawasina is exposed along the southern edge of the Jabal Akhdar in the Nizwa and Wadi Mu'aydin area. The Hawasina is a stack of intensely deformed thrust sheets consisting of hemipelagic to pelagic sediments and turbidites. It is the result of sedimentation along the continental rise and abyssal plain of the Hamrat Duru Basin. In addition to these sediments, remains of a carbonate platform, which may have been an island, a small archipelago or even a reef, and some residues from another ocean basin (Umar Basin) beyond this platform constitute this Supergroup (Lüdeling, 2004). The Hawasina rocks unconformably overlie the carbonates of the Hajar Supergroup or the sediments of the Aruma Group.

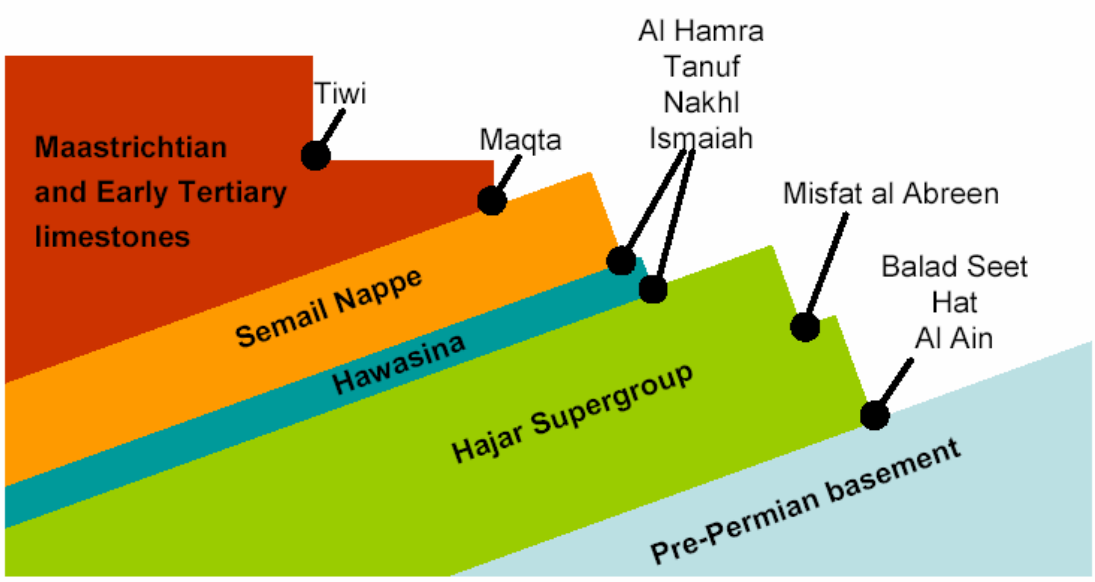

Figure 6.3: Stratigraphic relationship of the geological groups of the study areas and locations of the settlements within the stratigraphy. Al Hamra, Tanuf, Nakhl and Ismaiah were assigned two possible locations, as the Hawasina is not always present (Lüdeling, 2004).

The Semail Nappe forms a huge thrust sheet of mid Cretaceous oceanic lithosphere that was obducted onto the Arabian continental margin during the late Cretaceous (Lippard et al., 1986).The Semail Nappe is over 600 km long, up to 150 km wide, and between 5 to 10 km thick (Lippard et al., 1986). The Semail consists of mantle rocks (peridotites and harzburgites) in the structurally lower layers and igneous rocks higher up. Initially the structurally higher layers were characterized by gabbros, through which later basalts intruded, forming dykes in the gabbros and lava pillows on the ocean floor (Lüdeling, 2004).

The Maastrichtian and early tertiary limestones were deposited after obduction of the Semail Nappe at the bottom of a shallow sea on the continental shelf. The rather uniform carbonate formation ended abruptly about 35 Ma BP, when the Oman Mountain range was uplifted and the area was raised above sea level. These rocks are considered to provide good storage of water, where the thick carbonate sequences of these rocks tend to form caves and cavernous structures, very much like the rocks of the Hajar Supergroup (Lüdeling, 2004)

6.2.3 Climate

Oman's varied geography results in a wide range of climatic conditions. There are two seasons in Oman, summer and winter. Winters in Oman are relatively cool, with average coastal temperatures ranging from about 14 to 26 ^{o}C in January. In Salalah (southwestern Oman), humid weather with temperatures approaching 30 ^{o}C is common even in December. In mid June, average coastal temperatures range from about 30 to 39 ^{o}C (in the interior temperatures tend to be more extreme). Rainfall in

Oman is light but erratic and unpredictable. It can fall sporadically for weeks, or heavily for minutes, and can be incredibly localized.

The climate of Northern Oman is arid and characterized by warm winters with low humidity, very hot and sometimes humid summers, low and erratic rainfall, large variations in relative humidity and high rates of evapotranspiration. The long-term mean annual air temperature is 28.5 ^{o}C for the coastal areas (meteorological station at Seeb International Airport; 15 masl) and 17.8 ^{o}C in the mountains (meteorological station at Saiq; 1897 masl) (Weyhenmeyer et al., 2002). Precipitation is extremely variable in space and time, the mean annual precipitation ranges from < 50 to 300 mm (Wagner et al., 1999). In coastal areas the mean annual precipitation lies between 60 and 100 mm/yr, mountainous regions above 1000 m receive in excess of 200 mm/yr and more than 300 mm/yr in areas located above 2000 m (Weyhenmeyer et al., 2002). Two types of rainstorms predominate in the Sultanate (Wagner et al., 2000):

(i) Storms related to frontal depression systems, which originate over the Mediterranean Sea and trace into Oman during the winter months (mostly between December and March)

(ii) Local convective storm cells that form over the mountains during the very hot summers and cause short and heavy rainfall mostly in the mountainous regions (i.e., orographic rain).

6.3 Methods

6.3.1 Sampling

More than 20 samples have been taken between March 2002 and March 2004 from springs in oases in Northern Oman. The sampling was performed by the members of the Institute of Crop Science of the University of Kassel (Prof. Dr. A. Bürkert and E. Lüdeling) or their local collaborators. Samples were collected for the analysis of stable isotopes, noble gases, tritium, SF_6 and CFCs. The sampling covered two major areas: the first includes the oases of Balad Seet, Misfat Al Abreen, and Hat spring; the second includes the oases of Ismaiah, Umq Bir, and Maqta. Additional samples were taken from the Jabal Akhdar area, Al Ain and a thermal spring in Nakhl.

Sampling natural springs for dissolved gases can be quite difficult, because it is often impossible to make sure that no contact with air, possibly leading to gas exchange, has occurred before the point of sampling, especially in karstic areas. Furthermore, there is no way to increase water pressure in order to avoid degassing. The water was transferred into the sample containers through flexible PVC-tubing, which was inserted as far as possible into the spring outlets (usually fractures) to collect the water before it had contact with air.

6.3.2 Stable isotopes

Stable isotope samples were collected in 50 ml glass bottles and analyzed in the Heidelberg laboratory with a Finnigan MAT 252 mass spectrometer, using the measurement technique that has been described briefly in section 5.3.2.

6.3.3 Noble gases and tritium

Noble gas samples were collected in copper tubes sealed with stainless steel pinch-off clamps. Two slightly different designs of these samplers were used: The first samples collected in 2002 and early 2003 were taken in the samplers used by the noble gas lab of ETH Zurich, which contained either about 45 or 22 ml of water, whereas the later samples were taken with the 40-ml samplers of the Heidelberg lab. All noble gas analyses were performed at ETH Zurich, according to the procedures described in section 5.3.3 and in more detail by Beyerle et al. (2000).

Tritium analyses were also performed at ETH Zurich using the ^{3}He ingrowth method (Clarke et al., 1976). For the samples collected in the Zurich-type copper tubes, tritium was measured on the same water, which was re-sealed in the copper tube after having been degassed for the noble gas analysis. Otherwise, dedicated tritium samples were taken in glass or plastic bottles. The water was later degassed in the Heidelberg laboratory and flame-sealed in glass ampoules (see Bayer et al., 1989). In both cases, the degassed samples were stored for several months before being degassed again for analysis of the ingrown ^{3}He. The method used for tritium follows essentially the description given by Beyerle et al. (2000), except that the mass spectrometer was equipped with a specially designed compressor ion source (Baur, 1999), which increases the sensitivity for ^{3}He by about a factor of 100. Both the detection limit and the precision for tritium achieved with this technique were usually better than 0.1 TU.

6.3.4 SF_6

Samples for SF_6 were collected in 500 ml stainless steel cylinders (described in chapter 4, section 4.4). The samples taken in 2002 and January 2003 were extracted and measured in the tracer laboratory of EAWAG, Dübendorf (Switzerland) using a gas chromatograph (Carlo Erba, Milan) equipped with a molecular sieve 5 ^{o}A column (6 ft x 1/8 in., 80/100 mesh, Alltech) operated at room temperature and an electron capture detector (ECD Fisons 800) kept at 350 ^{o}C. The rest of the samples have been extracted and measured at the Institute of Environmental Physics in Heidelberg, Germany according to the method described in chapter 4, section 4.4.

6.3.5 CFCs

Water samples for CFC analysis were taken in the same copper tubes that are used for noble gas samples (section 6.3.3), the samples were extracted and measured at EAWAG (Switzerland) using the techniques described by Hofer and Imboden (1998). The dissolved gases were extracted from the water samples under vacuum and then collected in a trap cooled to -196 ^{o}C. After release from the trap by heating and flushing by carrier gas, the analysis was conducted using a gas chromatograph (Shimadzu GC-14 A, Kyoto, Japan) equipped with an electron capture detector (ECD) for the determination of CFCs.

6.4 Results and discussion

Table 6.1 provides an overview of the samples sorted by location. A short name code is introduced to identify the samples. In this code, the first two letters identify the location. The following number identifies different springs at each location. The last letter identifies the sampling campaign (Table 6.2).

Name	Location (Oasis)	Spring	Date	Temp [m]	Altitude of spring [m]	Est. recharge altitude [m]
BS1a	Balad Seet	Spring 6	09.03.2002	23.3	1115	1700-2100
BS1b	Balad Seet	Spring 6	25.11.2002	23	1115	1700-2100
BS2a	Balad Seet	Spring 13	19.03.2002	26	980	1700-2100
BS2b	Balad Seet	Spring 13	25.11.2002	26	980	1700-2100
HA1c	Hat	Spring Hat	15.01.2003	17	1305	1700-2100
HA1d	Hat	Spring Hat	12.06.2003	24	1305	1700-2100
HA1e	Hat	Spring Hat	18.08.2003	24.2	1305	1700-2100
MI1c	Misfat al Abreen	Spring Misfat (front left)	15.01.2003	27	917	1800-1200
MI2c	Misfat al Abreen	Spring Misfat (back)	15.01.2003	27	917	1800-1200
MA1a	Maqta	Spring F1293	12.03.2002	25	1008	1200-1600
MA2a	Maqta	Spring F1779	13.03.2002	26	1055	1200-1600
MA3a	Maqta	Spring WAZIN	13.03.2002	26	958	1200-1600
MA4b	Maqta	Spring F2680	29.11.2002	26	957	1200-1600
MA5c	Maqta	Spring F1789	15.01.2003	15	1196	1200-1600
MA6d	Maqta	Bdooa	10.06.2003	28	965	1200-1600
IS1c	Ismaiah	Spring Ismaiah	15.01.2003	33.5	439	1200-1600
IS1d	Ismaiah	Spring Ismaiah	09.06.2003	35	439	1200-1600
NA1d	Nakhl		11.06.2003	38.3	149	400-1200
AA1d	Al Ain		13.06.2003	23	1936	2000-2300
JA1f	Jabal Akhdar	lower spring	25.03.2004	19.8	1720	2000-2300
JA2f	Jabal Akhdar	Wadi Bani Habib	25.03.2004	23.1	1960	2000-2300
JA3f	Jabal Akhdar	Massara	26.03.2004	23.3	1059	1500-1800
UB1f	Umq Bir	upper spring	16.03.2004	21.6	767	1200-1300
UB2f	Umq Bir	upper spring	17.03.2004	25.3	767	1200-1300

Table 6.1: List of Oman samples

Location		Campaign	
BS	Balad Seet	a	2-Mar
HA	Hat	b	Nov. 02
MI	Misfat al Abreen	c	Jan. 03
MA	Maqta	d	3-Jun
IS	Ismaiah	e	Aug. 03
NA	Nakhl	f	4-Mar
AA	Al Ain		
JA	Jabal Akhdar		
UB	Umq Bir		

Table 6.2: Sample name code of Oman samples

6.4.1 Stable isotopes

The range of the stable isotope values reflects the recharge conditions temperature and altitude, as well as the moisture source. E.g., the most negative values of $\delta^{18}O$ and δD from the Oman samples may be related to recharge at high altitude in the mountain area (Table 6.3). The relationship between the stable isotope values and altitude has, however, not yet been defined in detail. It may be difficult to define such a relationship, because the stable isotope composition of precipitation in this area is strongly dependent on the moisture source. Weyhenmeyer et al. (2002) showed that stable isotope analyses of rainfall samples collected on the eastern Batinah coastal plain of northern Oman between 1995 and 1998 indicate two different principal water vapor sources for precipitation in the area: a northern, Mediterranean source and a southern, Indian Ocean source. As a result two new local meteoric water lines have been defined for the eastern Batinah region; the first one for precipitation originating from northern moisture sources (LMWL-N) with $\delta D = 5.0 \cdot \delta^{18}O + 10.7$ and the second for tropical rainfall from southern/ southeastern moisture sources (LMWL-S) with $\delta D = 7.2 \cdot \delta^{18}O - 1.1$.

Name	$\delta^{18}O$ (‰)	δD (‰)
HA1d	-4.03	-15.9
MA6d	-4.07	-19.1
IS1d	-3.84	-16.2
NA1d	-3.19	-11.9
AA1d	-3.39	-13.3
JA1f	-2.75	-11
JA2f	-3.85	-16.8
JA3f	-3.02	-11
UB1f	-5.24	-27
UB2f	-3.84	-16.6

Table 6.3: Stable isotope data (values in ‰ relative to V-SMOW)

Weyhenmeyer et al. (2002) also defined a local meteoric water line for the eastern Batinah region from isotopic analyses of groundwater samples from over 200 springs and wells. The Batinah meteoric water line ($\delta D = 5.3 \cdot \delta^{18}O + 2.7$) plots between the two local meteoric water lines (LMWL-N and LMWL-S), indicating that the origin of the water in the Batinah coastal alluvial aquifer is a combination of northern and southern moisture sources.

The stable isotope data obtained in this study from the springs in the Oman mountains lie on or near the Batinah meteoric water line (Figure. 6.4), indicating that the origin of groundwater in the investigation areas Jabal Akhdar, Hat spring, Umq Bir, Al Ain, Nakhl, Ismaiah and Maqta oasis is similar to that in the coastal plain, i.e. a combination between the northern and southern moisture sources.

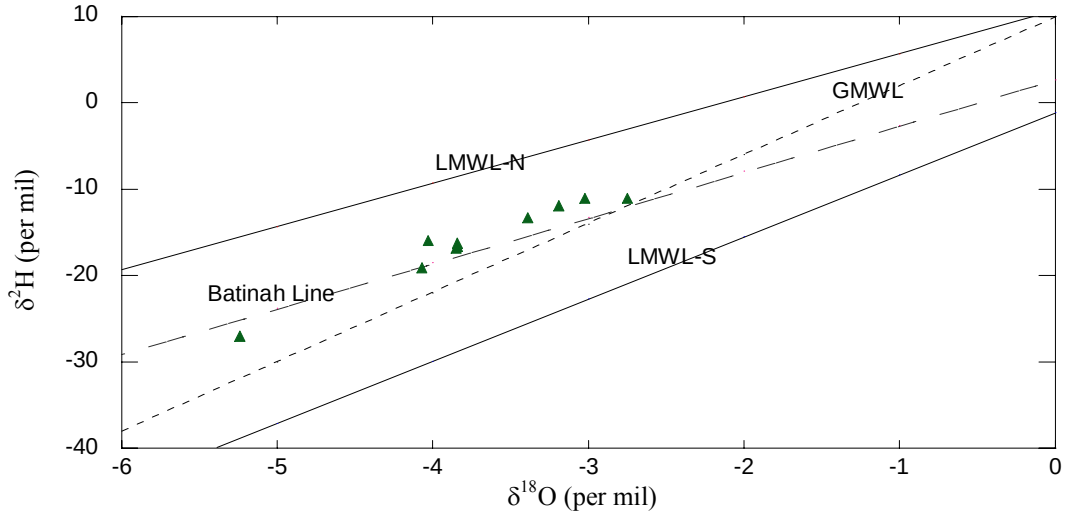

Figure 6.4: $\delta^{18}O/\delta D$ plot of groundwater samples from Oman Mountains containing the three meteoric water lines for the eastern Batinah region as defined by Weyhenmeyer et al. (2002) and the global meteoric water line (GMWL).

6.4.2 Noble gases and recharge altitude

The dependence of the equilibrium component of the measured noble gas concentrations C_i on pressure P, which in turn is related to the elevation H, and on recharge temperature T presents the possibility of using noble gases as recharge elevation tracers. If three or more dissolved gas concentrations are measured then a system of equations can in effect be solved simultaneously, using standard inverse techniques to determine the unknown parameters T, H, and A (excess air). This inverse problem can be solved by using the method described by Aeschbach-Hertig et al. (1999), employing χ^2 minimization. The method is described in section 2.4 and has been applied in section 3.4.2.

In this work three attempts have been performed to estimate the recharge altitude of Oman groundwater. Concentrations of the noble gases He, Ne, Ar, Kr, and Xe have

been measured, but the He concentrations were not used because of the terrigenic component. The first attempt to determine the recharge elevation is to treat pressure P together with temperature T and excess air A as a free parameter, i.e. to fit the parameter combination T-P-A, assuming no fractionation of the excess air component (otherwise the number of free parameters equals the number of constraints, which often leads to unrealistic solutions). The result of this attempt is summarized in Table 6.4. For the Balad Seet samples the altitude can be estimated for only one sample which is fitted with the model, the other samples do not fit. The estimated recharge altitude for this sample is 913 m with a large uncertainty of ± 500 m. This result is comparable to the sampling altitude of 980 m, but seems too low compared to the expected recharge altitude of 1700 – 2100 m (Table 6.1). Three of the Maqta samples yield good fits with the model with more or less realistic altitudes between 960 and 1750 m, but they have large uncertainties, while the other two give unrealistically high altitudes of 4400 and 9800 m, which are far above the maximum elevation of the mountains.

No.	Location	Sampling H[m]	χ^2	p [%]	T [°C]	A [ccSTP/kg]	Calculated H [m]
1	BS1a	1115	39.13	0.0	24.1 ± 1.9	0.00	1001 ± 418
2	BS2a	980	0.04	84.7	26.3 ± 2.4	0.04	913 ± 505
3	MA1a	1005	0.00		22.3 ± 11.4	0.61	1746 ± 550
4	MA2a	1060	0.00	99.1	23.9 ± 2.0	1.03	1522 ± 448
5	MA3a	958	0.28	59.9	28.4 ± 2.5	0.10	960 ± 509
6	BS1b	1115	9.76	0.2	0.00 ± 2.8	6.62	9396 ± 835
7	BS2b	980	4.89	2.7	32.4 ± 3.8	0.00	435 ± 713
8	MA4b	1200	7.22	0.7	0.00 ± 2.8	7.03	9813 ± 850
9	HA1c	1300	17.68	0.0	0.00 ± 2.7	7.37	8581 ± 812
10	MA5c	1196	0.05	82.5	6.8 ± 2.8	7.48	4401 ± 760
11	HA1d	1305	3.87	4.9	16.7 ± 2.6	1.69	2137 ± 620
12	IS1d	439	8.21	0.4	26.9 ± 3.0	2.36	1018 ± 659
13	MA6d	965	2.16	14.1	26.2 ± 3.1	0.57	1081 ± 663
14	NA1d	149	3.12	7.7	30.7 ± 3.5	6.09	-304 ± 742
15	AA1d	1936	5.13	2.3	20.3 ± 2.5	0.00	2076 ± 575
16	HA1e	1305	4.84	2.8	15.4 ± 2.5	1.72	2456 ± 619

Table 6.4: Results of fitting the parameters T, P, and A. Pressure P is converted to altitude H using the barometric formula (eq. 2.16). The probability is not calculated for MA1a because the Ne measurement failed for this sample.

The two Hat samples yield a good fit with the model, and the estimated altitudes of both samples are close to each other, the mean of the two estimated altitudes is about 2300 ± 620 m, and the mean NGT is 16.1 ± 2.5 °C. The sample from Al Ain yields a recharge altitude of 2080 ± 570 m and a NGT of 20.3 ± 2.5 $^{\circ}C$.

The T-P-A fit with the UA-model is not suitable to estimate the recharge altitudes, some samples do not fit with the model, while the ones that do fit give large uncertainties and sometimes unrealistic results. The large uncertainties are due to the

high correlation between the model parameters T and P, especially if excess air is present, as already noted by Aeschbach-Hertig et al. (1999).
The second attempt to estimate the recharge altitude of the Oman groundwater is to use the noble gas data to derive a set of best-fit H–T pairs for a given sample by specifying various values of H and fitting the respective T. Assuming that T is equal to the mean annual air temperature at all elevations (implying that the water table is near the land surface), the actual H and T for the sample should be the point of intersection between the almost linear set of best-fit solutions and a line representing the local atmospheric temperature lapse on a plot of H versus T (Figure 6.5). This approach has been proposed by Aeschbach-Hertig et al. (1999) and applied by Manning et al. (2003). However, as already noted by Aeschbach-Hertig et al. (1999), the relationship between the two model parameters T and H unfortunately resembles strongly the meteorological temperature-altitude relation (atmospheric lapse rate) thus limiting the use of the latter as an additional constraint.

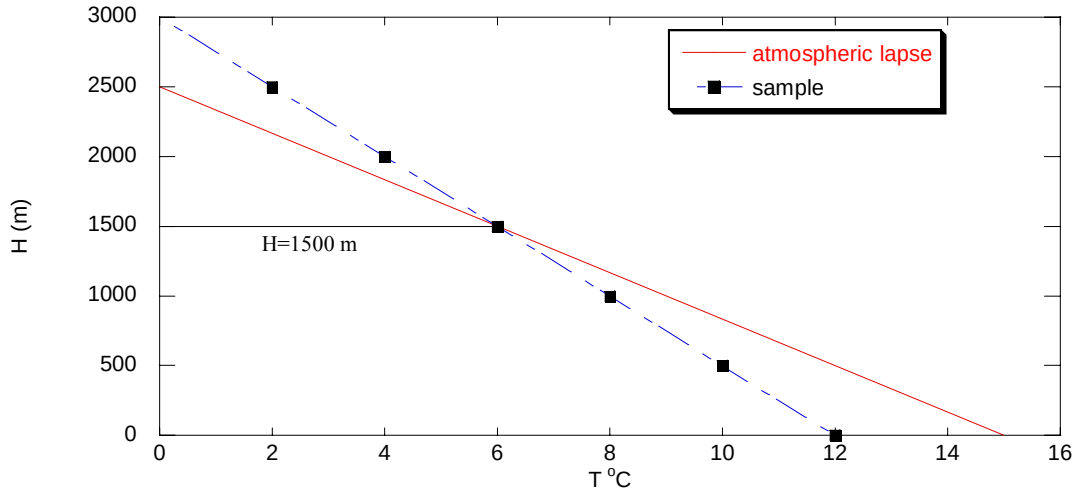

Figure 6.5: Method of determining recharge elevation H from noble gas concentrations proposed by Aeschbach- Hertig et al. (1999). A family of H–T solutions can be derived from the noble gas data by specifying different values of H: A unique recharge elevation is obtained at the intersection between the curve representing this family of H–T solutions and a line representing the local atmospheric lapse (mean annual air temperature vs. elevation). Modified from Manning et al. (2003).

A series of altitudes between 400 and 2400 m were prescribed and a CE-model fit (T, A and F as free parameters) was then performed for each altitude. The resulting noble gas temperatures (NGTs) define nearly straight lines in the T-H plain (Figure 6.6). The dependency of the mean annual air temperature (MAAT) on altitude H for the Oman Mountains was estimated from the climate data discussed above (section 6.2.3). These data provide two points of the MAAT-H relationship: 28.5 °C at sea level and 17.8 °C at an altitude of 1900 m. Assuming a linear relationship, a reasonable lapse rate of -5.6 °C/km is obtained, and T(H) is given by the following equation:

$$T(H) = 28.5^{o}C - 0.0056 \cdot H(m)$$

Unfortunately, there are almost no intersections of the lines representing the NGT-H relationship for each sample with the nearly parallel line representing the MAAT-H

dependency (Figure. 6.6), underscoring the difficulty to apply this method to determine the recharge altitudes. Most of the lines lie above the MAAT, which means

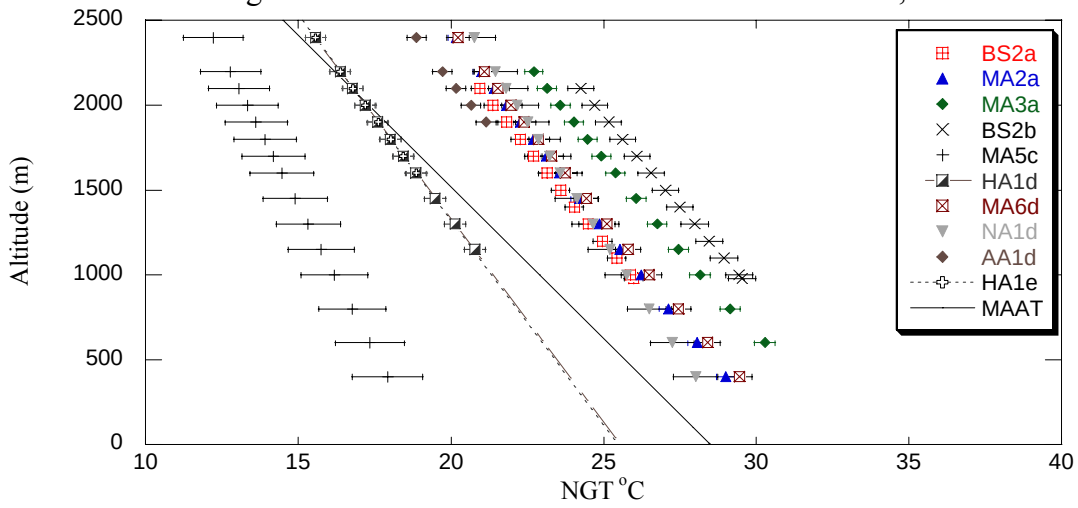

Figure 6.6: NGTs calculated by the CE model against altitude in m. Only points obtained from acceptable fits are shown. The line labeled MAAT shows the local atmospheric temperature lapse, as defined in the text.

the samples must have infiltrated at temperatures higher than the MAAT. This assumption may be supported by the results described by Beyerle et al. (2003), who found that in Niger the noble gas temperatures (NGTs) are elevated by about 3 °C above the MAAT. A relatively large difference between soil temperatures measured by the NGT and the MAAT may be characteristic for many sites in arid regions. Another reason for elevated NGTs could be that the unsaturated zone is very deep, so that the geothermal gradient significantly increases the temperature at the depth of final isolation from the air, where the noble gas signature is defined. There are three lines that lie below the MAAT, which means these samples must have infiltrated at temperatures lower than the MAAT, there is no clear interpretation for this phenomenon. Figure 6.6 shows that the MAAT line intersects the two lines of the Hat spring giving a recharge altitude between 1800 and 2200 m, which is quite close to the estimated recharge altitude (Table 6.1). Although this attempt successfully estimates the recharge altitude for the Hat location, it is still not useful for the rest of the samples.

The problem of the discrepancy between calculated NGTs and expected MAATs can also be illustrated in a different way, by carrying out fits with prescribed temperatures according to the above equation for the atmospheric lapse. It turns out that if both temperature and altitude are prescribed, no fit is achieved for nearly all samples from Oman. This shows that the assumption of "self-consistent" recharge altitudes and temperatures according to the atmospheric lapse equation is not in agreement with the noble gas data and has to be discarded.

The third attempt to estimate the recharge altitude was done by assuming that the recharge temperature is the same as the sampling temperature. Under this condition,

only P and A have to be fitted, avoiding the problem of parameter correlation and yielding much better defined altitude estimates. The problem of this approach is of course the assumption that the water temperature has not changed since recharge. This same assumption is often made in the age calculation from He, SF_6, or CFC data of young groundwaters. It may be quite reliable for young, shallow groundwater that was sampled under well controlled conditions. In the case of the springs in the Oman Mountains, the water temperature may have been affected by several effects, such as geothermal heating due to deep circulation in the mountains and temperature exchange with the environment before or during sampling at the spring sites.

A further problem that occurred when applying this approach to the Oman data was that most samples did not yield good fits with only P and A as free parameters. The situation is not significantly improved by including excess air fractionation as a third parameter, except that in this case the uncertainty of the derived altitudes increases strongly. For the few samples where satisfactory fits are achieved, the derived recharge altitudes are quite precise (better than $\pm$ 100 m) but often not realistic. Thus the usefulness of this approach is quite limited in the case of the Oman samples, but it may be an interesting option under more favorable circumstances.

In summary, the recharge altitudes could not be reliably estimated, neither from stable isotope nor from noble gas data. In the following, estimates of the altitudes based on the local topography are used.

6.4.3 ^3H-^3He ages

In this section, the results of the noble gas and tritium analyses are used to estimate the ^3H-^3He ages of groundwater samples. The noble gases information is mainly used to calculate the recharge temperature (using estimates of the recharge altitude) and to determine the excess air component. This information is important for the separation of the different He components and is later also used to calculate the solubility equilibrium components of SF_6 and CFCs to determine the respective ages (section 6.4.4). The interpretation of noble gas data is done by inverse modeling, which means that different conceptual models for noble gas concentrations in groundwater (including solubility equilibrium, excess air, fractionation, and degassing) are fitted to the data and the optimal parameter values of the models (including temperature) are determined (for more information see chapter 3).

In this study two different models have been used to interpret noble gas data. The first model is the UA-model, assuming that the excess air is due to total dissolution of entrapped air bubbles, the second is the CE-model, assuming that closed–system equilibrium between entrapped bubbles and water is attained. The UA-model is a special case of the CE-model, which leads to an excess air component that has the same composition as air, whereas in the general CE-case this composition can be fractionated relative to air (see chapter 3).

The interpretation of the Oman samples is unusually difficult due to several reasons:

(1) Sampling under not well-controlled conditions may have affected the samples (degassing, (partial) re-equilibration with the atmosphere). As a result, several samples could not be well fitted with the usual models, leading to uncertain recharge temperatures and excess air corrections.
(2) Tritium concentrations in modern Oman precipitation are very low (probably ~ 2 TU, compared to ~ 10 TU in mid-latitudes, although difficult to estimate due to the lack of monitoring stations in the region), hence the tritiogenic ^{3}He signal is tiny and very difficult to separate from the much bigger other ^{3}He components. This is the main reason for the unusually large age errors of several years obtained in this study.
(3) The recharge altitudes of the groundwater from a mountainous area are not exactly known, creating an additional uncertainty in all calculations.
(4) The ^{3}He/^{4}He ratio of the radiogenic He component could not be well constrained, leading to significant uncertainties in the correction for radiogenic ^{3}He for some samples.

Because of all these difficulties, it is hardly possible to evaluate and discuss all samples in the same manner. Before we start the individual discussion of each oasis or spring, some general features are noted here:

Because of the uncertainty of the recharge altitude, all samples have been evaluated for 4 different assumed altitudes: The elevation of the spring (lowest limit) and the lower limit, mean, and upper limit of the presumed range of recharge altitudes (these ranges were determined from the local topographic and geologic conditions by Lüdeling, personal communication). The results obtained for the mean value of the presumed elevation range are reported, other results are only discussed if they differ significantly. Usually, the large uncertainties caused by other difficulties are more important.

The calculation of ^{3}H-^{3}He ages is in principle best done by using the interpretation of all noble gas data (obtained from the inverse modeling) to estimate the atmospheric He components. However, this approach is not feasible for samples that yield no good fit to all noble gases (possibly due to the difficult sampling conditions), and may be problematic if very small differences between fitted and measured concentrations play a role, as it is the case here. Therefore, the classical age calculation based on He and Ne data only (see section 2.5) is used in this study. For samples with good noble gas fits, the recharge temperature and excess air fractionation needed in this calculation are taken from the fits of all noble gases. Otherwise, usually the sampling temperature is used as an estimate of the recharge temperature and the excess air is assumed to be unfractionated. Both quantities are quite critical in the age calculation. The He/Ne ratio of the excess air, L_{exc}, reflects the presence of excess air fractionation (section 2.5, eq. 2.29b), i.e. the choice between the UA- and CE-models. If the UA-model

applies, L_{exc} equals 0.2882. If the CE-model applies, L_{exc} can be reduced by up to about 15 %. This difficulty can be circumvented, and the age calculation further simplified, if the assumption of vanishing radiogenic He can be made (because eq. 2.30 can be used). This radical assumption yields smaller formal errors, but may not often be applicable. Figure 6.7 shows that several samples have a radiogenic He component and therefore the assumption of vanishing radiogenic He can not be applied for these samples. The occurrence of a radiogenic component can also easily be seen from the result of $^3He/^4He$ ratio (Table 6.5), as it leads to values below the atmospheric equilibrium ratio of about $1.36 \cdot 10^{-6}$.

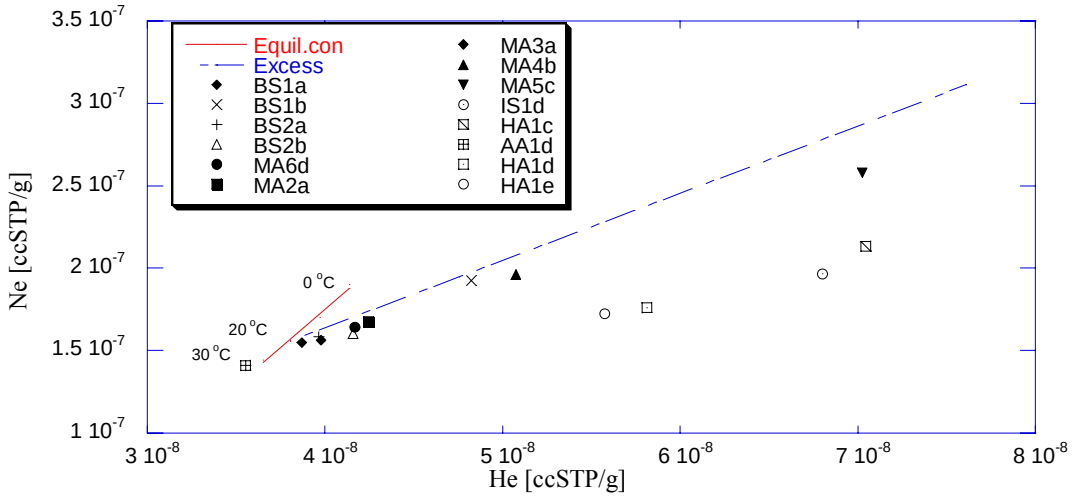

Figure 6.7: He versus Ne concentration of all samples. The line at the lower left indicates the concentrations in air equilibrated water at an altitude of 1400 m and at different temperatures. The broken line indicates addition of unfractionated excess air. Deviations from this line towards higher He concentrations indicate the presence of radiogenic He.

The $^3He/^4He$ ratio of the radiogenic component (R_{rad}) is an unknown parameter that often is assumed to be equal to the typical crustal value of $2 \cdot 10^{-8}$. In some cases, it can be estimated from tritium-free and He-rich samples. In this study, the sample from the thermal spring Nakhl is characterized by a very high non-atmospheric He excess (almost three orders of magnitude higher than any other sample). Assuming that this excess is purely radiogenic, R_{rad} can be estimated to be $1.22 \cdot 10^{-7}$ (see section 6.4.3.4). However, because the sample from Nakhl contains a significant tritium concentration, the assumption of a purely radiogenic excess is questionable and the derived value for R_{rad} can only be taken as an upper limit. Furthermore, it is not at all clear whether the radiogenic component present at Nakhl is representative for the entire study area. Therefore, ^3H-^3He ages were calculated using the standard R_{rad}-value of $2 \cdot 10^{-8}$. The use of the Nakhl-value would lead to younger ages for samples with high radiogenic He; this effect will be discussed where appropriate.

6.4.3.1 Balad Seet

In the oasis of Balad Seet, two springs have been sampled in March and November 2002. The two samples from spring 6 (BS1a, BS1b) have tritium concentrations of 1.8

and 1.7 TU, respectively. The two samples have quite different noble gas results: BS1a has a lower $^3He/^4He$ ratio (Table 6.5), indicating the presence of a radiogenic helium component, while BS1b has a higher ratio. BS1b has higher He and Ne, but lower Ar, Kr, and Xe, which is difficult to explain.

Neither of the two samples can be fitted with the inverse procedure, i.e., the noble gas signatures are not explained. The bad fits do not seem to be due to degassing or equilibration during sampling. Because of the bad fits the sampling temperatures of about 23 °C were used as estimates of the recharge temperature, although these temperatures are rather high for the presumed recharge altitude of ~1900 m, where the mean annual air temperature is expected to lie around 18 °C (see section 6.4.2).

Name	^3H [TU]	err ^3H [TU]	He (cm^3STP/g)	err He (cm^3STP/g)	Ne (cm^3STP/g)	err Ne (cm^3STP/g)	$^3He/^4He$	err $^3He/^4He$
BS1a	1.8	0.08	3.87E-08	1.79E-10	1.55E-07	1.22E-09	1.35E-06	1.10E-08
BS1b	1.7	0.06	4.85E-08	6.44E-10	1.93E-07	1.49E-09	1.38E-06	1.21E-08
BS2a	1.48	0.05	3.96E-08	1.78E-10	1.58E-07	1.92E-09	1.40E-06	1.38E-08
BS2b	1.74	0.07	4.16E-08	5.36E-10	1.60E-07	1.14E-09	1.40E-06	1.28E-08
HA1c	1.46	0.3	7.00E-08	1.09E-09	2.12E-07	2.39E-09	1.09E-06	7.57E-09
HA1d	1.54	0.3	5.81E-08	2.23E-10	1.76E-07	3.08E-09	1.10E-06	7.94E-09
HA1e	1.38	0.3	5.57E-08	2.18E-10	1.73E-07	3.01E-09	1.10E-06	1.02E-08
MA1a	2.27	0.12	4.00E-08	1.24E-10	lost	lost	1.33E-06	1.24E-08
MA2a	2.42	0.1	4.25E-08	1.71E-10	1.67E-07	2.00E-09	1.37E-06	7.82E-09
MA3a	1.39	0.04	3.98E-08	1.81E-10	1.56E-07	1.90E-09	1.40E-06	1.29E-08
MA4b	1.6	0.3	5.07E-08	6.55E-10	1.96E-07	1.39E-09	1.40E-06	1.17E-08
MA5c	0.32	0.05	6.92E-08	8.93E-10	2.54E-07	1.80E-09	1.37E-06	9.00E-09
MA6d	1.87	0.3	4.17E-08	1.67E-10	1.64E-07	2.88E-09	1.37E-06	9.25E-09
IS1d	1.19	0.3	6.80E-08	2.60E-10	1.97E-07	3.45E-09	1.04E-06	8.09E-09
NA1d	1.49	0.3	1.17E-05	4.47E-08	2.88E-07	5.04E-09	1.30E-07	2.28E-09
AA1d	1.92	0.3	3.56E-08	1.46E-10	1.41E-07	2.47E-09	1.39E-06	1.54E-08

Table 6.5: Tritium, He, Ne and $^3He/^4He$ for all Oman samples

For BS1b it can be assumed that no radiogenic He is present, i.e. only the He data are used to calculate the age, yielding an age of 3.0 ± 2.1 yr. For BS1a using only the He data yields a negative age, so that the age calculation for BS1a must include the Ne data, in order to estimate and correct for radiogenic He. Considering the Ne concentration shows that the recharge altitude must be at least 1450 m in order to obtain a positive Ne excess.

At the presumed altitudes of 1700 – 2100 m, ΔNe lies between 3 – 8 %. Despite the relatively small Ne excess, the calculation of the radiogenic He component depends critically on the assumed He/Ne ratio of the excess air, i.e. the value of L_{exc}. For example, the standard choice of $L_{exc} = L_{air} = 0.2882$ (UA-model) yields only very little radiogenic He (0.4 %) and the calculated age remains negative. Thus, excess air must be fractionated. The best guess for L_{exc} can be obtained from the fit of all noble gases (CE-model), although this fit is not really good. Using the respective value of $L_{exc} = 0.248$, a He_{rad} excess of 1.8 % and an age of 1.7 ± 2.3 yr are obtained.

The two samples from BS2 (spring 13) have tritium concentrations of 1.48 TU for BS2a and 1.7 TU for BS2b. The two samples have quite similar noble gas results, although they show the same phenomenon as the BS1 samples, but not so strong: BS2b has higher He and Ne, but lower Ar, Kr, and Xe, which in this case could be a temperature/excess air effect. Both samples have a similar $^3He/^4He$ ratio of about $1.40 \cdot 10^{-6}$, which should yield good ages.

Both samples are fitted very well with the CE-model, while the sample BS2b narrowly misses the usual criterion ($p > 0.01$) for a good fit with the UA-model. Assuming an altitude of 1900 m, the NGTs calculated by the CE-model for BS2a and BS2b are 22.9 and 27.1 °C, respectively. There is no clear interpretation for the temperature difference between the two samples. Yet, these fit results provide a solid basis for the age calculation.

The ^3H-^3He ages calculated for the samples from Balad Seet are summarized below in Table 6.6. The dependence of these ages on altitude and R_{rad} is small and leads to uncertainties of less than about ± 0.3 yr. The uncertainty due to the question of excess air fractionation (choice between UA and CE models) is larger (< ± 1 yr), but still small compared to the uncertainty due to experimental errors (about ± 3 yr).

Sample	Model	age (yr)	Remarks
BS1a	CE	1.7 ± 2.3	bad fit, but fractionation used
BS1b	-	3.0 ± 2.1	He_{rad} = 0 assumed (no excess air model needed)
BS2a	CE	8.9 ± 2.7	
BS2b	CE	10.1 ± 2.3	

Table 6.6: ^3H-^3He ages of the springs at the Balad Seet oasis.

6.4.3.2 Hat spring

In the oasis of Hat, one spring has been sampled three times, in January, June, and August 2003. The January sample (HA1c) was taken in a long drought phase, the June and August samples (HA1d and HA1e) shortly after new rainfalls. HA1c, HA1d and HA1e have tritium concentrations of 1.46, 1.54 and 1.38 TU, respectively.

HA1c has higher He and Ne concentrations than HA1d and HA1e, but lower Ar, Kr, and Xe. Only large differences in recharge temperature and excess air could explain this finding. An interesting observation in this respect is that HA1c has a much lower sampling temperature than HA1d and HA1e. This, however, is exactly opposite to what would be expected from the Ar, Kr, and Xe concentrations. It seems that the sampling temperatures are affected by the season, HA1c being taken in winter, the

other two samples in summer. This would indicate that the water had sufficient time for thermal exchange before or during sampling.

All three samples have a very low $^3He/^4He$ ratio (clearly below the equilibrium value), indicating radiogenic He (Figure 6.7) and complicating ^3H-^3He dating. The noble gas fits confirm that a significant radiogenic He component is present in the Hat spring. The presence of higher levels of radiogenic He than at Balad Seet might indicate higher ages.

HA1c can not be fitted with the inverse procedure, i.e., the noble gas signatures are not explained. The bad fit could be due to degassing, possibly during sampling, because the diffusive degassing model (DD-model, equation 3.3) provides a far better fit than any other model, although still not acceptable. It indicates that this sample had a large amount of excess air which was then lost in part due to degassing.

In contrast, HA1d and HA1e yield acceptable and quite similar fits, especially with the UA-model (but also the CE-model can be considered). The fits yield low recharge temperatures of about 17.8 °C (for H = 1900 m) for both samples. This is quite surprising in view of the much higher recharge temperatures obtained for Balad Seet, although the same altitude has been assumed. The cool temperatures are however quite consistent with the mean annual air temperature at the presumed high recharge altitude. Although HA1c is not fitted well with the DD-model, it yields a similar low temperature (18.0 °C). The low noble gas temperatures are consistent with the sampling temperature of HA1c, but not HA1d and HA1e, indicating that warming may have occurred at or before the sampling in summer.

The age calculation is straightforward for HA1d and HA1e due to good fits of the noble gas data. The choice between UA- and CE-model is not critical here; it only makes a small difference for HA1d. We therefore use the simpler UA-model.

For HA1c, despite the bad fits of the noble gases, a tentative age can be calculated from the He and Ne data. Using the sampling temperature of 17 ^oC and assuming unfractionated excess air, yields an age of 8.4 ± 5.0 yr (for H = 1900 m). Alternatively, using T = 18.0 °C, as indicated by the degassing model, gives an age of 7.4 ± 5.3 yr. These ages have to be interpreted as questionable, because the sample may be affected by degassing, which can hardly be corrected for. If degassing was active, the true age may be much higher.

The calculated ages are summarized in Table 6.7. The dependence of the age on altitude is very small (less than ± 0.1 yr). However, because of the large contributions of He_{rad} (about 40 % of the He expected at solubility equilibrium for all three samples), the uncertainty of the radiogenic isotope ratio R_{rad} is quite important. Using the Nakhl-value $R_{rad} = 1.22 \cdot 10^{-7}$ as a maximum estimate would reduce the ages by an amount comparable to the uncertainty due to experimental errors (about 4 yr for HA1d and HA1e).

Sample	Model	Age (yr)	Remarks
HA1c	UA	8.4 ± 5.0	bad fit, sampling temperature used
HA1d	UA	13.6 ± 3.4	
HA1e	UA	11.8± 4.0	

Table 6.7: ^{3}H-^{3}He ages of Hat spring

6.4.3.3 Maqta oasis

In the oasis of Maqta, six springs have been sampled between March 2002 and June 2003. Tritium concentrations are quite variable, ranging from only 0.3 TU for MA5c to 2.4 TU for MA2a. This variability indicates significant differences in age, with MA5c probably being very old or being mixed with an old component. Sample MA4b has unfortunately been lost during the tritium analysis, so that we assume a tritium concentration for this sample of 2.0 TU (close to the mean of the tritium concentrations of the other samples except MA5). Any ^{3}H-^{3}He age for this sample is therefore only a tentative result.

All six samples have $^{3}He/^{4}He$ ratios near the equilibrium value, indicating little radiogenic He and relatively young ^{3}H-^{3}He ages. Only the slightly lower ratio of MA1a clearly indicates the presence of radiogenic He.

For MA1a, the Ne measurement failed. This complicates the age calculation, but it is still possible based on the other noble gas data. Sample MA5c (with the low tritium concentration) stands out with high noble gas (He, Ne, Ar, Kr, and Xe) concentrations, probably indicating a high amount of excess air. The other samples have quite normal noble gas results.

The fitting works very well for MA1, MA2, MA3, and MA6, both with the UA- and CE-models. MA4 and MA5 may be affected by degassing; indeed for MA5 the diffusive degassing model provides an acceptable fit. The possibility of degassing complicates the dating considerably for these samples. Therefore, the samples with good fits are discussed first.

The fits for these samples yield reasonable temperatures, quite comparable to the sampling temperatures. With the UA-model and an altitude of 1400 m (mean of the presumed range), we obtain: 23.6 °C for MA1, 24.4 °C for MA2, 26.3 °C for MA3, and 24.8 °C for MA6. The CE-model yields slightly higher temperatures. As for Balad Seet, these temperatures are rather high for the presumed altitude (about 21 °C would be expected at 1400 m), but in good agreement with (or slightly lower than) the sampling temperatures, which range from 25 to 28 °C.

The fits corroborate that very little radiogenic He is present in all four samples, except for MA1. Therefore, the correction for He_{rad} has little influence on the ^3H-^3He ages. Because of the missing Ne, the age calculation for MA1 is based on all noble gases, for MA2, MA3, and MA6 it uses He and Ne data only but is based on the recharge temperature and excess air fractionation results from all noble gases. The ages are summarized in Table 6.8.

The dependence of the age on altitude and R_{rad} is small and generally leads to uncertainties of less than about ± 0.3 yr in the ages. The choice between UA and CE models affects only MA3 and MA6, but the difference is small compared to the uncertainty due to experimental errors. Thus, the age calculation is quite robust for these samples. Some caution should be exercised for MA1; because of the missing Ne value, which increases the uncertainty considerably. It should also be noted that this sample seems to have (almost) no excess air, which is unusual for groundwater and may indicate re-equilibration at the spring site before sampling.

Sample	Model	age (yr)	Remarks
MA1a	UA	4.7 ± 5.6	no Ne
MA2a	UA	1.7 ± 2.4	
MA3a	UA	8.3 ± 3.0	
MA4b	UA	5.1 ± 3.3	bad fit, no tritium
MA5c	UA	34.5 ± 5.5	bad fit, UA-model NGT used
MA6d	UA	3.4 ± 3.9	

Table 6.8: ^3H-^3He ages of springs at the Maqta oasis

Age dating for MA4 and MA5 is more problematic due to the bad fit for the noble gases. The standard attempt is to use the sampling temperature as a first estimate of the recharge temperature and to assume unfractionated excess air. A problem with this approach is that the sampling temperatures are very different: 26 °C for MA4 and 15 °C for MA5. Especially the latter seems unrealistic compared to the recharge temperatures derived above for the other Maqta samples. Nevertheless, this approach was carried out and it yields the following results for H = 1400 m: MA4: 5.1 ± 3.3 yr; MA5: 38.7 ± 4.7 yr. For MA4 this result can be used as a tentative age, because it should be remembered that only an estimated tritium value was used.

The UA-model fit for MA5 is not all too bad, and indicates a recharge temperature of 19.3 °C. Using this value reduces the age estimate to 34.5 ± 5.5 yr. MA5 has a radiogenic He component of about 10 % of the equilibrium value, thus using the Nakhl-value for R_{rad} would reduce the calculated age by about 1 yr. The high age of MA5 is due to the very low tritium concentration (0.32 TU). With such a low tritium value, ^3H-^3He dating becomes questionable, and the interpretation of this sample should essentially be that it is (mainly) of pre-bomb origin, i.e., older than about 40 yr. Of course, a small fraction of younger water could be mixed in.

6.4.3.4 Ismaiah, Nakhl and Al Ain

Finally, we discuss three samples taken in June 2003 from three completely different springs. Of the three springs, Nakhl stands out with an extremely high (almost three orders of magnitude higher than any other sample) concentration of He and a very low He isotope ratio. This clearly indicates a large contribution of radiogenic He, which is not unusual for thermal springs, such as Nakhl (sampling temperature 38.3 °C). It also indicates that this water circulates deep and presumably is very old. The overwhelming radiogenic He component makes ^{3}H-^{3}He dating practically impossible. The sample can however be used to estimate the (maximum) value of the radiogenic He isotope ratio, which is $1.22 \cdot 10^{-7}$, close to the value measured in the sample (Figure 6.8).

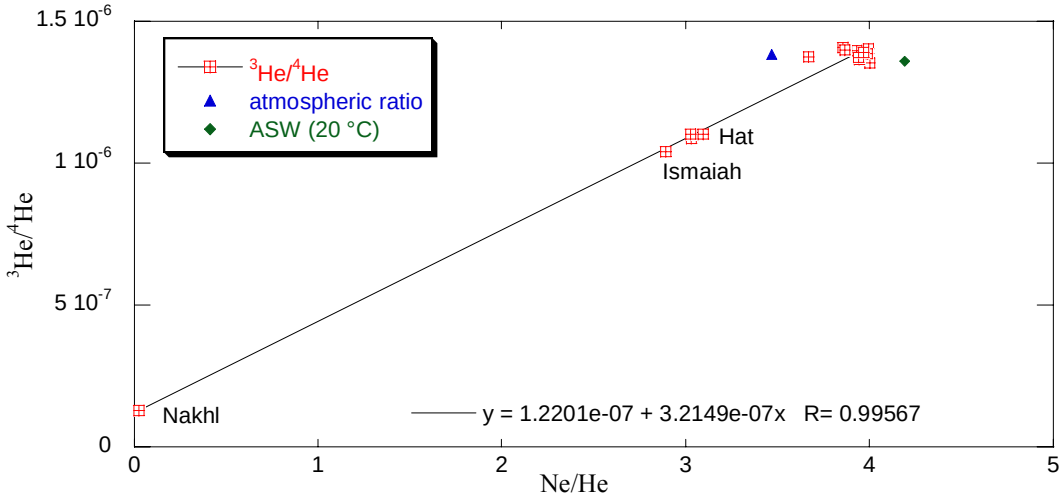

Figure 6.8: Measured ^{3}He/^{4}He ratio versus the measured concentration ratio of Ne to He for the Oman samples. If the He concentration approaches infinity, the Ne/He ratio approaches zero and the atmospheric gas contribution becomes negligible compared to the terrigenic contribution. Thus the intercept of the regression line can be interpreted as corresponding to $(^3\text{He}/^4\text{He})_{rad}$. The sample from the thermal spring Nakhl lies close to this hypothetical radiogenic endmember.

Ismaiah also has a low ^{3}He/^{4}He ratio and relatively high He concentration, indicating radiogenic He and complicating ^{3}H-^{3}He dating. With its high sampling temperature of 35 °C, Ismaiah also seems to be a thermal spring. Al Ain seems unaffected by radiogenic He and should be datable with ^{3}H-^{3}He.

For all three samples, the fits of the noble gases are not very good, but also not completely bad. Nakhl can be satisfactorily fitted with both the UA- and CE-models, Al Ain only with the UA-model (marginal with CE), and Ismaiah provides very marginal fits with both models, which usually would be rejected. There is no indication of degassing.

It seems to be best to rely on the more or less acceptable fits with the simple UA-model to estimate the recharge temperatures and ages. The obtained recharge

temperatures are 25.3 °C for Ismaiah (assuming a recharge altitude of 1400 m), 25.8 °C for Nakhl (assuming a recharge altitude of 800 m), and 20.1 °C for Al Ain (assuming a recharge altitude of 2150 m). These values appear to be more or less reasonable, although they are as usual substantially higher than the expected local mean annual air temperature. On the other hand they are clearly lower than the water temperature in the thermal springs. It should be noted that the good fits and comparatively low recharge temperatures are clear indications that the thermal waters of Nakhl and Ismaiah are of meteoric origin.

Ismaiah and Nakhl have quite high excess air components. In contrast, Al Ain has practically no excess air, which may indicate re-equilibration due to contact with air before sampling.

Although the sample from Nakhl is characterized by an extremely high concentration of He and a very low He isotope ratio, it has a significant tritium concentration of 1.49 TU, which indicates the presence of a recent water component in this spring. The presence of tritium in this sample is quite surprising. It indicates that the radiogenic $^3He/^4He$ ratio derived above may be too large due to the possible presence of tritiogenic ^3He. The dating of this sample by the ^3H-^3He method is practically impossible because of the presence of the high concentration of radiogenic He. The calculated age of the Nakhl sample using the value of $2 \cdot 10^{-8}$ for R_{rad} is about 100 years, which is of course out of the limit of the ^3H-^3He method. On the other hand, using the R_{rad} value of $1.22 \cdot 10^{-7}$ that was derived from this sample assuming only atmospheric and terrigenic (no tritiogenic) contributions, obviously yields a zero age. The most likely interpretation for this sample is a mixture of old water (large contribution of He_{rad}) with young water (tritium-bearing component).

The age derived for Ismaiah must also be regarded as very doubtful, because of the difficulty of correcting for the radiogenic He component, which amounts to about 53 % of the equilibrium He concentration. Assuming unfractionated excess air and using $R_{rad} = 2 \cdot 10^{-8}$ yields an age of 5.8 ± 6.5 yr. The calculated age using the Nakhl-value for R_{rad} is negative, corroborating that the Nakhl-value can only be taken as an upper limit of R_{rad}.

In contrast to Ismaiah and Nakhl, the sample from Al Ain, which has a tritium content of 1.92 TU and almost no radiogenic He can very well be dated. The only difficulty is that there is no excess air; indeed the Ne excess is slightly negative at the fitted recharge temperature. This fact makes it possible and necessary to use the simplified age calculation, without excess air correction and only based on the He data (eq. 2.30). This calculation yields an age of 8.0 ± 1.7 yr, which depends only slightly on the value of R_{rad}. The altitude-dependence of this result is however considerable, comparable to the uncertainty due to experimental errors. Varying the recharge altitude between 2000 and 2300 m would change the age by several years. The Ne concentration actually calls for a rather high altitude (2100 m or higher), because at lower altitudes the Ne deficit becomes significant. The age results are summarized in Table 6.9.

Sample	Model	age (yr)	Remarks
IS1d	UA	5.8 ± 6.5	bad fit, UA-model NGT used, high He_{rad}
NA1d	UA	-	dating impossible because of high He_{rad}
AA1d	UA	8.0 ± 1.7	no excess air

Table 6.9: ^{3}H-^{3}He ages of springs at Ismaiah, Nakhl, and Al Ain.

6.4.4 SF_6 and CFCs

The calculation of a water age from SF_6 and CFCs is based on the well-known temporal history of the concentrations of these anthropogenic trace gases in the atmosphere and the assumption that the water was in equilibrium with the atmosphere during infiltration and the trace gases behaved conservatively thereafter, as explained in more detail in chapter 4. In groundwater, a complication comes from the fact that excess air is present and has to be corrected for, which is especially important for SF_6 (see chapter 4, section 4.5). In our case, we have very significant excess air corrections for most samples.

In addition to the usual excess air problem, the Oman data set is an unusually difficult example of SF_6 dating, due to the following complications:

(1) High recharge temperatures resulting in low solubilities and thus leading to low concentrations and large excess air corrections.
(2) Uncertainties with regard to recharge altitude and recharge temperature.
(3) Possibility of artifacts due to difficult sampling conditions.
(4) Possibility of artifacts due to sample transport and storage and new laboratory procedures in Heidelberg.

More than in other examples, this study shows that it is of utmost importance to measure noble gases (at least Ne) in addition to SF_6, in order to have a handle on the unknown parameters recharge temperature and excess air concentration. Such data are present here for most samples. Thus, the results of the noble gas evaluation discussed in the previous sections provide the basis for the SF_6 age calculation. In accordance with the above noble gas evaluation and for reasons of simplicity, only unfractionated excess air will be considered for the excess air correction of the samples without noble gas data.

For the SF_6 age calculation, an explicit error propagation has been carried out, including the uncertainties of the raw data, the recharge temperature, and the excess air correction. The calculated age errors are on the order of 0.5 yr. However, the overall uncertainty of SF_6 ages, including possible effects of sampling and transfer techniques is estimated to be at least 1 year. Moreover, it has to be noted that some air

contamination during sampling, transport, and pre-analysis procedures, which would lead to too young ages, can not completely be ruled out for the SF_6 samples. It is also possible that natural SF_6 could be present in sulfur-rich crystalline or volcanic rocks (Harnisch and Eisenhauer, 1998), leading to enhanced SF_6 concentrations in the water. Thus, a conservative interpretation of SF_6 ages is to regard them only as minimum ages.

The problem of air contamination is less serious for CFC-12, but instead there is a higher potential for contamination of the groundwater from non-atmospheric sources. Such contamination is quite frequently observed in industrial regions, but would not be expected in the remote Oman Mountains. A certain danger of contamination may however come from the materials used during sampling, in particular plastic tubing and other synthetic materials may contain CFCs.

In the following sections, the results for the main oases are discussed and put into the context of the noble gas and ^3H-^3He results. The analytical results for SF_6 and CFC-12 are listed later in Table 6.10 together with an overview of all tracer ages for all samples from Oman.

6.4.4.1 Balad Seet

From Balad Seet, only one sample for SF_6 and CFC-12 is available: BS1b. This sample had a bad noble gas fit, thus in the age calculation we use the sampling temperature (~23 °C) as an estimate of the recharge temperature. With the assumption of no radiogenic He, a ^3H-^3He age of 3.0 ± 2.1 yr was obtained. BS1b has a quite large excess air component (ΔNe of ~ 35 %), leading to a similar and very important excess air correction (~37 %) for SF_6. The correction is much smaller (< 5 %) for CFC-12.

Assuming a recharge altitude of 1900 m, a recharge temperature of 23 °C, and applying the above excess air correction leads to ages of 8.4 yr from SF_6 and 13.3 yr from CFC-12. These ages are significantly higher than the ^3H-^3He age, which is difficult to explain if we remember that SF_6 ages may be seen as minimum ages. The ^3H-^3He age thus seems to be too young, which can not be due to the assumption of no radiogenic He, but could indicate a loss of ^3He, possibly by degassing or gas exchange with the atmosphere. A diffusive gas loss would affect He much more than SF_6 or CFCs, because of its higher diffusivity. In fact, the diffusive degassing model provides a better, although still not satisfying fit to the noble gas data than other models. The misfit between SF_6 and CFC-12 ages is also important, but may be expected under such difficult conditions.

6.4.4.2 Hat spring

In the oasis of Hat, one spring has been sampled three times for SF_6, in January, June, and August 2003. For the January sample (HA1c), CFC-12 is also available. HA1c could not be fitted, whereas HA1d and HA1e yielded acceptable fits with the UA-model and recharge temperatures of about 17.8 °C (for H = 1900 m) for both samples. These temperatures are used for the SF_6 calculation, whereas for HA1c a similarly low temperature (18.0 °C) obtained from the degassing model is used. The excess air correction is large for HA1c (ΔNe = 43 %), and moderate for HA1d and HA1e (ΔNe ~ 17 %).

For HA1c, an SF_6-age of 14.2 yr is obtained, which is much higher than the ^3H-^3He age of 7.4 yr (NGT = 18 ^oC). This SF_6 age is also comparable to the ^3H-^3He ages estimated for HA1d and HA1e. No age can be calculated from CFC-12 for HA1c, because the concentration is about a factor of 10 above the modern equilibrium concentration. This clearly indicates contamination with CFC-12. The source of the contamination is unknown, but could be related to the equipment used during sampling.

For HA1d, an SF_6-age of 2.3 yr is obtained, which is much lower than the ^3H-^3He age of 13.6 yr. For HA1e, no SF_6-age can be calculated, because the measured as well as the excess-air corrected concentration is higher than the modern equilibrium concentration (about 0.18 pg/kg for H = 1900 m and T = 17.8 °C). These results seem to indicate that the SF_6 concentration in HA1d and HA1e is elevated by an unknown effect other than excess air ("contamination"). This has most likely to be attributed to air contamination during storage or sample transfer before the analysis, or possibly to natural sources of SF_6.

6.4.4.3 Maqta

From the oasis of Maqta, for the later three of the six springs, MA4 – MA6, SF_6 samples have been taken. For MA4 and MA5 also CFC-12 data are available. Of the three springs, only from MA6 good noble gas fits can be used to estimate recharge temperature and excess air. For MA4 and MA5 assumptions in accordance with the ^3H-^3He evaluation are used: The sampling temperature of 26 °C is used for MA4 and the UA-model recharge temperature of 19.3 °C for MA5. Excess air is very high in MA5 (ΔNe = 62 %), moderate for MA4 (ΔNe = 32 %), and low for MA6 (ΔNe = 10 %)

With the above assumptions and excess air corrections, SF_6-ages of 7.3 and 7.0 yr are obtained for MA4 and MA5, respectively, whereas the SF_6 concentration in MA6 as well as the CFC-12 concentrations in MA4 and MA5 is too high to yield an age. Again, it seems that CFC-12 and in part SF_6 is affected by non-atmospheric sources (contamination). For MA4, the SF_6-age of 7.3 yr is in reasonable accordance with the ^3H-^3He age of 5.1 yr. For MA5, however, the SF_6-age of 7.0 yr is in strong disagreement with the very low tritium concentration of 0.3 TU and the ^3H-^3He age of

>35 yr. This indicates again that at least in MA5, non-atmospheric SF_6 could be present.

6.4.4.4 Ismaiah, Nakhl, and Al Ain

SF_6 is available for the three springs of Ismaiah, Nakhl, and Al Ain. For all three springs, the fits of the noble gases are not very good, but the more or less acceptable fits with the UA-model can be used to estimate the recharge temperatures and excess air component. Excess air is very high in Nakhl (ΔNe = 79 %), moderate for Ismaiah (ΔNe = 32 %), and zero for Al Ain. There is an additional SF_6 and CFC-12 sample from Ismaiah, taken in January 2003 (IS1c). For this sample, no corresponding noble gas data are available, which makes the excess air correction difficult.

An SF_6-age of 16.2 yr is obtained for Nakhl; an SF_6-age of 8.9 yr is obtained for IS1d, whereas the SF_6 concentration in Al Ain is too high to yield an age. For Ismaiah (IS1d), the SF_6 age of 8.9 yr is in reasonable agreement with the very uncertain ^3H-^3He age of 5.8 ± 6.5 yr. For Nakhl, however, the SF_6-age of 16.2 yr is in some disagreement with the assumption of a very high age based on the extremely high radiogenic He concentration (sample not datable with the ^3H-^3He method). At least it indicates in agreement with the He data that the water from Nakhl is comparatively old. For Al Ain, the high SF_6 concentration clearly shows that this sample is affected by contamination.

For IS1c, tentative SF_6 and CFC-12 ages can be calculated by assuming the same recharge temperature and excess air concentration as for IS1d. This assumption is not very reliable for the excess air correction, because excess air tends to be quite variable. With these assumptions, an SF_6-age of 19.9 yr is obtained for IS1c, whereas the CFC-12 concentration is too high to yield an age. The much higher age in IS1c compared to IS1d could partly be due to a too high excess air correction. For the extreme case of no excess air correction, the age drops to 15.1 yr. In any case, SF_6 indicates a rather high age for IS1c, a result that appears to be quite reliable despite the uncertainty of the excess air correction.

6.4.4.5 Misfat al Abreen

Two samples for SF_6 and CFCs have been taken from two outlets of a spring in Misfat al Abreen in January 2003. The evaluation of these samples is severely complicated by the fact that no noble gas measurements are available. Therefore, no reliable excess air correction can be made, which in the case of SF_6 can be very important, as the other samples show. The correction would be quite small for CFC-12, but unfortunately the samples seem to be affected by non-atmospheric CFC-12, as most of the other samples.

Assuming a recharge altitude of 1900 m (the expected range is 1800 to 2000 m) and taking the rather high sampling temperature of 27 °C as recharge temperature, the uncorrected SF_6 and CFC-12 concentrations lie above the modern equilibrium. Small to moderate excess air amounts have to be assumed in order to obtain positive SF_6 ages at least for SF_6.
Obviously, no reliable ages can be calculated for Misfat unless noble gas data are available to estimate the recharge temperature and the excess air correction.

In summary, SF_6- and CFC-dating seems questionable for most of the Oman springs, due to the presence of non-atmospheric sources or air contamination, although some SF_6-results appear reasonable. Under these circumstances, SF_6- and CFC-ages can be interpreted only as minimum ages, because contamination leads to artificially young apparent ages.

6.5 Summary

The stable isotope data lie on or near the Batinah meteoric water line indicating that the origin of groundwater in the investigation areas Jabal Akhdar, Hat spring, Umq Bir, Al Ain, Nakhl, Ismaiah and Maqta oasis is coming from a combination between the northern and southern moisture sources.

It has to be noted that the dating techniques based on gas tracers are not ideal for the setting encountered at the oases in the Oman Mountains. The open springs in karstic environment have a high probability of adverse effects, such as gas exchange, as shown by several samples where noble gas patterns can not be interpreted. Nevertheless, some general and approximate age information can be derived.

The best age information is obtained from the ^3H-^3He method, at least for samples with interpretable noble gas concentration patterns. SF_6 ages can only be used as minimum estimates, due to the possibility of air contamination. Surprisingly, CFC-12 is contaminated in almost all samples, which may be due to sampling materials, although they differed between the sampling campaigns. Radiogenic He is quite interesting, clearly but only qualitatively distinguishing three groups of samples (young/medium/old). A summary of the age information is given in Table 6.10.

It can be tried to relate the qualitative indication of radiogenic He to quantitative ages. It is quite clear that the label "young" from He_{rad} relates to ages of some years up to ~ 10 yr. There are not sufficient reliable ages for the "medium" samples from Hat and Ismaiah, but some SF_6 ages indicate that this range could be some decades (~ 10 – 20 yr).

The sample MA5 has a lower radiogenic He component than Hat and Ismaiah, but little tritium and a clearly high ^3H-^3He age. The sample from Nakhl appears old based on He_{rad}, but has significant tritium. These two samples show that the classification based on He_{rad} is not unequivocal.

The most critical factor in the age calculation for the Balad Seet samples is whether or not the excess air is fractionated, which unfortunately is not unequivocally indicated by the noble gas signature. Despite this uncertainty, it is clear that the water of BS1 is younger than that of BS2, and the November samples are older than those taken in March. The quite reliable ^3H-^3He ages indicate ages of 2 – 7 yr for BS1 and ~ 10 yr for BS2. The SF_6 and CFC results indicate somewhat higher ages for BS1b. Overall; Balad Seet seems to belong to the category "young", with ages up to ~ 10 yr, maybe with the exception of BS1b.

Hat samples have somewhat higher ages based on He_{rad}, although the ^3H-^3He ages are only slightly higher than at BS2. The SF_6 age of 14 yr for HA1c confirms this picture, the low SF_6 result for HA1d could be due to contamination. Overall, ages of 10 – 20 yr seem most likely for the Hat springs.

Name	SF_6 (pg/kg)	CFC-12 (pg/kg)	SF_6 age (yr)	CFC-12 age (yr)	^3H-^3He age (yr)	He radiogenic
BS1a					2 ± 2	young
BS1b	0.1524	149.9	(>) 8 ± 1	(>) 13 ± 3	3 ± 2	young
BS2a					9 ± 3	young
BS2b					10 ± 2	young
HA1c	0.1185	2654.3	(>) 14 ± 1		8 ± 5	medium
HA1d	0.2206		> 2		14 ± 3	medium
HA1e	0.2763				12 ± 4	medium
MA1a					5 ± 5	young
MA2a					2 ± 2	young
MA3a					8 ± 3	young
MA4b	0.1582	904.6	(>) 7 ± 1		~ 5	young
MA5c	0.2537	1733.6	(>) 7 ± 1		>~ 35	young-medium
MA6d	0.2034				3 ± 4	young
IS1c	0.0535	578.6	~ 20			
IS1d	0.1475		(>) 9 ± 1		~ 6	medium
NA1d	0.1361		(>) 16 ± 1			old
AA1d	0.2294				8 ± 2	young

Table 6.10: Analytical results for SF_6 and CFC-12 and overview of all tracer ages.

The Maqta springs seem to fall into the category "young", except for MA5. Ages below 10 yr are indicated by ^3H-^3He for MA1-MA3 and MA6, and by SF_6 for MA4. A higher age is clearly indicated by the tritium result for MA5, supported by a slightly elevated He_{rad} value, but in contrast with the SF_6 result. We consider the tritium and He data as more reliable than the SF_6-age. Possibly, MA5 is a mixture of old (> 40yr) water and a young component.

For Ismaiah, He_{rad} indicates medium ages, supported in part by the SF_6 results. Ages of 10 – 20 yr seem most likely. Nakhl is clearly old water based on He_{rad}, but the

presence of a significant tritium concentration and the apparent SF_6 age of 16 yr indicate a mixture of old water and a young component.

Al Ain has a young age of about 8 yr according to the ^3H-^3He method. For Misfat a precise dating is not possible with the presently available data (only SF_6).
In conclusion, the ages of the spring waters in the Oman Mountains range from a few years to about 20 yr, with the exception of the samples from MA5 and Nakhl, which probably represent mixtures between old and young components. The ages of the order of 10 yr explain why the springs do not fall dry even during prolonged periods of drought. Obviously the groundwater reservoirs feeding the springs used by the different oases are sufficiently large and the water flow in the catchment area is sufficiently slow to store precipitation over many years, thus providing a relatively steady and secure water supply to the settlements in the oases.

Summary and outlook

Environmental tracers such as stable isotopes, CFCs, SF_6 and noble gases are important tools to study the origin, evolution and the age of groundwater, and to obtain paleoclimate records. Applications of these methods, especially the use of CFCs and SF_6 to date groundwater, have several challenges such as the formation of excess air, which leads to concentrations above equilibrium and consequently to underestimated calculated ages. In contrast, the degassing process results in concentrations below the equilibrium and consequently the calculated age will overestimate the true age. The theoretical models (UA, PR and CE models) introduced by several authors to overcome these problems depend mainly on the use of noble gas concentrations are discussed. In this work one can easily notice that the closed-system equilibration (CE) model is the best model for excess air correction, as it is in most cases in perfect agreement with the noble gas concentration data within experimental uncertainty both for individual samples and for complete data sets, while the PR- model fits only with some individual samples and not for the complete data set.

The closed-system model can also be used as a model to describe degassing in groundwater samples. It has been successfully used to account for about 50% of the degassed samples from the Ledo-Paniselian aquifer (Belgium). This result indicates the need to conduct more research in this direction to reach a better understanding of the degassing process, e.g., under which conditions and how it takes place in different types of aquifers. Once this process is understood, it is not difficult to develop the different methods to overcome the problem, which presently limits the use of environmental tracers to study groundwater in such systems.

The main project in this work was the use of environmental tracers to study groundwater in the area south-west of the Nile Delta in Egypt, which is characterized by a very arid climate. The obtained results can be summarized as follows:

(1) The main source of recharge is Nile water. (2) Most of the recharge took place before the completion of the Aswan High Dam, corresponding to groundwater ages larger than 40 yr. (3) Only few wells located close to the surface water were recharged by Nile water after the completion of the Aswan High Dam and have ages younger than 25 yr.

These results indicate the limited extent of recharge, especially for the wells located further away from the surface water. Therefore only a limited amount of groundwater is available for pumping in a sustainable resource management regime. These results demonstrate that, at the present extraction rate, the groundwater reserves of the aquifers in the study area are being mined. By expanding the presently established well fields to their full capacity, the water levels will continuously decline, possibly causing further increase of groundwater salinity, which limits the use of groundwater for drinking or for agriculture. To avoid groundwater depletion in the shallow aquifer

and to ensure sustainable development of this precious natural resource in the area of study, the present extraction rate has to be lowered to be equal to the rate of recharge. The rate of recharge can be estimated if the age of groundwater is calculated and the properties of different aquifers are defined. As mentioned, the ages have been calculated for the few wells that are located close to the surface water and have a significant amount of ^{3}H and SF_6 indicating young water. The majority of the wells have no or very low concentration of ^{3}H and SF_6, so that other techniques should be used to date these groundwaters, which have ages older than 50 years. The relatively low concentrations of radiogenic He and the uniform NGTs for these samples indicate recharge during the Holocene period (ages <10,000 yr). ^{14}C will be used in the near future to prove this assumption.

This study shows that significant insight in the groundwater recharge conditions in an arid place like Egypt can be gained from applications of environmental tracers. In the future, environmental tracer techniques could be applied in different locations in Egypt, where the Egyptian government adopted aggressive policies to develop new agricultural communities outside the overpopulated Nile valley and Nile Delta. Several national projects have been started, e.g. the Tushka Canal project, which will divert Nile River water from Lake Nasser to the Baris Depression in the Western Desert. The goal of this project is the use of surface water (Nile water) and groundwater to cultivate thousands of feddans (1 feddan = 0.4 ha) in this area. About 50 % of this project depends on groundwater, so that environmental tracers can be applied to determine the origin and the recharge rate of groundwater in this area. If these studies are performed, one can easily decide if the withdrawn amount of groundwater is available for pumping in a sustainable way or not. The same studies would be quite important for the new reclaimed areas around the Nile valley e.g., the reclaimed areas around the new cities of Assiut and El-Minia in the southern part of Egypt.

Environmental tracers have also been applied to study groundwater from springs in the mountains of Oman; this area is also characterized by an extremely arid climate. Stable isotopes have been applied to determine the origin of groundwater, which mainly is from a combination between the northern and southern moisture sources.

In the Oman study it was tried to estimate the recharge altitude by different methods. The main one is the use of the least squares method with pressure considered as a fit parameter. Quite erratic results and large errors are obtained for the pressure and altitude. The determination of recharge altitude is hampered because the model parameters temperature T and pressure P (i.e. altitude) are badly identifiable, especially if excess air is present. The only possible way to obtain well defined altitude estimates is to prescribe the recharge temperature, if it can be accurately estimated.

Dating groundwater from the springs in Oman is quite difficult, especially for SF_6 and CFCs, because of sampling under unconventional and not well controlled conditions. The calculated age refers to young groundwater in most samples while some springs

are characterized by at least a component of water older than 40 yr. Despite the unusual difficulties encountered in the Oman study, the environmental tracers still provide useful information on the time scale of groundwater renewal, which is mostly in order of one to two decades. This is sufficient to explain that the studied springs can sustain the related oases even during several consecutive years of drought.

References

Abdel Baki, A. A. (1983). Hydrogeological and hydrogeochemical studies in the area west of Rosetta branch and south of El Nasr canal. Ph.D. Thesis, Fac.Sci., Ain Shams University.

Abdel Rahman (1996). Geophysical study on the groundwater conditions in the area southwest of the Nile Delta between Abu Roash and El Khataba road. M. Sc. Thesis, Fac.Sci., Ain Shams University.

Aeschbach-Hertig, W., R. Kipfer, M. Hofer, D. M. Imboden and H. Baur (1996). Density-driven exchange between the basins of Lake Lucerne (Switzerland) traced with the ^{3}H-^{3}He method. Limnol. Oceanogr., 41, 707-721

Aeschbach-Hertig, W., F. Peeters, U. Beyerle, and R. Kipfer (1999). Interpretation of dissolved atmospheric noble gases in natural waters. Water Resour. Res., 35, 2779 -2792.

Aeschbach-Hertig, W., F. Peeters, U. Beyerle and R. Kipfer (2000). Palaeotemperature reconstruction from noble gases in ground water taking into account equilibration with entrapped air. Nature 405, 1040-1044

Aeschbach-Hertig, W., U. Beyerle, J. Holocher, F. Peeters, and R. Kipfer (2002). Excess air in groundwater as a potential indicator of past environmental changes. In: Study of Environmental Change Using Isotope Techniques. IAEA, Vienna, pp. 174-183.

Aeschbach-Hertig, W., R. Kipfer, P. C. Blaser and K. Walraevens, (2003). A noble gas palaeotemperature record from the Ledo-Paniselian aquifer in Belgium. EGS 28th General Assembly, Nice. Geophys. Res. Abstr., 5, 14209.

Andrews, J. N., and D. J. Lee (1979). Inert gases in groundwater from the Bunter sandstone of England as indicators of age and paleoclimatic trends. J. Hydrol., 41, 233–252.

Andrews, J. N., J. E. Goldbrunner, W. G. Darling, P. J. Hooker, G. B. Wilson, M. J. Youngman, L. Eichinger, W. Rauert and W. Stichler (1985). A radiochemical, hydrochemical and dissolved gas study of groundwaters in the Molasse basin of Upper Austria. Earth Planet. Sci. Lett., 73, 317-332.

Andrews, J. N., S. N. Davis, J. Fabryka-Martin, J.-C. Fontes, B. E. Lehmann, H. H. Loosli, J.-L. Michelot, H. Moser, B. Smith and M. Wolf, (1989). The in situ production of radioisotopes in rock matrices with particular reference to the Stripa granite. Geochim. Cosmochim. Acta., 53, 1803-1815.

Andrews, J. N., (1991). Noble gases and radioelements in groundwaters. In: Applied Groundwater Hydrology, A British Perspective, R. A. Downing and W.B. Wilkinson, Eds., 243-265, Clarendon Press, Oxford.

Andrews, J. N. (1992). Mechanisms for noble gas dissolution by groundwaters. In: Isotopes of Noble Gases as Tracers in Environmental Studies, pp. 87- 110. IAEA, Vienna.

Ashton, J. T., R. A. Dawe, K. W. Miller, E. B. Smith, and B. J. Stickings (1968). The solubility of certain gaseous fluorine compounds in water. J. Chem. Soc., (A), 1793–1796.

Baur, H. (1999). A noble-gas mass spectrometer compressor source with two orders of magnitude improvement in sensitivity. American Geophysical Union, Fall Meeting, San Francisco, American Geophysical Union.

Bayer, R., P. Schlosser, G. Bonisch, H. Rupp, F. Zaucker, and G. Zimmek (1989). Performance and blank components of a mass spectrometric system for routine measurement of helium isotopes and tritium by the ^{3}He ingrowth method Sitzungsberichte der Heidelberger Akademie der Wissenschaften, Mathematisch-naturwissenschaftliche Klasse, Jahrgang 1989, 5. Abhandlung, Springer-Verlag.

Benson, B. B. and D. Krause (1976). Empirical laws for dilute aqueous solutions of nonpolar gases. J. Chem. Phys., 64(2), 689-709.

Benson, B. B. and D. Krause (1980). Isotopic fractionation of helium during solution: A probe for the liquid state. J. Solution Chem., 9(12), 895-909.

Beyerle, U. (1999). Groundwater Dynamics, Paleoclimate and Noble Gases. Ph.D. Thesis, ETH Nr. 13078, ETH Zürich.

Beyerle, U., W. Aeschbach-Hertig, D. M. Imboden, H. Baur, T. Graf, and R. Kipfer (2000). A mass spectrometric system for the analysis of noble gases and tritium from water samples. Env. Sci. Technol., 34(10), 2042-2050.

Beyerle, U., J. Rueedi, M. Leuenberger, W. Aeschbach-Hertig, F. Peeters, R. Kipfer, and A. Dodo, (2003). Evidence for periods of wetter and cooler climate in the Sahel between 6 and 40 kyr BP derived from groundwater. Geophys. Res. Lett., 30(4), 1173, doi:10.1029/2002GL016310.

Bullister, J. L., D. P. Wisegarver, and F. A Menzia (2002). The Solubility of Sulfur Hexafluoride in Water and Seawater. Deep Sea Res., I, 49, 175-187.

Busenberg, E., and L. N. Plummer (1992). Use of chlorofluorocarbons (CCl3F and CCl2F2) as hydrologic tracers and age-dating tools: Example-The alluvium and terrace system of central Oklahoma: Water Resour. Res., 28, 2257–2284.

Busenberg, E., and L. N. Plummer (1997). Use of sulfur hexafluoride as a dating tool and as a tracer of igneous and volcanic fluids in ground water. Geol. Soc. Am. Abstr. Programs., 29(6), A-78.

Busenberg E., and L. N. Plummer (2000). Dating young ground water with sulfur hexafluoride: Natural and anthropogenic sources of sulfur hexafluoride. Water Resour. Res., 36(10), 3011-3030

Clark, J. F., P. Schlosser, M. Stute, and H. J. Simpson (1996). SF_6-^3He tracer release experiment: A new method of determining longitudinal dispersion coefficients in large rivers. Environ. Sci. & Technol., 30,1527-1532.

Clark, I. D. and P. Fritz (1997). Environmental isotopes in hydrogeology. Lewis Publishers, Boca Raton, FL, 328 pp.

Clarke, W. B., W. J. Jenkins, and Z. Top (1976). Determination of tritium by mass spectrometric measurement of ^3He. Int. J. appl. Radiat. Isotopes., 27, 515-522.

Clever, H. L. (1979a). Helium and neon - gas solubilities. In: Solubility data series, Vol. 1 (Ed. by IUPAC). Pergamon Press, Oxford.

Clever, H. L. (1979b). Krypton, xenon and radon - gas solubilities. In: Solubility data series, Vol. 2 (Ed. by IUPAC). Pergamon Press, Oxford.

Clever, H. L. (1980). Argon. In: Solubility data series, Vol 4 (Ed. by IUPAC). Pergamon Press, Oxford.

Cook P. G. and D. K. Solomon (1995). The transport of atmospheric trace gases to the water table: Implications for groundwater dating with chlorofluorocarbons and Krypton-85. Water Resour. Res., 31(2), 263–270.

Cook P. G. and A. L. Herczeg (2000). Environmental tracers in subsurface hydrology Kluwer Academic Publishers, Boston, 529 pp.

Cosgrove, B. A., and J. Walkley (1981). Solubilities of gases in H_2O and $2H_2O$. J. Chromatogr., 216, 161–167.

Cotton, F. A., and G. Wilkinson (1972). Advanced Inorganic Chemistry. 3rd ed. Interscience Publishers, New York.

Dahab. K., M. A. Sadek, and M. A. El-Fakharany (1999). Replenishment and mineralization processes of lower Miocene aquifer at Wadi El-Farigh area and its vicinities, using environmental isotopes and hydrochemistry. Sci. J. Fac. Sci., Menufia Univ. Vol. XIII.

El Ghazawi, M. M., and S. M. Atwa (1994). Contributions of some structural elements to the groundwater conditions in the southwestern portion of the Nile Delta. Geological Society of Egypt, Cairo, Egypt. 38(2), 649-667.

Fekry, A. M. (1993). Hydrogeological studies of the southern region west of the Nile Delta. Ph.D. Thesis, Fac. Sci., Ain Shams University.

Friedman, H. L. (1954). The solubility of sulfur hexafluoride in water and of rare gases, sulfur hexafluoride and osmium tetroxide in nitromethane. J. Am. Chem. Soc. A, 76, 1793–1796.

Geller, L. S., J. W. Elkins, J. M. Lobert, A. D. Clarke, D. F. Hurst, J. H. Butler, and R. C. Myer (1997). Tropospheric SF_6: Observed latitudinal distribution and trends, derived emissions and interhemispheric exchange time. Geophys. Res. Lett., 24, 675–678.

Gill, A. E. (1982). Atmosphere-Ocean Dynamics. Academic Press, San Diego, 662 pp.

Glennie K. W., M. G. A. Boeuf, M. W. Hughes Clarke, M. Moody-Stuart, W. F. H. Pilaar, and B. M. E. Reinhardt (1974). Geology of the Oman Mountains. Verh. Kon. Ned. Geol. Minjnb. Gen 32.

Glynn, P. D., and E. Busenberg (1996). Unsaturated zone investigations and chlorofluorocarbon dating of ground waters in the Pinal Creek basin, Arizona, in Morganwalp, D. W., and Aronson, D.A., eds., U.S. Geological Survey Toxic Substances Hydrology Program-Proceedings of the Technical Meeting, Colorado Springs, Colorado, September 20-24, 1993: U.S. Geological Survey Water-Resources Investigations Report 94-4015.

Gomaa, M. A. A. (1995). Comparative hydrogeological and hydrogeochemical study on some aquifer west of Nile Delta, Egypt. Ph.D. Thesis, Fac. Sci., Ain Shams University.

Grothe, J. (1992). Datenerfassung und Datenauswertung am Heidelberger Low-Level-Tritium-Meßsystem. Diploma-thesis, Institute of Environmental Physics, University of Heidelberg.

Hanna S. S. (1990). The Alpine deformation of the central Oman Mountains. In The Geology and Tectonics of the Oman Mountains, Vol. 49 (ed. A. H. F. Robertson, M. P. Searle, and A. C. Ries), pp.341-359. Geological Society of London.

Harnish, J., and A. Eisenhauer (1998). Natural CF_4 and SF_6 on Earth. Geophys. Res. Lett., 25, 2401-2404.

Heaton, T. H. E. and J. C. Vogel (1979). Gas concentrations and ages of groundwaters in Beaufort Group sediments, South Africa. Water SA., 5(4), 160-170.

Heaton, T. H. E. (1981). Dissolved gases: Some applications to groundwater research Trans. Geol. Soc. S. Afr., 84, 1–97.

Heaton, T. H. E., and J. C. Vogel (1981). Excess air in groundwater. J. Hydrol., 50, 201-216.

Herzberg, O., and E. Mazor (1979). Hydrological applications of noble gases and temperature measurements in underground water systems: Examples from Israel J. Hydrol., 41, 217–231.

Hofer, M., and D. M. Imboden (1998). Simultaneous determination of CFC-11, CFC-12, N_2 and Ar in water. Anal. Chem., 70(4), 724-729.

Holocher, J., F. Peeters, W. Aeschbach-Hertig, W. Kinzelbach, and R. Kipfer (2003). Kinetic model of gas bubble dissolution in groundwater and its implications for the dissolved gas composition. Env. Sci. Technol., 37, 1337-1343.

Horst, W., M. Nagieb, and S. Siebert (2002). Water as a natural resource in oases of the Oman Mountains. Deutscher Tropentag, October 9-11, 2002, Witzenhausen. Abstr., Subgroup 1b: Irrigated and Dryland Farming.

IAEA/WMO (2004). Global Network of Isotopes in Precipitation. The GNIP Database. Accessible at: http://isohis.iaea.org.

Ibrahim, S .M. (2000). Groundwater hydrology of El-Khatatba area and its vicinities, west Nile Delta, Egypt. M.Sc. Thesis. Fac. Eng. Ain Shams University.

Ingraham, N. L., E. A. Caldwell, and B. T. Verhagen (1998). Arid Catchments, in: Kendall, C., J. J. McDonnell, (eds.), Isotope Tracers in Catchment Hydrology. Elsevier, Amsterdam, 435-465.

Jähne, B., G. Heinz, and W. Dietrich (1987). Measurement of the diffusion coefficients of sparingly soluble gases in water. J. Geophys. Res., 92(C10), 10767-10776.

Jenkins, W. J. and W. B. Clarke (1976). The distribution of ^{3}He in the western Atlantic Ocean. Deep Sea Res., 23, 481-494.

Kipfer R., W. Aeschbach-Hertig, F. Peeters, and M. Stute (2002). Noble gases in lakes and ground waters. In. Noble Gases in Geochemistry and Cosmochemistry, Vol. 47 (eds. D. Porcelli, C. Ballentine, and R. Wieler), pp. 615–700. Mineralogical Society of America, Geochemical Society, Washington, DC.

Klement, R., (2005). Optimierung von SF_6 Grundwasserprobenahme-Methoden. Diploma-thesis, Institute of Environmental Physics, University of Heidelberg, Heidelberg.

Ko, M. K. W., N. D. Sze, W.-C. Wang, G. Shia, A. Goldman, F. J. Murcray, D. G. Murcray, and C. P. Rinsland (1993). Atmospheric sulfur hexafluoride: Sources, sinks and greenhouse warming. J. Geophys. Res., 98(D6), 10499–10507.

Kulongoski, J. T., D. R. Hilton, and E. T. Selaolo (2004). Climate variability in the Botswana Kalahari from the late Pleistocene to the present day. Geophys. Res. Lett., 31, L10204, doi:10.1029/2003GL019238.

Law, C. S., A. J. Watson, and M. I. Liddicoat (1994). Automated vacuum analysis of sulfur hexafluoride in seawater: Derivation of the atmospheric trend (1979–1993) and potential as a transient tracer. Mar. Chem., 48, 57–69.

Lippard S. J., A. W. Shelton, and I. E. Gass (1986). The Ophiolite of Northern Oman. Vol (11), pp. 178. Geological Society of London.

Lippmann J., M Stute, T. Torgersen, D. Moser, J. A. Hall, L. Lin, M. Borcsik, R. E. S. Bellamy, and T. C. Onstott (2003). Dating ultra-deep mine waters with noble gases and ^{36}Cl, Witwatersrand Basin, South Africa. Geochim. Cosmochim. Acta., 67 (23), 4597-4619

Lovelock, J. E. (1971). Atmospheric fluorine compounds as indicators of air movements. Nature 230, 379.

Lüdeling, E. (2004). Geological and topographic determinants of oasis locations in the Oman Mountains-a remote sensing approach. Diploma-thesis, University of Kassel.

Maiss, M. (1992). Schwefelhexafluorid (SF_6) als Tracer für Mischungsprozesse im westlichen Bodensee. Ph.D. Thesis, Institute of Environmental Physics, University of Heidelberg, Heidelberg.

Maiss, M., and I. Levin (1994). Global increase of SF_6 observed in the atmosphere. Geophy. Res. Lett., 21, 569–572.

Maiss, M., L. P. Steele, R. J. Francey, P. J. Fraser, R. L. Langenfelds, N. Trivett, and I. Levin (1996). Sulfur hexafluoride - A powerful new atmospheric tracer. Atmos. Environ., 30, 1621–1629.

Maiss, M., and C. A. M. Brenninkmeijer (1998). Atmospheric SF_6: trends, sources, and prospects. Environ. Sci. Technol., 32, 3077-3086.

Mamyrin. B. A and I. N. Tolstikhin (1984). Helium isotopes in nature. Elsevier, Amsterdam, 273 pp.

Manning, A. H. and D. K. Solomon (2003). Using noble gases to investigate mountain-front recharge. J. Hydrol., 275, 194-207.

Mather, J. R. (1984). Water resources, distribution, use, and management. John Wiley & Sons, Inc. and V.H. Winstzons & Sons, New York, Silver Spring Maryland, 439 pp.

Matthess, G. (1982). The Properties of Groundwater. John Wiley, New York, 1982, 406 pp.

Mazor, E. (1972). Paleotemperatures and other hydrological parameters deduced from noble gases dissolved in groundwaters: Jordan Rift Valley, Israel. Geochim. Cosmochim. Acta., 36, 1321–1336.

Morrison, T. J., and N. B. Johnstone (1955). The salting out of nonelectrolites, III, The inert gases and sulfur hexafluoride. J. Chem.Soc., 3655–3659.

Neubert, R. (1998). Messung der stabilen Isotopomere des atmosphärischen Kohlendioxids. PhD Thesis, Institute of environmental physics, University of Heidelberg, Heidelberg.

Ozima, M. and F. A. Podosek (1983). Noble gas geochemistry. Cambridge Univ. Press, Cambridge, London, New York.

Patra, P. K., S. Lal, B. H. Subbaraya, C. H. Jackman, and P. Rajaratnam (1997). Observed vertical profile of sulfur hexafluoride and its atmospheric applications. J. Geophys.Res., 102(D7), 8855-8859.

Peeters, F., U. Beyerle, W. Aeschbach-Hertig, J. Holocher, M. S. Brennwald, and R. Kipfer (2003). Improving noble gas based paleoclimate reconstruction and groundwater dating using $^{20}Ne/^{22}Ne$ ratios. Geochim. Cosmochim. Acta., 67(4), 587-600.

Plummer, L. N., S. A. Dunkle, and E. Busenberg (1993). Chlorofluorocarbons (CCl_3F and CCl_2F_2) as Dating Tools and Hydrologic Tracers in Shallow Ground Water of the Delmarva Peninsula--Data Tabulation. U.S. Geol. Surv. Open File Rep., 93-484, 56 p.

Plummer, L. N. and E. Busenberg (1999). Chlorofluorocarbons in P. Cook and A. Herczeg, (eds.), Environmental Tracers in Subsurface Hydrology: Kluwer Academic Publishers: Boston; pp. 441-478.

Ravishankara, R. A., S. Solomon, A. A. Turnipseed, and R. F. Warren (1993). Atmospheric lifetimes of long-lived species. Science 259, 194-199.

REGWA. (1990). Hydrogeological inventory and groundwater development plan, western Nile Delta Region. Internal report,

Robertson A. H. F., M. P. Searle, and A. C. Ries (1990). The Geology and Tectonics of the Oman Region. In Geological Society Special Publications, Vol (49), pp. 845. Geological Society of London.

Said, R., 1962. The geology of Egypt. Amsterdam, New York. Elsevier CO., 380 pp.

Schlosser P., M. Stute, C. Sonntag, and K. O. Munnich (1989). Tritiogenic ^3He in shallow groundwater. Earth Planet. Sci. Lett., 94, 245-256.

Schlosser, P., G. Bönisch, B. Kromer, K. O. Münnich, and K. P. Koltermann (1990). Ventilation rates of the waters in the Nansen Basin of the Arctic Ocean derived from a multitracer approach. J. Geophys. Res., 95, 3265–3272.

Schlosser, P. (1992). Tritium/^3He dating of waters in natural systems. In: Isotopes of noble gases as tracers in environmental studies, pp. 123-145. IAEA, Vienna.

Shafei, A. A. (1972). Wadi El Natrun Nasser Farm. General company for research and groundwater (REGWA).

Shiklomanov, I. A., and J. C. Rodda (2003). World Water Resources at the Beginning of the Twenty-First Century. Cambridge University Press, Cambridge, 450 pp.

Smith, S. P. and B. M. Kennedy (1983). Solubility of noble gases in water and in NaCl brine. Geochim. Cosmochim. Acta., 47, 503-515.

Solomon, D. K., R. J. Poreda, S. L. Schiff, and J. A. Cherry (1992). Tritium and helium 3 as groundwater age tracers in the Borden aquifer. Water Resour. Res., 28(3), 741-755.

Stute, M. (1989). Edelgase im Grundwasser - Bestimmung von Palaotemperaturen und Untersuchung der Dynamik von Grundwasserfliesssystemen. Ph.D. Thesis, University of Heidelberg. Heidelberg

Stute, M. and P. Schlosser (1993). Principles and applications of the noble gas paleothermometer In P. K. Swart, K. C. Lohmann, J. McKenzie and S. Savin (eds), Climate Change in Continental Isotopic Records: American Geophysical Union, Washington, DC. Vol. 78, pp. 89-l00.

Stute, M., M. Forster, H. Frischkorn, A. Serejo, J. F. Clark, P. Schlosser,W. S. Broecker, and G. Bonani (1995). Cooling of tropical Brazil (5^{o}C) during the last glacial maximum. Science 269, 379-383.

Stute, M., J. Deak, K. Revesz, J. K. Bohlke, E. Deseo, R. Weepernig, and P. Schlosser, (1997). Tritium/He-3 dating of river infiltration: An example from the Danube in the Szigetkoz area, Hungary. Ground Water, 35(5), 905-911.

Stute, M., and A. S. Talma (1998). Glacial temperatures and moisture transport regimes reconstructed from noble gases and delta ^{18}O, Stampriet aquifer, Namibia. In: Isotope techniques in the study of environmental change. IAEA-SM-349, Vienna, pp. 307-318.

Stute M., and P. Schlosser (2000). Atmospheric noble gases. In P. Cook,. and A. L. Herczeg (eds.), Environmental tracers in subsurface hydrology: Kluwer Academic Publishers: Boston; pp. 349-377.

Thompson, G. M. and J. M. Hayes (1979). Trichloroflouromethane in groundwater - a possible tracer and indicator of groundwater age. Water Resour. Res., 15(3), 546-554.

Tolstikhin, I. N. and I. L. Kamenskiy (1969). Determination of ground-water ages by the T-^{3}He Method. Geochemistry International, 6, 810-811.

Van der Kemp, W. J. M., C. A. J. Appelo, and K. Walraevens. (2000). Inverse chemical modeling and radiocarbon dating of palaeogroundwaters: The Tertiary Ledo-Paniselian aquifer in Flanders, Belgium. Water Resour. Res., 36, 1277-1287.

von Rohden, C., and J. Ilmberger (2001). Tracer experiment with sulfur hexafluoride to quantify the vertical transport in a meromictic pit lake. Aquat. Sci., 63, 417-431.

Wagner, W. and M. A. Geyh (2000). Application of Environmental Isotope Methods for Groundwater Studies in the ESCWA Region (Economic and Social commission for Western Asia), Geologisches Jahrbuch Reihe C, Band C 67.

Wanninkhof, R., J. R. Ledwell, and A. J. Watson (1991). Analysis of sulfur hexafluoride in seawater. J. Geophys. Res., 96(C5), 8733–8740.

Wanninkhof, R. (1992). Relationship between gas exchange and wind speed over the ocean. J. Geophys. Res., 97, 7373-7381.

Warner, M. J., and R. F. Weiss (1985). Solubilities of chlorofluorocarbons 11 and 12 in water and seawater. Deep Sea Res., 32, 1485–1497.

Watson, A. J., and M. I. Liddicoat (1985). Recent history of atmospheric trace gas concentrations deduced from measurements in the deep sea: Application to sulfur hexafluoride and carbon tetrachloride. Atmos. Environ., 9, 1477–1484.

Watson, A. J., and J. R. Ledwell (2000). Oceanographic tracer release experiments using sulphur hexafluoride. J. Geophys. Res., 105, 14325-14337.

Weiss, R. F. (1970). The solubility of nitrogen, oxygen and argon in water and seawater. Deep Sea Res., 17, 721-735.

Weiss, R. F. (1971). Solubility of helium and neon in water and seawater. J. Chem. Eng. Data., 16(2), 235-241.

Weiss, R. F. and T. K. Kyser (1978). Solubility of krypton in water and seawater. J. Chem. Eng. Data., 23(1), 69-72.

Weiss, R. F. and B. A. Price (1989). Dead Sea gas solubilities. Earth Planet. Sci. Lett., 92(l), 7-10.

Weyhenmeyer, C. E., S. J. Burns, and H. Niklaus Waber (2002). Isotope study of moisture sources, recharge areas, and groundwater flow paths within the eastern Batinah coastal plain, Sultanate of Oman. Water Resour. Res., 38(10), 1184, doi:10.1029/2000WR000149.

Wilhelm, E., R. Battino, and R. J. Wilcox (1977). Low-pressure solubility of gases in liquid water. Chem. Rev. Washington, D. C., 77, 219–262.

Wilson, R. D., and D. M. Macky (1996). SF_6 as a conservative tracer in saturated media with high intragranular porosity of high organic carbon content. Ground Water, 34(2), 241-249.

Wilson, G. B. and G. W. McNeill (1997). Noble gas recharge temperatures and the excess air component. Appl. Geochem., 12(6), 747-762.

Appendix

Appendix 1: Noble gas solubilities

The coefficients and constants that were used to calculate the solubility of noble gases (He, Ne, Ar, Kr, and Xe) in water are listed in the following.

Moist air equilibrium concentrations C_i^{eq} are calculated according to Weiss (1970b, 1971) and Weiss and Kyser (1978), using the following equation, which can be applied for He, Ne, Ar, and Kr:

$$\ln\left(C_i^{eq}(T,S,P_0)\right) = \left\{ A_1 + A_2\frac{100}{T} + A_3\cdot\ln\left(\frac{T}{100}\right) + A_4\frac{T}{100} + S\cdot\left[B_1 + B_2\frac{T}{100} + B_3\left(\frac{T}{100}\right)^2 \right] \right\} / 1000$$

$C_i^{eq}(T,S,P_0)$ is the equilibrium concentration of noble gas i in water with moist air at a total atmospheric pressure of $P_0 = 1$ atm in cm^3STP/gH_2O, T is the temperature in Kelvin, and S is the salinity in ‰. The constants are listed in Table A1.1.

For Xe, the mole fraction solubility X_{Xe} in fresh water is calculated from (Clever, 1979b):

$$X_{Xe} = \exp(A_1 + A_2\cdot(100/T) + A_3\cdot\ln(T/100))$$

The salt dependence is given by the salting coefficient of Smith and Kennedy (1983)

$$k_{s,xe} = B_1 + B_2\cdot(100/T) + B_3\cdot\ln(T/100)$$

The equilibrium concentration of Xe as a function of T, S, and P is then calculated by eq. 2.14. The constants are listed in Table A1.1.

Noble gas	A_1	A_2	A_3	A_4	B_1	B_2	B_3
He	-167.218	216.3442	139.2032	-22.6202	-0.04478	0.023541	-0.00343
Ne	-170.602	225.1946	140.8863	-22.629	-0.12711	0.079277	-0.01291
Ar	-178.173	251.8139	145.2337	-22.2046	-0.03873	0.017171	-0.00213
Kr	-112.684	153.5817	74.469	-10.0189	-0.01121	-0.00184	0.00112
Xe	-74.7393	105.21	27.4664		-14.1338	21.8772	6.5527

Table A1.1: Constants of Weiss (1970, 1971) for calculating moist-air equilibrium concentrations of He, Ne, Ar, and Kr in water; and of clever (1979b) and Smith and Kennedy (1983) for the equilibrium concentration of Xe

Appendix 2: SF_6 solubilities

The temperature and salinity effects on Henry's law coefficients for SF_6 are given by the equation (Bullister et al., 2002):

$$\ln K' = a_1 + a_2\left(\frac{100}{T}\right) + a_3 \ln\left(\frac{T}{100}\right) + S\left[b_1 + b_2\left(\frac{T}{100}\right) + b_3\left(\frac{T}{100}\right)^2\right]$$

Constants for the calculation of K' in gravimetric (mol $kg^{-1}atm^{-1}$) and volumetric (mol l^{-1} atm^{-1}) forms for SF_6 as given by Bullister et al. (2002) are listed in the following table:

K`	Gravimetric	Volumetric
a_1	-98.7264	-96.5975
a_2	142.803	139.883
a_3	38.8746	37.8193
b_1	0.02687	0.031069
b_2	-0.03344	-0.03564
b_3	0.007084	0.007433

The following equation is used to determine the solubility function G, which is used to calculate equilibrium concentrations for trace components in moist air at a total pressure of 1 atm:

$$\ln G = a_1 + a_2\left(\frac{100}{T}\right) + a_3 \ln\left(\frac{T}{100}\right) + S\left[b_1 + b_2\left(\frac{T}{100}\right) + b_3\left(\frac{T}{100}\right)^2\right]$$

Constants for the calculation of G in gravimetric (mol kg^{-1}) and volumetric (mol l^{-1}) forms for SF_6 as given by Bullister et al. (2002) are listed in the following table:

G	Gravimetric	Volumetric
a_1	-82.1639	-80.043
a_2	120.152	117.232
a_3	30.6372	29.5817
b_1	0.02932	0.033518
b_2	-0.0352	-0.03739
b_3	0.007401	0.007749

Appendix 3: CFC solubilities

The temperature and salinity effects on Henry's law coefficients for CFCs are given by the equation (Warner and Weiss, 1985)

$$\ln K' = a_1 + a_2\left(\frac{100}{T}\right) + a_3 \ln\left(\frac{T}{100}\right) + S\left[b_1 + b_2\left(\frac{T}{100}\right) + b_3\left(\frac{T}{100}\right)^2\right]$$

where K' is the solubility in mol kg^{-1} atm^{-1} (gravimetric form) or in mol l^{-1} atm^{-1} (volumetric form). It has been measured in pure water and see water for CFC-11 and CFC-12 (Warner and Weiss, 1985), and for CFC-113 (Bu and Warner, 1995). S is the salinity in ‰, and T is the temperature in Kelvin. Constants for calculation of K' are listed in the following tables.

CFC	a_1	a_2	a_3	b_1	b_2	b_3
CFC-11	-136.269	206.115	57.2805	-0.1486	0.095114	-0.01634
CFC-12	-124.44	185.4299	51.6383	-0.14978	0.094668	-0.016
CFC-113	-136.129	206.475	55.8957	-0.02754	0.006033	----------

Table A3.1: Constants for the calculation of K' in gravimetric form (Warner and Weiss, 1985; Bu and Warner, 1995)

CFC	a_1	a_2	a_3	b_1	b_2	b_3
CFC-11	-134.154	203.2156	56.232	-0.14445	0.092952	-0.016
CFC-12	-122.325	182.5306	50.5898	-0.14563	0.092509	-0.01566
CFC-113	-134.243	203.898	54.9583	-0.02632	0.005874	----------

Table A3.2: Constants for the calculation of K' in volumetric form (Warner and Weiss, 1985; Bu and Warner, 1995)

Acknowledgements

I would like to thank the following people whose support and encouragement during my study in the Institute of Environmental Physics contributed greatly to the work described here.

Prof. Dr. Werner Aeschbach-Hertig, his helpful remarks and his confidence in me were a continual source of encouragement, forming the foundation on which my work was built, introducing great advice during the interpretation of my results, checking over and correcting the English of the final version of this thesis. He provided me financial support after finishing the time of my mission, this helped me to finish my work without stress. (I would like to say Prof. Aeschbach-Hertig is the best person I met in Germany).

Dr. Kamal Dahab and his group, they supported me with all hydrogeological and hydrochemical information about the study area in Egypt. They also introduced great advice, which helped me during the interpretation of the results.

Dr. Christoph Von Rohden showed me how to collect, how to measure, and how to evaluate SF_6 samples.

Dr. Reinhold Bayer helped me to finish and overcome some official problems, which took place during my work in the Institute of Environmental Physics.

Markus Pettinger supported me with information about the measurement technique of stable isotope samples.

The members of the GP-research group, especially my dear Prof. Werner Aeschbach-Hertig, Ronny Friedrich, Andreas Kreuzer, and Rainer Klement who did a lot of work to test the new technique to transfer SF_6 samples from stainless steel cylinders to the ususl glass bottles.

Finally, my warmest thanks go to my family. My parents and my brother encouraged me and gave me every possible support during my study. Without the emotional encouragement of my wife and here belief in me, completion of this work would not have been possible; she gave me all the freedom I required to bring this work to a successful conclusion. My lovely daughters Al-Zahraa and Tasabeeh helped me many times to relax from the stress of work.